

Argonne National Laboratory

REVIEW OF OXIDATION RATES OF DOE SPENT NUCLEAR FUEL:

PART 1: METALLIC FUEL

by

BRUCE A. HILTON



Argonne National Laboratory, Argonne, Illinois 60439
operated by the University of Chicago
for the United States Department of Energy under Contract W-31-109-Eng-38

Argonne National Laboratory, with facilities in the states of Illinois and Idaho, is owned by the United States Government and operated by The University of Chicago under the provisions of a contract with the Department of Energy.

DISCLAIMER

This report was prepared as an account of work sponsored by an agency of the United States Government. Neither the United States Government nor any agency thereof, nor The University of Chicago, nor any of their employees or officers, makes any warranty, express or implied, or assumes any legal liability or responsibility for the accuracy, completeness, or usefulness of any information, apparatus, product, or process disclosed, or represents that its use would not infringe privately owned rights. Reference herein to any specific commercial product, process, or service by trade name, trademark, manufacturer, or otherwise, does not necessarily constitute or imply its endorsement, recommendation, or favoring by the United States Government or any agency thereof. The views and opinions of document authors expressed herein do not necessarily state or reflect those of the United States Government or any agency thereof, Argonne National Laboratory, or The University of Chicago.

Available electronically at <http://www.doe.gov/bridge>

Available for a processing fee to U.S. Department of Energy and its contractors, in paper, from:

U.S. Department of Energy
Office of Scientific and Technical Information
P.O. Box 62
Oak Ridge, TN 37831-0062
phone: (865) 576-8401
fax: (865) 576-5728
email: reports@adonis.osti.gov

ANL-00/24

ARGONNE NATIONAL LABORATORY

P.O. Box 2528

Idaho Falls, Idaho 83403

Review of Oxidation Rates of DOE Spent Nuclear Fuel

Part 1: Metallic Fuel

by

Bruce A. Hilton

Nuclear Technology Division

Argonne National Laboratory

November 2000

TABLE OF CONTENTS

	<u>Page</u>
ACRONYMS	x
ABSTRACT	xi
I. INTRODUCTION	1
A. Background	2
1. Grouping	2
2. Compositions and Fuel Types	2
B. Fundamentals of Oxidation and Corrosion	4
1. Thermodynamics	5
2. Kinetics and Reaction Processes	6
3. Temperature Dependence	10
C. Measurement and Analysis Techniques	12
1. Reaction Rate Measurements	12
2. Reaction Product Characterization	13
3. Unit Conversion Factors	14
4. Software	15
II. OXIDATION RATES OF URANIUM METAL	15
A. Mechanisms of Uranium Metal Oxidation	16
1. Uranium/Oxygen Reaction	16
2. Uranium/Water Vapor Reaction	17
3. Uranium/Water Reaction	21
B. Kinetics of Uranium Metal Oxidation	23
1. Uranium/Oxygen Reaction	23
2. Uranium/Water Vapor Reaction	29
3. Uranium/Water Reaction	36
4. Summary	39
C. Irradiation Effects on Uranium Metal Oxidation	40
D. Uranium-Hydride Effects on Uranium Metal Oxidation	43
III. OXIDATION RATES OF URANIUM METAL ALLOYS	45
A. Factors Affecting Uranium Alloy Oxidation	45
1. Microstructural Effects on Oxidation	45
2. Discontinuous Failure	47
B. Kinetics of Uranium-Molybdenum Oxidation	48
1. U-Mo/Water Vapor Reaction	48
2. U-Mo/Water Reaction	49
C. Kinetics of Uranium-Niobium Oxidation	51
1. U-Nb/Water Reaction	51
D. Kinetics of Zirconium-Uranium Oxidation	53
1. Zr-U/Oxygen Reaction	54
2. Zr-U/Water Reaction	54
E. Irradiation Effects on Uranium Alloy Oxidation	55
F. Summary of Uranium Alloy Oxidation	56

IV.	OXIDATION RATES OF ALUMINUM-BASED DISPERSION FUELS	57
A.	Oxidation Mechanisms of Aluminum-Based Dispersion Fuels	58
1.	Microstructural Effects on Oxidation.....	59
2.	Oxidation Mechanism of Aluminum-Based Dispersion in Water	62
B.	Kinetics of Aluminum Alloy Oxidation	62
1.	Al-Alloy/ Water Reaction	62
C.	Kinetics of Aluminum Matrix-Uranium Aluminide Oxidation.....	64
1.	Al-UAl _x /Water Vapor Reaction.....	64
2.	Al-UAl _x /Water Reaction.....	65
D.	Kinetics of Aluminum Matrix-Uranium Oxide Oxidation	66
E.	Kinetics of Aluminum Matrix-Uranium Silicide Oxidation.....	66
1.	Al-U _x Si _y /Water Reaction	67
2.	U _x Si _y /Oxygen Reaction.....	68
3.	U _x Si _y /Water Reaction	69
F.	Summary of Aluminum-Based Dispersion Fuel Oxidation	70
V.	CONCLUSIONS	71
VI.	ACKNOWLEDGMENTS	75
VII.	REFERENCES	76

LIST OF FIGURES

Figure 1.	Schematic representation of metals oxidation: (a) adsorption of oxygen molecules, (b) dissociation of adsorbed oxygen molecule, and (c) continued growth by diffusion or migration of oxygen and metal ions through oxide.4
Figure 2.	Schematic illustration of the kinetic rate equations representing metal oxidation.7
Figure 3.	Oxidation mechanisms represented by linear kinetics (a) surface reaction (b) parabolically growing oxide that periodically cracks and (c) weight gain versus time for (b).9
Figure 4.	Paralinear oxidation described by an inner, coherent layer that transforms to an outer, porous oxide at a linear rate resulting in a constant thickness inner layer.....9
Figure 5.	Rate-determining processes resulting in direct logarithmic kinetics (a) electron movement through potential energy barrier and (b) oxygen ion diffusion through mutually blocking pores.11
Figure 6.	Rate-determining step of inverse logarithmic kinetics described by the movement of ions under the influence of the electric potential gradient.....12
Figure 7.	Schematic of uranium/oxygen oxidation mechanism by oxygen adsorption, ionization, and oxygen anion diffusion through outer porous and inner protective layers to metal-oxide interface.....17
Figure 8.	Schematic of uranium/water vapor oxidation mechanism by (a) adsorption and dissociation of H_2O_v on oxide surface at oxygen interstitial sites, (b) diffusion of OH^- and O^- ion complexes through outer porous and inner coherent oxide layers and formation of fresh oxide and hydrogen ions at metal/oxide interface, and (c) migration of $\sim 85\%$ of the H^+ to oxide surface where it evolves as H_2 gas and remaining 15% reacts with metal to form UH_319

Figure 9.	Schematic of uranium/oxygenated water vapor oxidation described by adsorption mechanism and simultaneous reaction with O ₂ and H ₂ Ov. Three regions of behavior dependent on oxygen and water vapor pressures are (a) less than 10vppm oxygen content, uranium oxidizes at the anoxic water vapor rate since adsorption sites are available for attachment and dissociation of H ₂ Ov, (b) between 10-1000vppm O ₂ and <2-4%RH, a monolayer of chemisorbed O ²⁻ forms at the oxide/gas interface blocking direct adsorption of OH ⁻ on oxide surface, resulting in inhibited rate proportional to the water vapor pressure, and (c) between 2-90%RH, a monolayer of hydroxyl ions completely cover O ²⁻ layer resulting in reaction rate intermediate to dry air and anoxic water vapor rates, independent of both oxygen and water vapor pressure.	21
Figure 10.	The temperature dependence of oxygen solubility in water for pure oxygen and air atmospheres. A threshold concentration of 4wppm oxygen, inferred from the observed transition in rate behavior at 70°C, is depicted separating the regions of the uranium/anoxic (gray area) and uranium/oxic (white area) water reactions.	22
Figure 11.	Summary of Arrhenius expressions derived for uranium oxidation in oxygen at temperatures less than 300°C. The regression fits by Shell, Abrefah, Trimble, and this author were all based on data compiled in Pearce ¹⁵ and are essentially identical, overlaying each other.	24
Figure 12.	Reanalysis of Ritchie's ¹⁸ Arrhenius rate expression of the uranium/oxygen reaction.....	25
Figure 13.	Summary of Arrhenius expressions derived for uranium oxidation in water vapor with vapor pressure less than 101 kPa and temperatures less than 302°C.	30
Figure 14.	Reanalysis of Ritchie's ²⁵ Arrhenius rate expression of the uranium/anoxic water vapor reaction.....	31
Figure 15.	Summary of Arrhenius expressions derived for uranium oxidation in oxygenated water vapor at temperatures less than 302°C.	33
Figure 16.	Summary of Arrhenius expressions derived for uranium oxidation in anoxic water and temperatures less than 302°C. Regression fits by this author and Trimble and the expressions derived from Burkart and Troutner completely overlay one another.....	36
Figure 17.	Reanalysis of irradiation enhancement factor dependence on swelling at temperatures between 100 and 300°C (after Bennett, et al. ^{22, 24}).....	41

Figure 18.	Reaction rates of N-reactor SNF with oxygen and with water vapor along with the temperature dependencies of uranium metal reactions determined in this work	42
Figure 19.	Arrhenius dependencies of the uranium-hydride/oxygen reaction rate (Totemeier, et al. ⁸⁰) and uranium metal/oxygen reaction rate (this work).....	44
Figure 20.	Uranium-molybdenum phase diagram indicating equilibrium gamma phase at a minimum temperature of 550°C and 12 at.% molybdenum.....	46
Figure 21.	Uranium-niobium phase diagram indicating equilibrium gamma phase at a minimum temperature of 647°C and 13.3 at.% niobium.....	46
Figure 22.	Zirconium-Uranium phase diagram indicating equilibrium gamma phase at a minimum temperature of 615°C and 68 to 75 at.% zirconium.....	47
Figure 23.	Summary of uranium-molybdenum alloy/water reaction rate at temperatures between 100 and 440°C.....	51
Figure 24.	Summary of uranium-niobium alloy/water reaction rates at temperatures 100 to 343°C.....	52
Figure 25.	Summary of reaction rate of uranium-zirconium alloy with water and with oxygen at temperatures below 500°C.....	53
Figure 26.	Reaction rates of irradiated uranium-molybdenum and uranium-niobium alloys in water at temperatures between 100 and 400°C.....	56
Figure 27.	Typical microstructures of aluminum-based dispersion fuels irradiated to 80-90% burnup with Al matrix (light phase) and fuel dispersions (dark phase) of (a) UAl _x , (b) U ₃ Si ₂ , and (c) U ₃ O ₈ . ⁹⁶	59
Figure 28.	Phase diagram of the aluminum-uranium system.....	60
Figure 29.	Phase diagram of uranium-silicon system.....	61
Figure 30.	Summary of reaction rates of aluminum alloys (types 6061 and 8001) with water and saturated water vapor at temperatures between 30 and 360°C.....	63
Figure 31.	Summary of reaction rates of aluminum-based dispersions with uranium aluminide (equivalent to Al-1.9-53 wt%U alloys) and uranium-oxide with water and saturated water vapor at temperatures less than 360°C.....	64
Figure 32.	Summary of reaction rates of uranium-silicide intermetallic alloys and defected aluminum-based uranium silicide dispersion fuels with oxygen and water at temperatures below 550°C.....	68

- Figure 33. Summary of reaction rates of uranium metal, zirconium-uranium alloy and uranium silicide intermetallic with oxygen at temperatures less than 550°C.....73
- Figure 34. Summary of reaction rates of uranium metal, uranium alloys and aluminum-based dispersion fuels with water at temperatures less than 350°C.....74

LIST OF TABLES

Table 1.	DOE SNF groups used in the Total System Performance Assessment in FY 1999 ¹	2
Table 2.	Composition of fuel types reviewed in this report and the DOE SNF for which they are prototypical.....	3
Table 3.	Free energy of formation of some metal oxides relevant to DOE SNF.....	6
Table 4.	Conversion factors to metal loss units for uranium metal, alloys, and intermetallics reactions with oxygen, water vapor, and water.....	14
Table 5.	Summary of uranium/oxygen reaction rate expressions.....	28
Table 6.	Summary of uranium/anoxic water vapor reaction rate expressions.....	32
Table 7.	Summary of uranium/oxygenated water vapor reaction rate expressions at intermediate (2-90%RH) and 100%RH relative humidity.....	35
Table 8.	Summary of uranium/water reaction rate expressions at temperatures less than 350°C.	38
Table 9.	Summary of rates of reaction for uranium with oxygen, water vapor, oxygenated water vapor and water at temperatures less than 300°C.....	39
Table 10.	Nominal composition of N-Reactor fuel samples used in the corrosion study.....	41
Table 11.	Linear reaction rates of uranium-molybdenum alloys in humid air at 75°C and 50%RH (after Waber ⁶).....	49
Table 12.	Corrosion rates of non-irradiated and irradiated (gamma quenched) uranium alloys. ⁸⁷	55
Table 13.	Summary of rates of reaction for uranium-molybdenum, uranium-niobium and zirconium-uranium alloys with oxygen and water at temperatures less than 500°C.	57
Table 14.	Summary of rates of reaction of aluminum alloys, aluminum matrix uranium aluminide dispersions and uranium silicides with oxygen and water at temperatures less than 550°C.....	70
Table 15.	Summary of rates of reaction for uranium metal, uranium alloys and aluminum-based dispersion fuels with oxygen, water vapor, oxygenated water vapor, and water at temperatures less than 300°C.	72

ACRONYMS

ANL	Argonne National Laboratory
ANL-W	Argonne National Laboratory-West
ATR	Advanced Test Reactor
DOE	Department of Energy
EBR-II	Experimental Breeder Reactor II
EF	Enhancement Factor
FFTF	Fast Flux Test Facility
HFBR	High Flux Beam Reactor
HWCTR	Heavy Water Component Test Reactor
INEEL	Idaho National Engineering and Environmental Laboratory
LWBR	Light Water Breeder Reactor
MTHM	Metric Tons of Heavy Metal
PNNL	Pacific Northwest National Laboratory
ppm	Parts Per Million
PWR	Pressurized Water Reactor
RERTR	Reduced Enrichment of Research and Test Reactor
SNF	Spent Nuclear Fuel
SRS	Savannah River Site
TFA	Test Fuel Assembly
TRIGA	Training Research Isotopes General Atomic
XPS	X-ray Photoelectron Spectroscopy
XRD	X-Ray Diffraction

Review of Oxidation Rates of DOE Spent Nuclear Fuel
Part 1: Metallic Fuel

by

Bruce A. Hilton

ABSTRACT

The long-term performance of Department of Energy (DOE) spent nuclear fuel (SNF) in a mined geologic disposal system depends highly on fuel oxidation and subsequent radionuclide release. The oxidation rates of nuclear fuels are reviewed in this two-volume report to provide a baseline for comparison with release rate data and technical rationale for predicting general corrosion behavior of DOE SNF. The oxidation rates of nuclear fuels in the DOE SNF inventory were organized according to metallic, Part 1, and non-metallic, Part 2, spent nuclear fuels. This Part 1 of the report reviews the oxidation behavior of three fuel types prototypic of metallic fuel in the DOE SNF inventory: uranium metal, uranium alloys and aluminum-based dispersion fuels. The oxidation rates of these fuels were evaluated in oxygen, water vapor, and water. The water data were limited to pure water corrosion as this represents baseline corrosion kinetics. Since the oxidation processes and kinetics discussed in this report are limited to pure water, they are not directly applicable to corrosion rates of SNF in water chemistry that is significantly different (such as may occur in the repository). Linear kinetics adequately described the oxidation rates of metallic fuels in long-term corrosion. Temperature dependent oxidation rates were determined by linear regression analysis of the literature data. As expected the reaction rates of metallic fuels dramatically increase with temperature. The uranium metal and metal alloys have stronger temperature dependence than the aluminum dispersion fuels. The uranium metal/water reaction exhibited the highest oxidation rate of the metallic fuel types and environments that were reviewed. Consequently, the corrosion properties of all DOE SNF may be conservatively modeled as uranium metal, which is representative of spent N-Reactor fuel. The reaction rate in anoxic, saturated water vapor was essentially the same as the water reaction rate. The long-term intrinsic reaction rates of irradiated and unirradiated fuel were determined to be similar. The apparent reaction rate of irradiated metallic fuel increases as a function of swelling due to the increased surface area.

I. INTRODUCTION

The long term performance of the Department of Energy (DOE) spent nuclear fuel (SNF) in a mined geologic disposal system depends highly on the fuel oxidation, fuel dissolution, microstructure changes, and radionuclide partitioning within the fuel as related to fuel corrosion. Based on preliminary results, the radionuclide releases due to fuel oxidation and dissolution from any one of the DOE SNF fuel designs appears to be bounded by the N-reactor fuel design in the DOE SNF inventory. It has been proposed that the corrosion and dissolution properties of all DOE SNF will be conservatively modeled as DOE spent N-reactor fuel in the High Level Waste Repository performance assessment evaluation. The technical basis for this modeling approach is being evaluated by additional release rate testing of a number of prototypical DOE SNF compositions and by a comprehensive review of oxidation rate data published in the literature.

There is no simple correlation between corrosion rate data and release rate data. The corrosion rate is the rate at which a material physically degrades. It is based on the total amount of material reacted. The release rate is the rate that material is transported away from the sample. The release rate is related to the corrosion rate, but it depends on a number of other factors. Some of these factors include structural adherence of oxide, solubility, colloid formation and sequestration of radionuclides in alteration products. The oxidation rate data in this report are literature data that were limited to pure oxygen and water environments with low conductivity and negligible impurity levels. This represents baseline corrosion kinetics. (Since the corrosion of metals always occurs by an oxidation reaction and this report is limited to oxidation, the three terms, corrosion, oxidation, and reaction are used interchangeably in this report.) This review of literature data is intended only to provide a baseline for comparison with and to support the release rate testing data. The release rate test program may not generate sufficient data to describe comprehensively the corrosion of the fuel. It is impractical to perform release rate testing for every possible combination of fuel type and environmental condition. The oxidation rate expressions will be used for comparison with specific effect tests to identify parameter dependencies, like water chemistry differences in conductivity, pH, and specific ions.

This document is a two-volume compilation and analysis of reaction rate data published in peer-reviewed literature, technical reports, and in consultation with technical experts of specific nuclear fuel types. The two volumes address metals and non-metals. Part 1 reviews the oxidation rates of uranium metal, uranium alloys and aluminum-based dispersion fuels. Part 2 reviews the oxidation rates for the non-metal fuel groups: oxides, hydrides, carbides, and nitrides. The corrosion aspect of this review is limited to pure water corrosion; corrosion data for water chemistry expected in the repository environment were not available at the outset of this project. The report provides: (1) a comprehensive summary of DOE SNF oxidation and corrosion rates of reaction and oxidation mechanisms and (2) a report providing insight into commonalities of fuel types and technical rationale for predicting general corrosion behavior of DOE SNF in a permanent repository.

A. Background

1. Grouping

The DOE SNF inventory includes more than 200 fuel designs. That inventory has been grouped into 11 categories (shown in Table 1) for evaluating the corrosion and radionuclide release rate performance.¹ Group 1 was excluded from this report because the fuel will be addressed elsewhere. Part of the group 2 inventory consists of Na-bonded fuel and will require treatment to remove the Na metal and is also excluded from this report. For this report, the ten remaining categories were rearranged into seven fuel types with similar fuel matrices thus similar chemical compositions and oxidation behaviors (see Table 2). Fuel groups 4, 6, and 8 were condensed into an oxide fuel type. Fuel groups 3 and 5 were condensed into a carbide fuel type. The remainder fuel groups, due to their uniqueness, were placed under their own fuel types: fuel group 7 as U metal, fuel group 2 as uranium alloys, fuel group 9 as Al-based dispersion fuel, fuel group 11 as hydride fuels, and fuel group 10 as nitride fuels. Presenting the data as major fuel types summarizes DOE SNF reaction rates within similarly behaving fuels and facilitates discussions of performance differences among many fuel varieties.

The first major fuel group, uranium metal is treated as a separate group from alloys for two reasons: (1) for this study Uranium metal is considered the bounding fuel type because of its high chemical reactivity, and (2) Uranium metal is the major portion of the DOE SNF inventory in terms of metric tons of heavy metal (MTHM). Uranium alloys are the second group and are distinguished from the metal generally by improved corrosion resistance. The third group, the aluminum-based dispersion fuels, are used in research and test reactors. Dispersion fuels reaction rates are largely determined by the corrosion rate of the aluminum matrix material containing the dispersed fuel particles. The fourth group, oxide fuels, includes uranium oxide, thorium/uranium oxide, mixed plutonium-uranium oxide and others. The oxides are very stable and exhibit much slower reaction rates than uranium metal. The next three groups, hydrides, carbides and nitrides, are small but distinct families, justifying separate treatment. Typical fuel compositions of the seven fuel groups are discussed in the next section.

Table 1. DOE SNF groups used in the Total System Performance Assessment in FY 1999¹

Fuel Groups	Fuel Matrix
1	Classified
2	Pu/U alloy ^a
3	Pu/U carbide
4	MOX and Pu oxide
5	U/Th carbide
6	U/Th oxide
7	U metal
8	U oxide
9	Aluminum-based fuels
10	Unknown/miscellaneous
11	U-ZrH _x

^a Part of the Pu/U alloy inventory is Na-bonded fuel, and will require treatment to remove the Na metal.

2. Compositions and Fuel Types

The materials reviewed in this report correspond to the major fuel groups of the DOE SNF inventory. While each major fuel group contains SNF from a number of sources, generally one or two reactors or reactor types discharged most of the fuel from that group in the inventory, based on the mass of heavy metal. The composition of the major fuel groups and subgroups reviewed in this report and the corresponding DOE SNF for which they are prototypical are compiled in Table 2. Generally, the composition of the fuel subgroups for which reaction rates have been reviewed bounds the composition of the most significant DOE SNF type. This was the case for the uranium metals, alloys and aluminum-based dispersion fuels.

Table 2. Composition of fuel types reviewed in this report and the DOE SNF for which they are prototypical.

Fuel Types	SNF Subgroup	DOE SNF Group	Composition of Subgroups	Representative SNF	Nominal Composition of Representative SNF
U Metal	U Metal	7	U Metal	N-Reactor Fuel	
Uranium Alloys		2			
	U-Mo		U-<8 wt% Mo	Fermi Blanket	U-3 wt% Mo
			U->8 wt% Mo	Fermi Driver	U-10 wt% Mo
	U-Zr		U->20 wt% Zr	SRS HWCTR	U-90.7 wt% Zr
Al-Based Dispersion Fuels		9			
	UAl _x		U-Al (1.8-53 wt%)	ATR	UAl ₃
	U _x Si _y		U->3.8 wt%Si	Research Reactors	U ₃ Si ₂
	U ₃ O ₈ -Al			HFBR	9.4 wt% U ₃ O ₈ , 90.6% Al
Oxide Fuels					
	UO ₂	8		Shippingport PWR	UO ₂
	(U, Th)O ₂	6		Shippingport LWBR	3% UO ₂ , 97% ThO ₂
	MOX	4		FFTF Driver	≈20 wt% PuO ₂
Hydride Fuels	U-ZrH _x	11	U-ZrH _{1.0-1.7}	Standard TRIGA	U-ZrH _{1.6}
Carbide Fuels					
	(U, Th)C ₂	5	(U, Th)C ₂ , ThC ₂	Ft. St. Vrain; Peachbottom	4% UC ₂ , 96% ThC ₂ ; 16% UC ₂ , 84% ThC ₂
	Pu/U Carbide	3		FFTF-TFA	
Nitride Fuels	U Nitride	10	U ₃ N ₄	FFTF	

B. Fundamentals of Oxidation and Corrosion

The fundamentals of corrosion are briefly defined in this section, along with the concepts of reaction mechanisms and kinetics that pertain to nuclear fuel materials. A discussion of the thermodynamic characteristics is followed by an explanation of kinetic expressions commonly used in oxidation modeling, including possible processes the expressions represent. For an expanded discussion of these principles, the interested reader is referred to a number of excellent texts (Scully, Uhlig, Evans, and Kofstad^{2,3,4,5}). Finally, the measurement techniques employed in oxidation studies are summarized and conversion factors for translating the data to units of mass of metal loss per unit surface area per unit time are compiled.

Metal oxidation occurs when metal reacts with another atom or molecule and loses electrons. In an oxidation reaction electrons transfer from one species to another. The species losing electrons is oxidized and the species gaining electrons is reduced.

The net oxidation reaction of a metal with oxygen, O_2 , is the sum of two separate reactions occurring simultaneously. For the case of a metal, Me, with valence, z, reacting with oxygen, O_2 , the reactions are

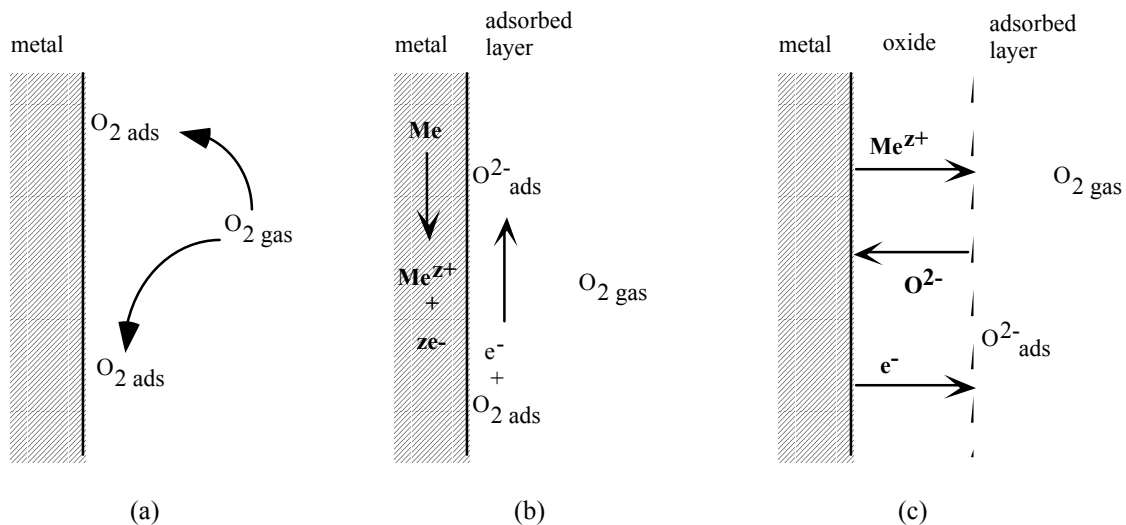
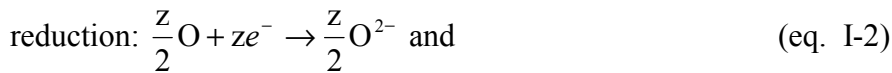


Figure 1. Schematic representation of metals oxidation: (a) adsorption of oxygen molecules, (b) dissociation of adsorbed oxygen molecule, and (c) continued growth by diffusion or migration of oxygen and metal ions through oxide.

The oxidation process is shown schematically in Figure 1. First, the oxidizing molecules (e.g., oxygen or water) are adsorbed, attached to the surface of the metal (a). Next, the adsorbed molecules dissociate and are ionized (b). The charge is delivered from electrons liberated by the metal lattice as it forms metal ions. Across this layer of adsorbed oxygen ions and metal ions there is a potential difference of around one volt. For very thin films, less than 10 Å, this creates a very strong electric field that drives ion migration and growth of the oxide film. The oxide film can also grow by diffusion since a concentration gradient is established. The concentration of metal ions will be greatest near the metal-oxide interface where they originate and the concentration of oxygen or hydroxyl ions will be greatest near the oxide-gas interface. Metal cations (positive ions) combine with the oxygen or hydroxyl anions (negative ions) to form oxide. Subsequent oxygen or water molecules adsorption occurs on the oxide surface, followed by dissociation and ionization. The oxygen ions, metal ions or both move through the oxide to combine with the other species and form more oxide. As the oxide film grows, the strength of the electric field decreases rapidly becoming negligible at a thickness of approximately 10-40 Å. The driving force of the concentration gradient also decreases with thickness. As the oxide grows, a stress develops in the oxide due to the different sizes of the oxide and metal structures. The stress is proportional to the volume ratio of the oxide/metal, which is commonly referred to as the Pilling Bedworth ratio for their original work on this topic. The size mismatch results in a compressive stress or a tensile stress depending on whether the volume ratio is greater or less than 1, respectively. Initially, a compressive stress helps the oxide adhere and provide a protective film. Eventually, the stress will increase as the oxide film grows until it causes fracture and a porous, nonprotective layer. As long as the oxide remains adherent and protective, the oxidation rate decreases with time and eventually becomes very small. When the oxide is porous or cracks due to high stress, open pathways allow movement of the oxidizing species and the oxidation rate tends to reach a constant value.

1. Thermodynamics

The Gibb's free energy, G , is a thermodynamic function that indicates the spontaneity of a reaction and the most stable reaction product. The change in free energy that is calculated for a reaction is equal to the work done or absorbed during the process. If the reaction performs work (i.e., the change in free energy is negative) it can occur spontaneously, furthermore the reaction that performs the most work, i.e., has the largest negative free energy, will be the most favored. Examples of the free energy of formation for uranium and other metal oxides relevant to DOE SNF are presented in Table 3. The free energy of all the oxides listed are negative, which is typical of metals and indicates the spontaneity of metal oxidation. Theoretically, based on thermodynamic considerations alone, a metal should spontaneously react with oxygen or water (an oxidant) to form metal oxide and should continue to react until the metal is totally consumed. However, in practice metals exposed to an oxidizing environment may not exhibit this behavior, which illustrates the importance of kinetic parameters in addition to thermodynamic considerations in predicting the outcome of oxidation reactions. Uranium oxidation is one example of this. Of uranium oxides, U_3O_8 has the largest negative free energy of the uranium oxides and consequently is the most stable. While U_3O_8 is the most stable uranium oxide, UO_2 is the reaction product reported in most oxidation studies under 300°C, due to the reaction kinetics.

Table 3. Free energy of formation of some metal oxides relevant to DOE SNF.

Oxide	$\Delta G_f(298.15)$, kJ/mol
Al ₂ O ₃	-1582.3
MoO ₂	-533.0
SiO ₂	-856.3
ZrO ₂	-1042.8
UO ₂	-1031.8
UO ₃	-1145.7
U ₃ O ₇	-3242.9
U ₃ O ₈	-3369.5

2. Kinetics and Reaction Processes

The rate of reaction is explained by two theories, collision theory and transition state theory. In collision theory, the reacting particles (i.e., atoms, ions, molecules) are constantly colliding with each other at a frequency much higher than can be accounted for by the actual reaction rate. Most collisions do not result in a reaction because the particles do not have enough energy for the collision to be effective. In transition state theory the reactants and reaction products are separated by a transition state that has a higher potential energy than either the reactants or reaction products. In order for the reaction to proceed, the reactants must absorb this difference in energy between the transition state and their unreacted state, termed activation energy, Q , of the reaction. The activation energy can be attained by sufficiently high temperature, by the electric potential gradient, or the concentration gradient in an oxide. The reactions generally have different activation energies, thereby allowing determination of the mechanism. Activation energy analysis is discussed in the context of the temperature dependence (cf. Section 1.2.3). The oxidation mechanisms can also be understood by the kinetics of the reaction rate.

Kinetics deals with the time dependence or rate of reactions and is usually described in terms of a mathematical relationship found between the oxide thickness (equivalent to weight gain or metal loss) and time. In this report, the reaction rates are reported in terms of metal loss per unit surface area, which is most applicable to radionuclide release rate calculations. Conversion factors from weight gain units to metal loss units for the fuel groups in this report are presented at the end of this section. The oxidation rate is usually normalized by surface area since the reaction rate is proportional to the surface area. Likewise if there is another known parameter dependence (e.g., the one-fifth power of oxygen pressure at low oxygen pressures, or the square root of the water vapor pressure for the uranium/water vapor reaction) the reaction rate is reported on a unit basis normalized by the parameter. In the case of water vapor, the reaction rate will be reported in units of metal loss rate per surface area per square root of the vapor pressure (mg metal/cm²/h/kPa^{0.5}).

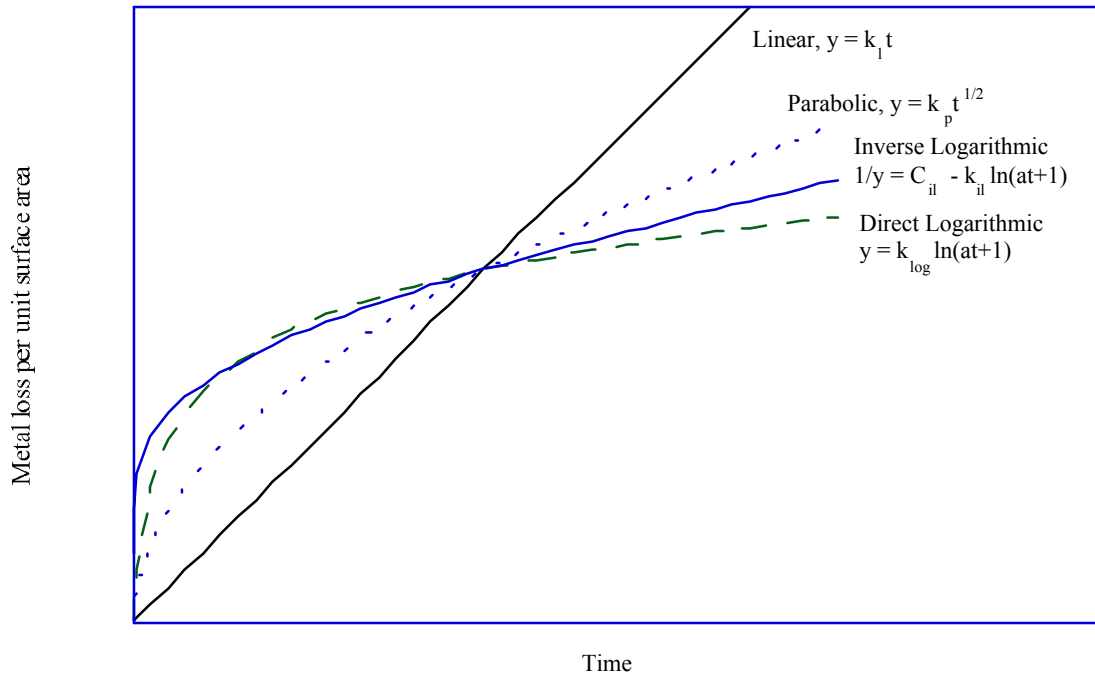


Figure 2. Schematic illustration of the kinetic rate equations representing metal oxidation.

The mathematical expressions typically used to model oxidation kinetics are linear, parabolic, paralogarithmic, direct logarithmic, and inverse logarithmic (see Figure 2). The time dependence of each of these kinetic expressions represents different rate-determining oxidation steps. A general power-law expression is used to identify the most appropriate kinetic expression for modeling the data. The power-based expression is written as

$$y = kt^n \tag{eq. I-4}$$

or in logarithmic forms as

$$\ln y = \ln k + n \ln t \tag{eq. I-5}$$

where y is the metal loss per unit surface area, k is the reaction rate, and n is the exponent indicative of the kinetic model. For example, an exponent equal to one indicates linear kinetics, 0.5 indicates parabolic kinetics and an intermediate value might indicate logarithmic or paralogarithmic kinetics. The logarithmic form of the power-law expression (eq. I-5) is useful in visually distinguishing between logarithmic and paralogarithmic behavior since the latter will exhibit a definite change in slope from 0.5 at short times to unity at longer times. To facilitate discussions of data reviewed in this report, each of the kinetic oxidation expressions is defined and their associated mechanisms are summarized.

Linear

In linear kinetics the reaction rate remains constant with time and is described as

$$y = k_l t + C_l . \quad (\text{eq. I-6})$$

For true linear kinetics the intercept constant, C_l , is zero. Linear kinetics is often indicative of a rate determining surface or interface reaction or process (see Figure 3a). For example, the limiting surface or interface reaction may involve the adsorption of oxidant on the surface or the conversion of metal to oxide at the metal-oxide interface. Alternatively, linear behavior may result from a series of parabolic growth segments (Figure 3c). In this mechanism the oxide film grows to critical thickness by parabolic oxidation, whereupon the oxide can crack or spall to reveal bare metal again. Such cyclic oxidation and spallation of the product can result in pseudolinear kinetics. Linear kinetics can also be explained as a coherent oxide layer of constant thickness as in the case of paralineer kinetics, described below.

In addition to these mechanisms represented by linear kinetics, metal oxidation by more complex kinetic mechanisms can be suitably approximated at long times by linear kinetics (see Figure 2). In using linear kinetics to approximate non-linear kinetics (which initially have a large initial oxide growth), the total metal loss can be predicted by including a non-zero intercept constant in the linear kinetics expression.

Parabolic

Parabolic kinetics generally describes metal oxidation at higher temperatures. The rate of oxide growth is initially rapid, but decreases with time as the oxide film thickens. The form of the equation is

$$y = k_p t^{1/2} . \quad (\text{eq. I-7})$$

The parabolic time dependence usually implies that the reaction is limited by a thermal diffusion or charged particle migration process. The driving force is a concentration or electric potential gradient for diffusion and migration, respectively. The oxidizing species diffuse or migrate from the oxide-reactant interface to the metal-oxide interface, as the oxide grows. In both diffusion and migration the rate is inversely proportional to the thickness, hence the reaction rate (i.e., the amount of metal reacting per unit time) decreases with time as the oxide film grows.

Paralinear

In some metals the rate-determining oxidation mechanism changes over time. One situation is paralinear kinetics, which is a combination of parabolic and linear oxidation. Initially, oxidation proceeds by a parabolic process, then eventually changes to a linear process. The mathematical expression is written as

$$y = k_l t + k_p t^{1/2} \quad (\text{eq. I-8})$$

Paralinear oxidation involves an inner coherent layer that transforms at a linear rate into an outer, porous and nonprotective layer (see Figure 4). In this mechanism, the oxidizing species easily penetrate the outer porous layer, at a rate determined by diffusion through the inner oxide layer to the metal-oxide interface. At long times, the rate is essentially linear since the inner layer remains at constant thickness, growing at the same rate that it transforms into the outer porous layer.

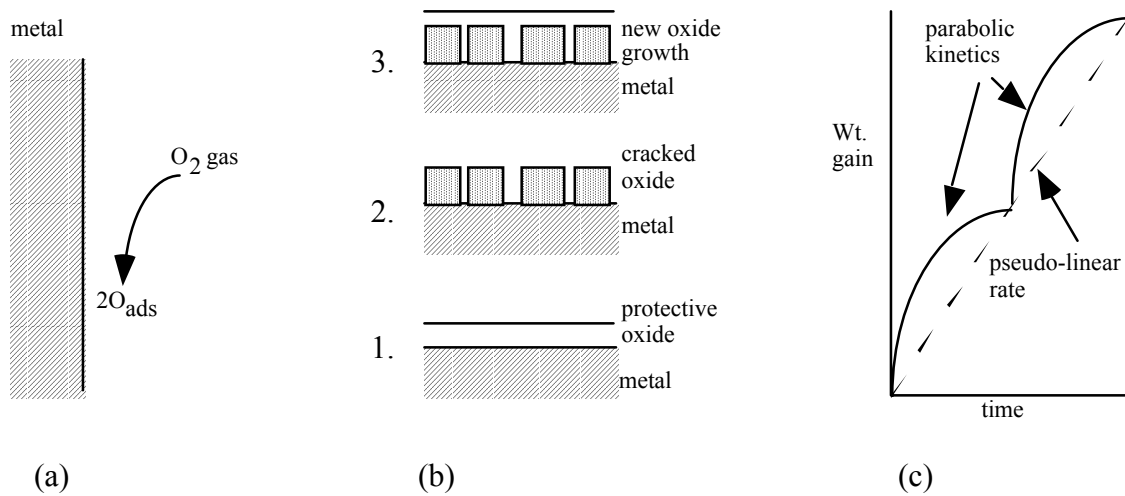


Figure 3. Oxidation mechanisms represented by linear kinetics (a) surface reaction (b) parabolically growing oxide that periodically cracks and (c) weight gain versus time for (b).

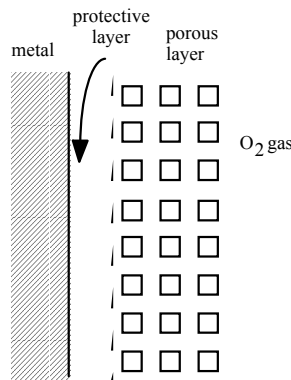


Figure 4. Paralinear oxidation described by an inner, coherent layer that transforms to an outer, porous oxide at a linear rate resulting in a constant thickness inner layer.

Direct and Inverse Logarithmic

Logarithmic kinetics is generally used to describe oxidation at low temperatures. The oxidation reaction rate begins rapidly, but quickly drops off to low or negligible values. The time dependence of the direct logarithmic oxidation is expressed as

$$y = k_{\log} \log_e (at + t_o) . \quad (\text{eq. I-9})$$

Direct logarithmic kinetics represents a rate determining mechanism controlled by (1) electronic transport as opposed to ionic transport or (2) ion movement through mutually-blocking pores (see Figure 5).

The inverse logarithmic kinetics describes oxide growth limited by the migration of ions under an electric potential gradient (see Figure 6). Time dependence of inverse logarithmic kinetics is given as

$$1/y = C_{il} - k_{il} \log(at + t_o) . \quad (\text{eq. I-10})$$

This correlation is valid at low temperatures where the ions do not have enough thermal energy to pass beyond the potential barrier and move under influence of the electric potential gradient that exists across the oxide film.

3. Temperature Dependence

The metal oxidation reaction rate is limited by the movement of particles (e.g., atoms, ions, or electrons), whether the driving force is diffusion, migration or some other mechanism. The movement of particles can be described as discrete jumps from one position of low potential energy to another adjacent position of low potential energy. In between the adjacent positions of low energy is a transition state with a high potential energy, and the particle will only be able to jump from one to the other if it acquires a minimum energy equal to the potential energy of the transition state, which is a characteristic of the oxidation mechanism. The number of particles, N , that will have a certain minimum energy, E_{\min} , is given by the exponential function of E_{\min} divided by the absolute temperature, T , and the gas constant, R ,

$$N \propto \exp \left[\frac{-E_{\min}}{RT} \right] . \quad (\text{eq. I-11})$$

Since the reaction rate constant, k , is limited by the number of particles that can move, N , then k will have the corresponding energy and temperature dependence as in eq. I-11. This dependency for a macroscopic reaction system is valid only if a single mechanism is rate-determining and independent of temperature over the temperature range of interest.

Arrhenius Expression

In the case of a single rate-determining step, the logarithm of reaction rate, $\log k$, is directly proportional to the inverse temperature, $1/T$, wherein the constant of proportionality is related to the activation energy, Q , of the reaction. The temperature dependence of oxidation rates of reaction is given by the empirical Arrhenius expression,

$$k = k_0 \exp\left[\frac{-Q}{RT}\right], \quad (\text{eq. I-12})$$

where Q is the activation energy given in kJ/mol , R is the gas constant equal to 8.314 J/mol/K and T is the absolute temperature in K . In an Arrhenius plot of $\log k$ versus $1/T$, the slope of the straight line equals Q/R , where Q equals the activation energy of the reaction. The pre-exponential factor, k_0 , is found to be independent of temperature. The values for k_0 and Q for a specific reaction can be determined empirically from an Arrhenius plot of the data (as $\log k$ versus $1/T$), wherein the slope of the plot equals $-Q/R$ and the unit intercept equals $\log k_0$.

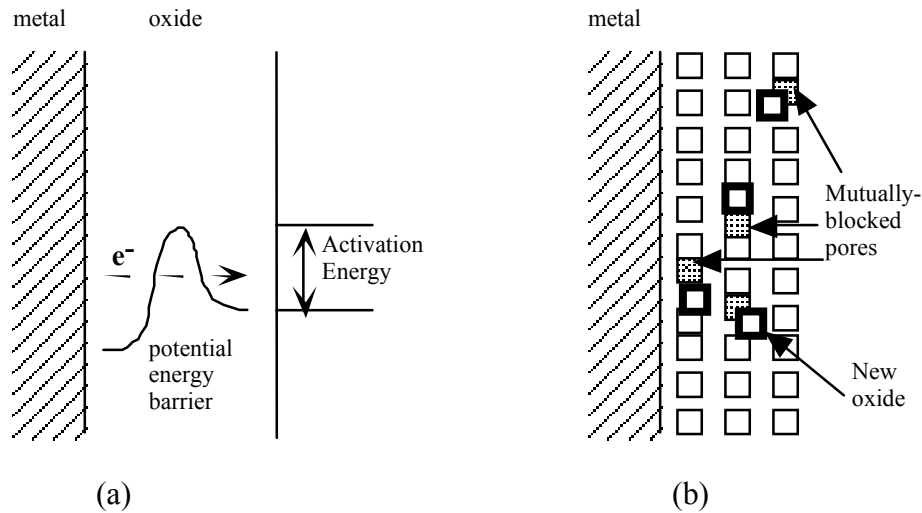


Figure 5. Rate-determining processes resulting in direct logarithmic kinetics (a) electron movement through potential energy barrier and (b) oxygen ion diffusion through mutually blocking pores.

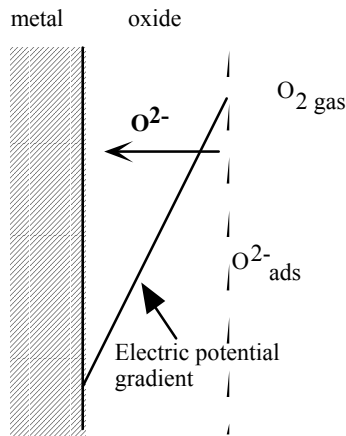


Figure 6. Rate-determining step of inverse logarithmic kinetics described by the movement of ions under the influence of the electric potential gradient.

Activation Energy

In terms of reaction rate theory, Q is related to the free-energy barrier between the initial state and the final state. In this interpretation, the activation energy of the oxidation reaction rate may correlate to physical properties of metals and oxides depending on the rate-determining mechanism. For example in parabolic oxidation, the rate-limiting step is the diffusion or transport of ions through the oxide layer.

Generally speaking, the activation energy is independent of temperature, unless temperature changes induce a change in mechanism. Specifically, activation energy is a constant in the Arrhenius function that is independent of temperature, a steady slope that describes the correlation of the dependent to the independent variables. Therefore, a change in mechanism can be identified by a change in slope of an Arrhenius plot. Comparisons of the slopes on an Arrhenius plot of rate expressions for different environments can also indicate whether mechanisms are similar.

C. Measurement and Analysis Techniques

1. Reaction Rate Measurements

During oxidation, the material gains weight as long as the oxide film remains attached to the material surface. While there is a weight gain due to the reacted oxidant (e.g., oxygen or water), there is a material loss due to the conversion of metal (or oxidizable compound) to the metal-oxide. As oxide gain and metal loss are both aspects of the oxidation process, reaction rates are generally quantified as weight gain or metal loss, depending on the investigators' methods. Additionally, the reaction rate may be determined by measuring a secondary reaction product such as hydrogen gas in the water oxidation reaction. In this report the reaction rates are given in units of metal loss.

Weight Gain

The most straightforward technique for determining reaction rates is measuring the weight gain. For metal oxidation, weight gain is the mass of oxygen that has reacted with the metal during oxidation. Weight gain is measured ex situ by periodic weighing and in situ by thermogravimetry. Periodic weighing requires halting the test and removing the sample from the experiment chamber, which introduces some variability into the data. In tests with water vapor or immersion there is an added factor of uncertainty due to the possibility of adsorbed moisture on the samples or to the drying step that removes this moisture. Thermogravimetry is a very sensitive technique that measures small weight changes via an electromechanical response. Care must be taken to eliminate errors due to convection currents, buoyancy forces, vibrations, and temperature gradients in the reaction chamber. Both weight gain techniques are also susceptible to errors caused by oxide spalling. Generally, thermogravimetry is sensitive enough that a sharp weight loss, typical of spalling, can be identified and taken into account. While measuring weight gain data is the most straightforward technique, it does not, by itself, provide information on the amount of metal reacted. The amount of metal reacted can be derived from weight gain measurements only indirectly with knowledge of the composition of the end reaction product.

Metal Loss

The metal loss rate (i.e., rate of metal oxidized whether pure U or U-X in the case of uranium alloys) of uranium in different environments is determined by removing the oxide scale from a sample and measuring the mass difference between the descaled sample and the original sample. Most of the data reported from 1950 to 1960 for corrosion in water are in units of metal loss or weight loss. Typically, the oxide was dissolved using a nitric acid rinse, since nitric acid attacks the oxide but only slowly reacts with uranium metal. A tightly adhering oxide layer often remained after the nitric acid rinse. If the acid was reacted with the sample for longer time, it was possible that the acid rinse also removed some metal. While reaction rate data reported in metal loss units require no conversion factor, there is uncertainty introduced by the dissolution step due to the likelihood of either leaving a thin layer of oxide or removing an unquantified amount of underlying metal.

Hydrogen Gas Generation or Oxygen Gas Depletion

In reactions of metal with water vapor or water, hydrogen is generated. The amount of hydrogen gas evolved during the oxidation reaction can be quantified to derive the amount of metal reacted. The difficulty of this technique is that not all the hydrogen generated in the reaction combines to form hydrogen gas.

A technique involving oxygen gas depletion in a closed system can quantify oxidation rates. A high sensitivity manometer has been used for studying oxidation at low temperatures or initial growth. The disadvantage of the system is the limited oxidant volume for conducting tests, which essentially precludes using the application in long-term studies or at high temperatures.

2. Reaction Product Characterization

A variety of techniques have been used in the corrosion kinetics research for characterizing the chemistry, structure, and source of the reaction products. The composition and

structure have been investigated via x-ray diffraction (XRD) and electron diffraction. The microstructure has been characterized by metallography and electron microscopy. Identification of the reacting species has been provided by isotope tracer techniques and x-ray photoelectron spectroscopy (XPS).

3. Unit Conversion Factors

A review of reaction rates covering data published during the last fifty years encounters a range of experiment techniques. Consequently, oxidation of uranium metal, its alloys, and aluminum-based dispersion fuels are reported in many units. In this report, the data are presented in a single set of units allowing comparison of reaction rates reported in the same conditions by different investigators and comparison of reaction rates in different media. The units are expressed as mass of metal loss per unit surface area per unit time. Conversion factors used for the uranium, uranium alloys and the aluminum-based dispersion fuels are shown in Table 4. Conversions for uranium metal are straightforward because the reaction product is well characterized. Stoichiometric UO_2 is the assumed product in all environments. This assumption results in a small overestimation of metal loss in dry air/oxygen and water vapor environments, where the oxide is slightly hyperstoichiometric with nominal compositions of $\text{UO}_{2.08}$ and $\text{UO}_{2.2}$, respectively. Much of the water corrosion data for the uranium alloys is originally reported as metal loss, requiring no unit conversion. A conversion factor for the zirconium/oxygen reaction rate data was derived from the oxide composition given in the original publications. Conversion factors for the aluminum matrix-uranium aluminum dispersions and uranium intermetallics reaction rates are based on oxide compositions reported in the original papers or other literature. Conversion factors for the aluminum matrix-uranium silicide dispersion fuels reaction rate were derived using the following simplifying assumptions: (a) the aluminum matrix and dispersed fuel oxidized independently of each other, (b) the net oxide composition was the surface area weighted average of the aluminum oxide and uranium-silicide oxide compositions, and (c) the surface area fractions of matrix and dispersed fuel were equal to the respective volume fractions.

Table 4. Conversion factors to metal loss units for uranium metal, alloys, and intermetallics reactions with oxygen, water vapor, and water.

Reaction	Reaction Product ^a	Original Units	Conversion Factor to mg metal/cm ² /h
U/O ₂ , U/H ₂ Ov, U/O-H ₂ Ov, U/H ₂ O	UO ₂	mg wt gain/cm ² /h	7.44
U-Zr/O ₂	40.8%U-37.6%Zr-21.6%O	mg wt gain/cm ² /h	3.63
U-Al/O ₂ , U-Al/H ₂ O	Al ₂ O ₃ •H ₂ O	mg wt gain/cm ² /h	0.818
Al/O ₂ , Al/H ₂ O	Al ₂ O ₃ •H ₂ O	mg wt gain/cm ² /h	0.818
U-Si/O ₂ , U-Si/H ₂ O	79%U-4%Si-16%O	mg wt gain/cm ² /h	5.25
UH ₃ /O ₂ , UH ₃ /H ₂ O	UO ₂	mg wt gain/cm ² /h	8.21

^a Reaction product represented by chemical formula or weight fraction. Actual phases may differ from chemical formula.

4. Software

In preparing this report, the following computer software were used:

Word Processing

- Microsoft Word and Excel from Macintosh Microsoft Office 98 by Microsoft
- Microsoft Word and Excel from Personal Computer Microsoft Office 98 by Microsoft

Technical Drawings and Graphics

- Canvas Macintosh Version 3.5 by Deneba Software
- KaleidaGraph Macintosh Version 3.0 by Abelbeck Software

Linear Regression Analyses

Linear regression analyses were performed with a standard curve fitting routine of the KaleidaGraph application.

II. OXIDATION RATES OF URANIUM METAL

Uranium metal oxidation has been investigated for more than five decades by researchers from countries throughout the world. Interest in this topic spans research communities in weapons development, reactor fuel development, and repository disposal with a motivation to understand behavior during process operations, interim fuel storage and long term repository disposition. The United States and United Kingdom completed a great portion of research in efforts to store safely uranium metal produced in their weapons programs. Uranium metal oxidation forms non-protective oxides that are generally described by linear kinetics. The rate data in the literature exhibit a large scatter (i.e., two orders of magnitude) which highlights the difficulties inherent in determining reaction kinetics and the variability due to experiment methods, sample microstructure, and oxidation conditions.

This chapter reviews the reaction rates of uranium metal with oxygen, anoxic and oxygenated water vapor and water. The first section is an overview of the reaction steps of U-metal oxidation in the various environments. Next, the kinetics and temperature dependencies of uranium oxidation in the above environments are reviewed. Arrhenius-type expressions reported in the literature are reanalyzed and compared with Arrhenius expressions developed by regression analyses of data published up to 1999. The strengths and weaknesses of the various Arrhenius expressions are discussed; and later summarized at the end of each subsection. Two sections address topics that relate the reaction rates of unirradiated uranium to the DOE inventory of spent nuclear uranium fuel. One section discusses the general effects of irradiation on uranium metal oxidation kinetics and one addresses the effects of uranium hydride in light of uranium hydride reaction rates reported in recent work. The conclusions and recommended rate expressions for uranium metal oxidation in the different environments are summarized in the last section.

A. Mechanisms of Uranium Metal Oxidation

Uranium oxidation process has been studied for many years, but a good understanding of the mechanisms has only been obtained fairly recently and is not conclusive under all environments.^{6, 7, 8, 9} Research in this area is still ongoing as reflected by recent publications.^{10, 11, 12} The kinetics, pressure dependence, and activation energy behavior offer insights into the uranium oxidation mechanisms, as do micro chemistry and materials observations using isotopic tracer analysis, x-ray photoelectron spectroscopy (XPS), and electron microscopy. Descriptions of the oxidation process in various environments (i.e., oxygen, water vapor, oxygenated water vapor and water) are presented in this section. The reacting species and rate determining steps are discussed, as far as data are available. Unresolved issues are identified in parallel with the major proposed hypotheses. Kinetics is discussed only as it relates to mechanistic understanding; a review of reaction kinetics is presented in a separate section.

1. Uranium/Oxygen Reaction

Uranium reacting with oxygen at temperatures less than 300°C results in a black, tightly adherent oxide that eventually spalls off. The reaction product is hyperstoichiometric dioxide (UO_{2+x}) with x generally accepted as between 0.06 and 0.1.^{9, 13, 14, 15} While some previous work^{16, 17} and reviews^{7, 18} reported values of x between 0.2 and 0.4, the data are considered systematically high due to further oxidation during measurement. The chemical reaction can be written as



The oxidation rate has a weak oxygen pressure dependence ($p^{0.2-0.3}$) up to 5.3 kPa and is independent of oxygen content above this pressure. Oxidation occurs by diffusion of oxygen anions, O^{2-} .^{9, 19} Oxygen ions enter the oxide at the oxide-gas interface and move towards the metal-oxide interface where they react with metal to form new oxide. The oxygen ions move by an interstitialcy mechanism concluded from the pressure dependence⁹ and the activation energy of ~ 70 kJ/mol²⁰. The initial reaction rate follows parabolic kinetics;^{9, 15, 21} however, the long term oxidation of uranium with an existing ‘mature’ oxide layer is generally treated as linear kinetics^{9, 18, 22, 23, 24} and is so treated in this review.

Initially in the reaction, the parabolic term is dominant due to the formation of a thin adherent, diffusion-limiting oxide layer. As the reaction proceeds and the film thickness increases, the tensile stresses cause the outer portion of the film to fracture and limit the thickness of the adherent portion to approximately 1 micron. Therefore, at longer times, the linear component dominates, accounting for greater total oxidation. The change to linear kinetics occurs when the oxide thickness exceeds a critical value, forming an outer fractured layer of increasing thickness and maintaining an adherent inner layer of constant thickness (see Figure 7).

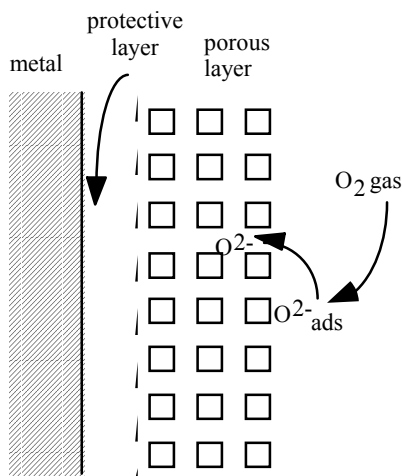


Figure 7. Schematic of uranium/oxygen oxidation mechanism by oxygen adsorption, ionization, and oxygen anion diffusion through outer porous and inner protective layers to metal-oxide interface.

2. Uranium/Water Vapor Reaction

The uranium/water vapor reaction proceeds at a much higher rate than uranium oxidation in oxygen. Many investigators have studied the uranium/water vapor reaction in a range of conditions from moist inert gas to moist air to saturated steam. The uranium oxidation in water vapor mechanism is extensively reviewed by Colmenares⁹ and also by Ritchie,²⁵ Orman,⁷ and Pearce¹⁵. The kinetics and mechanism of the reaction are dependent on the water vapor and oxygen pressures in the environment. Therefore, the water vapor reaction mechanisms for anoxic (no oxygen) and oxygenated conditions are discussed separately.

Anoxic Water Vapor

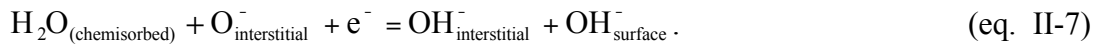
Uranium oxidation in anoxic water vapor occurs at a much higher rate than in dry air. The reaction at temperatures up to 350°C produces a porous, non-adherent oxide. A laminar structure is generally observed^{26, 27, 28}; however a highly porous cellular structure that formed on extruded bar samples has also been reported.²⁷ The difference in metal microstructures of the foil and bar samples was suggested as a possible explanation for the porous oxide structures. The oxide laminae, approximately 0.1 μm thick, grow and crack under stresses induced by the oxide/metal volume mismatch and eventually spall in sheets of approximately 1 μm thickness.²⁶ The reaction product is UO_{2+x} with x between 0.13 and 0.20, which is slightly more hyperstoichiometric than the U/O_2 reaction product. The chemical reaction of uranium oxidation in water vapor can be written as



Some researchers also report evidence of hydride formation, and explain it as an intermediate product according to the reactions^{7, 14, 29, 30}



The reaction kinetics of eq. II-2 is linear for temperatures up to 300°C.¹⁵ At pressure less than 101 kPa, which is the range for most of the data, the water vapor reaction rate varies as the square root of the pressure ($p^{0.5}$).^{14, 26, 31, 32, 33, 34} Trimble reviewed the scant data at higher pressures³⁵ and proposed a linear pressure dependence ($p^{1.0}$) for pressure above 101 kPa. Reanalysis of that work by this author demonstrates that a square root dependence was also valid considering the variability of the data. The linear reaction kinetics implies a rate independent of total oxide thickness similar to the dry air reaction, in which the gross oxide structure consists of an outer porous layer increasing in thickness and an inner coherent layer of constant thickness that moves into the metal at a constant rate. Water molecules are adsorbed on the metal (clean) or oxide surface and dissociate to hydroxyl, OH^- , and hydrogen, H^+ , ions. Colmenares proposed dissociation of chemisorbed water at oxygen lattice or interstitial sites since these reactions are exothermic and energetically favorable to other reactions (see Figure 8),



The reacting species are the singly charged ions OH^- and O^- rather than the doubly charged oxygen ion, O^{2-} , in the case of oxygen gas oxidation. The OH^- and O^- diffuse through the oxide film in ion complexes, most probably by an interstitialcy mechanism, and produce UO_2 and H^+ at the oxide-metal interface. Most of the hydrogen ions diffuse through the oxide to recombine at the oxide surface and evolve hydrogen gas, H_2 , but the net hydrogen generated is less than the stoichiometric amount derived from measurements of the metal reacted. The discrepancy between hydrogen gas evolved and the total hydrogen produced from corrosion is approximately 15%, the difference partly due to uranium hydride formation.

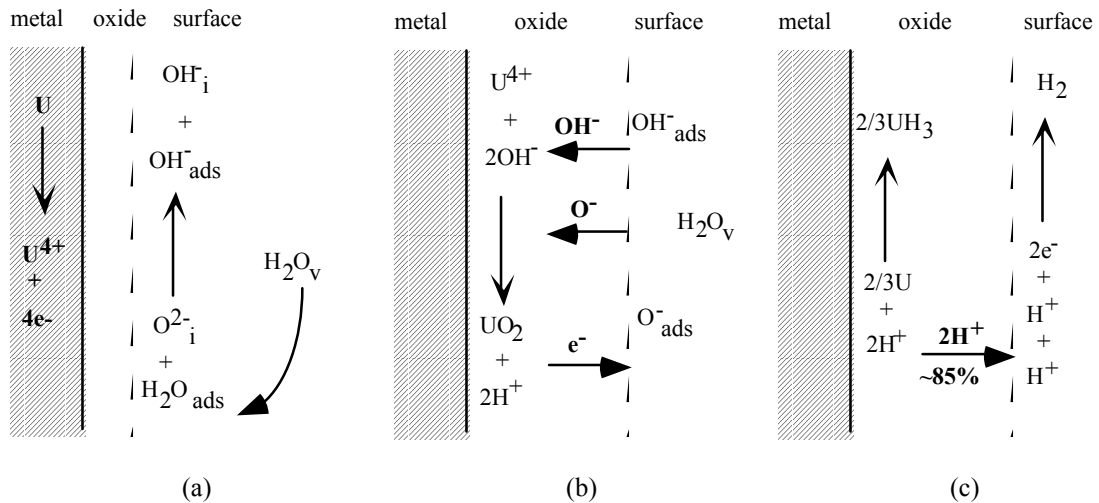


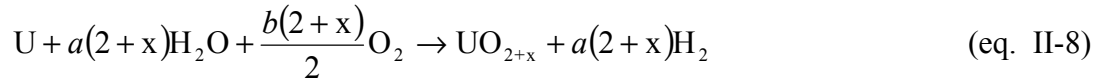
Figure 8. Schematic of uranium/water vapor oxidation mechanism by (a) adsorption and dissociation of H_2O_v on oxide surface at oxygen interstitial sites, (b) diffusion of OH^- and O^- ion complexes through outer porous and inner coherent oxide layers and formation of fresh oxide and hydrogen ions at metal/oxide interface, and (c) migration of $\sim 85\%$ of the H^+ to oxide surface where it evolves as H_2 gas and remaining 15% reacts with metal to form UH_3 .

Oxygenated Water Vapor

The rates for the uranium/oxygenated water vapor reaction fall between the reaction rates of uranium with oxygen and uranium with anoxic water vapor. The reaction kinetics is linear for temperatures up to $300^\circ C$. The reaction product is hyperstoichiometric (x is between 0.17 and 0.24), having slightly more oxygen than the anoxic water vapor reaction product.^{9, 26} The reaction product also has a slightly different morphology of coherent plates/layers that spall when approximately $1\mu m$ thick.^{9, 14} The reaction rate is a complex function of water vapor and oxygen pressure. In oxygen environments (e.g., air) with small amounts of moisture, the reaction rate increases rapidly with increased water vapor up to approximately 2 to 4% relative humidity (%RH).^{10, 14, 16, 18, 32} In moist inert gas atmospheres at temperatures up to $325^\circ C$, small amounts of oxygen between 10 and 1000vppm decrease the uranium oxidation kinetics by a factor of approximately 10 to 15.^{9, 14} At intermediate O_2 and H_2O pressures, the reaction rate is essentially independent of oxygen content and water vapor pressure,^{10, 32, 36} although some researchers report a very weak water vapor pressure dependence ($p^{-0.2}$).^{9, 14, 26}

The roles of oxygen and water vapor in the oxidation process have been investigated for many years using isotope tracer studies and surface analysis techniques. Based on these studies, some researchers have proposed that U/O- H_2O oxidation occurs via a single source of oxidant, such as only water vapor^{37, 38} or only oxygen.^{9, 34, 39} However McGillivray et al.¹⁰ have

convincingly shown that both water vapor and oxygen react simultaneously with U metal to form oxide. The general chemical reaction of U/O-H₂O_v can be written as



where *a* and *b* are the fractional contributions of oxidant in the oxide from water vapor and oxygen, respectively. At temperatures of ~80 to 90°C, oxygen from the water vapor constitutes ~70 to 75% of the oxide, while approximately 25 to 30% is contributed from oxygen in the atmosphere.¹⁰ The reacting species are probably O²⁻, from the oxygen, and OH⁻, from the water, which diffuse through the oxide and react with the metal, forming the oxide at the metal/oxide interface as discussed above for reactions with the separate atmospheres. The U/O-H₂O reaction is reasonably described by a Langmuir type adsorption mechanism,^{10, 18, 40} where the reaction rate increases proportionately to the H₂O surface coverage up to complete coverage when the rate is constant (see Figure 9). While the specific mechanism by which oxygen inhibits the anoxic water vapor reaction remains to be determined, the overall oxidation process is well understood and can be summarized in the following salient features.

- Oxygen from the oxygen gas and from the water vapor, probably as O²⁻ and OH⁻, respectively, react simultaneously with the uranium metal.
- Oxygen adsorption, dissociation, diffusion, and reaction are unaffected by H₂O addition.
- Oxygen above a threshold concentration of 10 to 1000 vppm inhibits the anoxic water vapor reaction. Two proposed mechanisms that describe this effect are (a) a chemisorbed layer of oxygen ions at the oxide/gas interface that limits direct access of OH⁻ and (b) the mass flux of slower moving O²⁻ impedes the diffusion of the OH⁻ through the oxide, since O²⁻ and OH⁻ are both transported by an interstitialcy mechanism.
- The reaction rate becomes independent of oxygen pressure and water vapor pressure when the reacting surface is completely covered by the respective species.

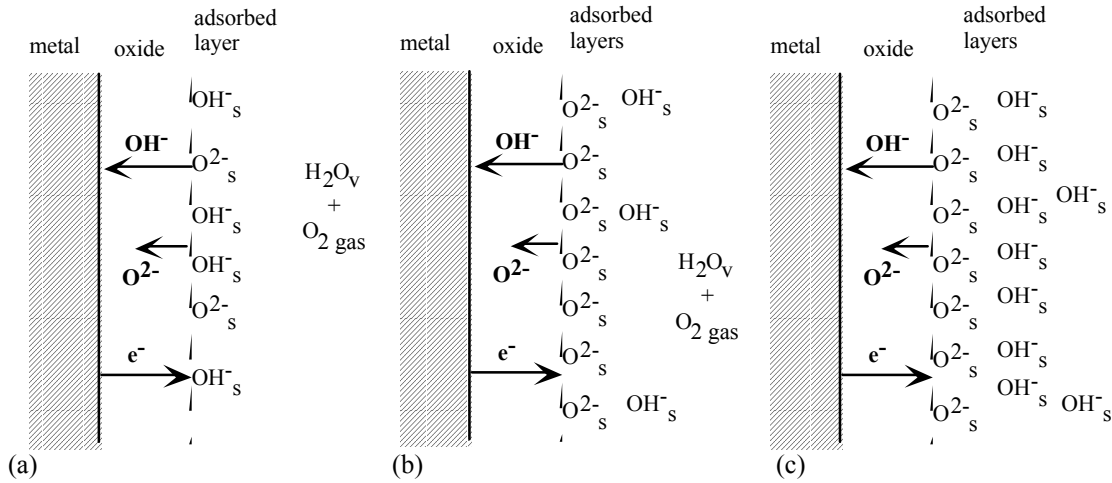
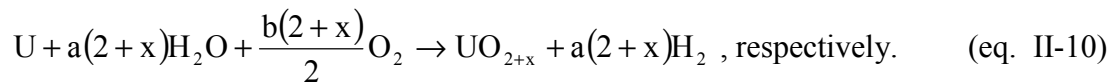
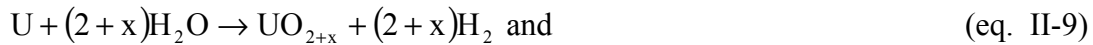


Figure 9. Schematic of uranium/oxygenated water vapor oxidation described by adsorption mechanism and simultaneous reaction with O_2 and H_2O_v . Three regions of behavior dependent on oxygen and water vapor pressures are (a) less than 10vppm oxygen content, uranium oxidizes at the anoxic water vapor rate since adsorption sites are available for attachment and dissociation of H_2O_v , (b) between 10-1000vppm O_2 and <2-4%RH, a monolayer of chemisorbed O^{2-} forms at the oxide/gas interface blocking direct adsorption of OH^- on oxide surface, resulting in inhibited rate proportional to the water vapor pressure, and (c) between 2-90%RH, a monolayer of hydroxyl ions completely cover O^{2-} layer resulting in reaction rate intermediate to dry air and anoxic water vapor rates, independent of both oxygen and water vapor pressure.

3. Uranium/Water Reaction

Uranium corrosion in immersed water obeys linear kinetics at temperatures below $300^\circ C$ and proceeds at a rate similar to the water vapor reaction at saturation pressure. Due to the rate similarity, the same mechanism probably controls water immersion oxidation as well as water vapor oxidation. The chemical reactions for uranium oxidation by anoxic and oxygenated water immersion are the same as for water vapor,



The reaction product UO_{2+x} is almost stoichiometric with x less than 0.1. The hydrogen evolved as gas is typically 70 to 95% of stoichiometric. The discrepancy, though not completely understood, is partially explained as uranium hydride formation.^{30, 41}

The effect of oxygen on the U/H_2O reaction is a function of temperature and time. At temperatures less than $70^\circ C$, oxygen has a strong inhibiting effect on the initial corrosion rates of

uranium with water.^{41, 42, 43} After 42 hours in 70°C aerated water (i.e., reaction vessel was continuously sparged with air for the 1800-hour test), the reaction rate is forty times less than the anoxic water rate. However after 1200 to 1800 hours the oxidic water reaction rate is essentially the same as the anoxic rate.^{42, 43} At lower temperatures, the time to reach the anoxic reaction rate increases. The transition between oxygenated and anoxic behavior at 70°C in water can be likened to the transition observed in water vapor reaction rates at a threshold oxygen concentration of 10 to 1000 vppm in the vapor phase. The solubility of oxygen in water is a strong function of temperature, which decreases by a factor of two between 25°C and 70°C (see Fig. 10). The dissolved oxygen content of 4 wppm in air-saturated water at 70°C is a threshold oxygen concentration that delineates the oxidic/anoxic reaction transition in liquid phase water. The similar threshold concentrations of 4 wppm oxygen in oxidic immersion and the 10 to 1000 vppm, in water vapor phase support the hypothesis that the same mechanism determines uranium oxidation in water and in water vapor. While the oxygen dependence of the U/H₂O reaction at initial times can be rationalized, more research is necessary to understand the low temperature transition occurring at long times from U/O-H₂O rates to anoxic water rates.

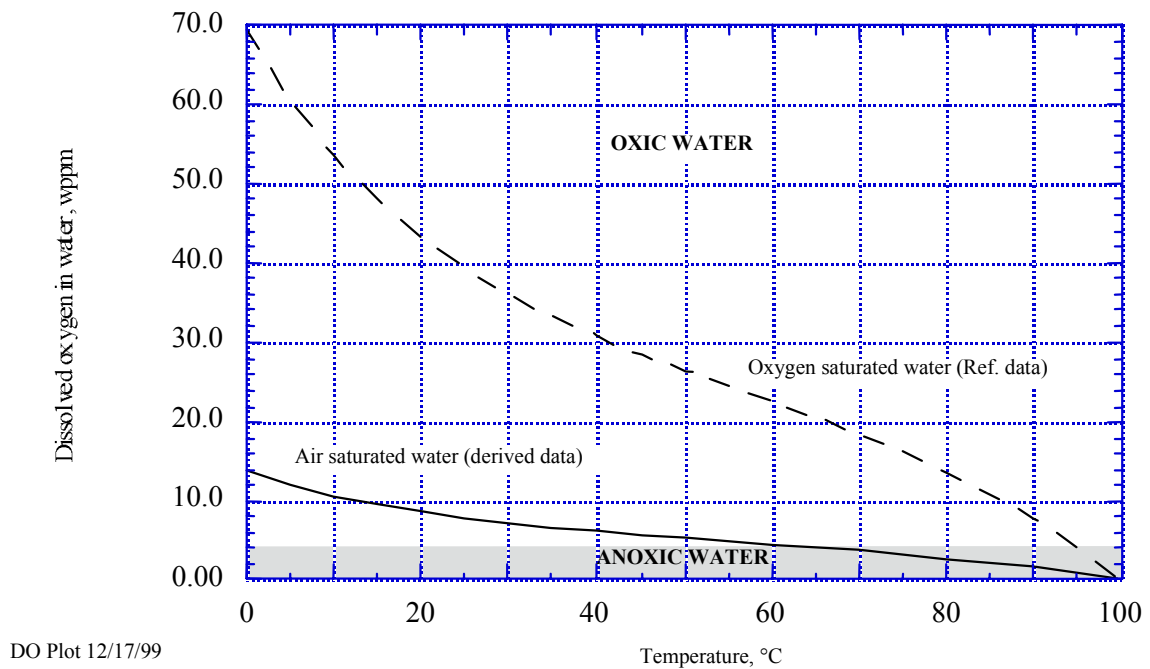


Figure 10. The temperature dependence of oxygen solubility in water for pure oxygen and air atmospheres. A threshold concentration of 4wppm oxygen, inferred from the observed transition in rate behavior at 70°C, is depicted separating the regions of the uranium/anoxic (gray area) and uranium/oxidic (white area) water reactions.

B. Kinetics of Uranium Metal Oxidation

1. Uranium/Oxygen Reaction

Many investigators have reviewed the kinetics and mechanism of uranium oxidation in oxygen and dry air atmosphere over a span of fifty years.^{7, 8, 9, 15, 18, 30, 36, 41, 44, 45} The work was motivated by the need to understand the corrosion behavior of uranium stockpiles in the weapons programs during interim storage.^{15, 18, 30, 36, 46} Researchers in the United States, United Kingdom and Canada contributed over a hundred papers on the subject. The data cover temperatures from 25°C to above the melting temperature in atmospheres ranging from parts per million (ppm) levels to pure oxygen. Data collection, over many years, employed a wide variety of test techniques, some less sophisticated than others. Oxidation kinetics have been determined (a) by rudimentary discreet mass measurements resulting in net weight gain or weight loss after dissolving away the oxide, (b) by sensitive gas pressure measurements to detect the amount of oxygen reacted, and (c) by in situ weight gain measurements using modern thermogravimetric analysis (TGA) instruments. These widely varying techniques are partly responsible for the one to two orders of magnitude scatter in the data. Other factors contributing to variability were inherent sample differences due to impurity levels, variations in surface finishes, and the low magnitude of the reaction rate, particularly at temperatures below 100°C. In spite of the large propensity for differences, there is broad consensus on the magnitude and temperature dependence of the reaction rate of unirradiated uranium metal with oxygen. The reaction rate is small compared with the rate of water-driven corrosion and is a strong function of temperature. However, the irradiated uranium reaction rate at low levels of irradiation has not been conclusively determined. While there are relatively few data, the irradiation effects have been related to irradiation-induced swelling and are thus small to negligible at low burnup. (This subject is detailed in a separate section.)

The uranium in oxygen reaction rate is a strong function of temperature that is best expressed in an Arrhenius form. This review evaluated and reanalyzed prominent Arrhenius expressions and their supporting data reported by Pearce,¹⁵ Colmenares,⁹ Ritchie,¹⁸ Trimble,⁴⁷ Shell,⁴⁸ and Abrefah.⁴⁶ A revised Arrhenius expression determined by linear regression analysis of literature data is compared with the above reported Arrhenius expressions and presented in Figure 11. A discussion of each follows.

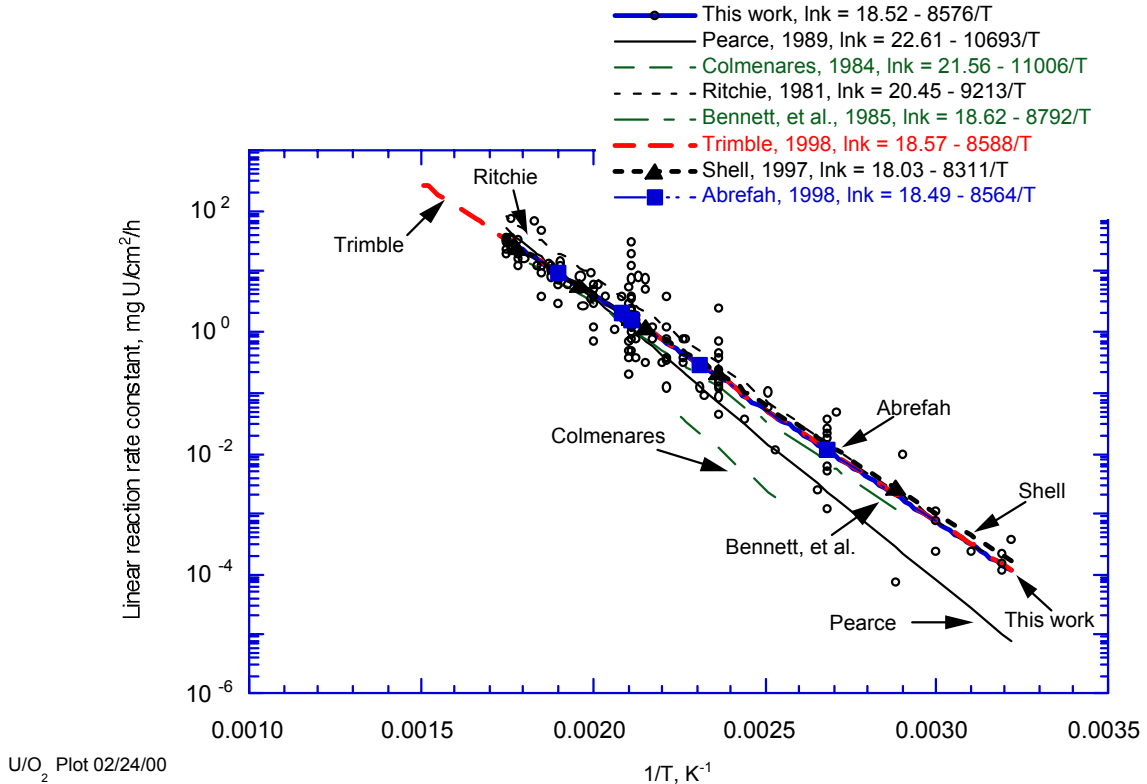


Figure 11. Summary of Arrhenius expressions derived for uranium oxidation in oxygen at temperatures less than 300°C. The regression fits by Shell, Abrefah, Trimble, and this author were all based on data compiled in Pearce¹⁵ and are essentially identical, overlaying each other.

Ritchie reviewed the uranium with oxygen reaction rate data reported before 1981 for the temperature range 40 to 300°C. He reported a temperature dependence of the reaction rate, based on linear kinetics,¹⁸

$$k_l = 7.59 \times 10^8 \exp\left[\frac{-76.6 \text{ kJ/mol}}{RT}\right] \text{ mg U/cm}^2/\text{h.} \quad (\text{eq. II-11})$$

The data cited by Ritchie^{17, 30, 49, 50, 51, 52, 53} were reanalyzed in this review in an effort to qualify his expression. Figure 12 depicts the data cited in Ritchie's review, Ritchie's recommended expression, and the corresponding linear regression fits generated in this review for all the data without outliers and all the data excluding Bennett (Bennett's data was excluded in an attempt to replicate Ritchie's fit). While Ritchie's expression provides a "reasonable fit" to the data, Ritchie's expression was not equal to the temperature dependence determined by regression analyses of the data. Therefore, it appears to be an approximate visual fit rather than a true regression fit.

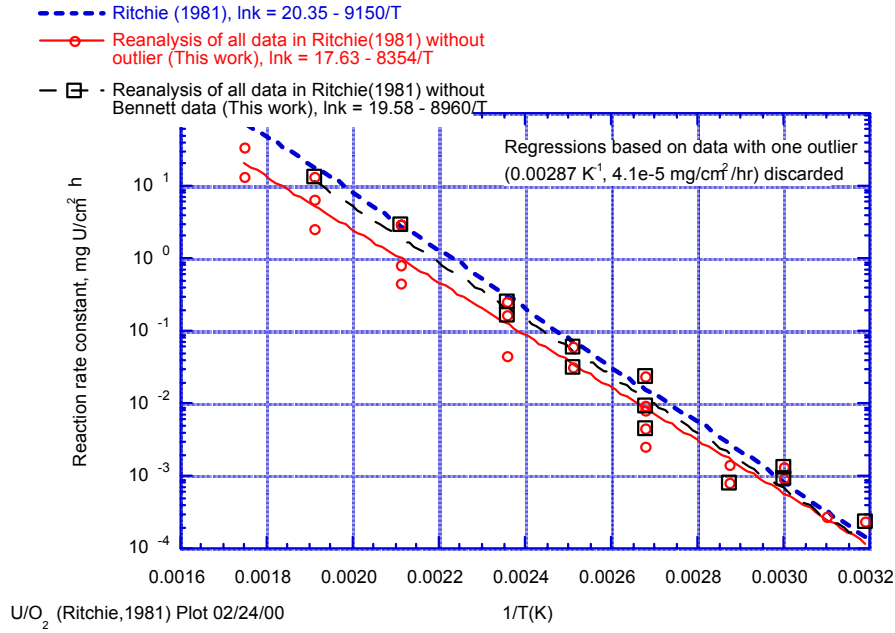


Figure 12. Reanalysis of Ritchie's¹⁸ Arrhenius rate expression of the uranium/oxygen reaction.

Bennett and co-workers studied the oxidation of uranium in dry air in the temperature range 50-300°C.²² They reviewed the reaction rate data in the literature and modeled the temperature dependence according to linear kinetics. The Arrhenius expression they proposed was based on linear kinetics and was originally published by Bennett, et al.²² Pearce and Abrefah referred to this expression as representative of uranium/oxygen reaction rates.

$$k_l = 1.21 \times 10^8 \exp\left[\frac{-73.1 \text{ kJ/mol}}{RT}\right] \text{ mg U/cm}^2/\text{h.} \quad (\text{eq. II-12})$$

Colmenares fit his data to parabolic kinetics and derived the temperature dependence from rate data in the temperature range 117–177°C. The parabolic and linear reaction rate constants he derived were⁹

$$k_p = 2.31 \times 10^4 \exp\left[\frac{-42.4 \pm 2.5 \text{ kJ/mol}}{RT}\right] \text{ mg U/cm}^2/\text{h}^{1/2} \text{ and} \quad (\text{eq. II-13})$$

$$k_l = 2.31 \times 10^9 \exp\left[\frac{-91.5 \pm 4.5 \text{ kJ/mol}}{RT}\right] \text{ mg U/cm}^2/\text{h.} \quad (\text{eq. II-14})$$

Colmenares also fit his data to a power law expression, which was very nearly linear⁹

$$\Delta w/A = kt^{0.8} + 1.4 \text{ mg U/cm}^2 \text{ where} \quad (\text{eq. II-15})$$

$$k = 3.25 \times 10^7 \exp\left[\frac{-70.9 \pm 2.4 \text{ kJ/mol}}{RT}\right] \text{ mg U/cm}^2/\text{h.} \quad (\text{eq. II-16})$$

The nearly linear dependence of the regression fit, as indicated by the exponent of 0.8 in eq. II-14, demonstrates the predominance of the linear component in the rate expression. The linear dependence further illustrates that reaction rates of uranium with oxygen for long reaction times can be modeled by linear kinetics.

Pearce reviewed the data up to 1989 for oxidation of uranium in oxygen and modeled the reaction rate according to parabolic kinetics. Although he reviewed the world body of literature, Pearce recommended Arrhenius expressions for the parabolic and linear reaction rate constants based solely on his own data.¹⁴ All the literature data were plotted on summary figures, but the data were not used to determine the recommended Arrhenius relations. Pearce recommended the reaction rate constants¹⁵

$$k_p = 5.25 \times 10^3 \exp\left[\frac{-36.8 \text{ kJ/mol}}{RT}\right] \text{ mg U/cm}^2/\text{h}^{1/2} \text{ and} \quad (\text{eq. II-17})$$

$$k_l = 6.58 \times 10^9 \exp\left[\frac{-88.9 \text{ kJ/mol}}{RT}\right] \text{ mg U/cm}^2/\text{h.} \quad (\text{eq. II-18})$$

The Arrhenius dependencies of Pearce's recommended reaction rates on temperature were very similar to the values reported by Colmenares, eqs. II-12 and II-13 above, whose derivation was also based on parabolic kinetics. However, the linear reaction rate varied significantly from the linear rate expressions derived for linear kinetics (eqs. II-10 and II-11). Since Pearce did not include a 'best fit' based on regression analysis, a number of researchers have subsequently done this based on the data he compiled.

Shell and Ballinger, at the Massachusetts Institute of Technology, performed a regression analysis of the linear reaction rate data compiled (but not analyzed) by Pearce.⁴⁸ The data were extracted indirectly from the summary plot in Pearce's report. Shell's Arrhenius expression for uranium oxidation in oxygen in the temperature range 38 to 300°C was⁴⁸

$$k_l = 6.76 \times 10^7 \exp\left[\frac{-69.1 \text{ kJ/mol}}{RT}\right] \text{ mg U/cm}^2/\text{h.} \quad (\text{eq. II-19})$$

The coefficient and activation energy of Shell's Arrhenius expression, based on linear kinetics, were very different than the linear rate expression Pearce reported (eq. II-17), which was derived from parilinear kinetics. However, the regression fit was similar to the regression fit Bennett, et al. reported (eq. II-11).

Trimble also performed a statistical analysis of the data reported in Pearce's review.⁴⁷ As many of the references cited by Pearce were unavailable, Trimble extracted the data indirectly from the summary plot in Pearce's report.⁵⁴ This indirect extraction contributed some variability to their analysis, especially due to the logarithm scale used in the plot. Trimble determined that the regression fit of the linear reaction rate constant in the temperature range 38 to 450°C was⁴⁷

$$k_l = 1.16 \times 10^8 \exp\left[\frac{-71.4 \text{ kJ/mol}}{RT}\right] \text{ mg U/cm}^2/\text{h.} \quad (\text{eq. II-20})$$

Trimble's expression had essentially the same activation energy determined by Shell's regression analysis (eq. II-18), but the magnitude was double. The difference between these expressions (i.e., a factor of two) was attributed to the different temperature ranges fit by the authors and to the variability introduced by extracting data from the summary plot in Pearce.

Abrefah, et al., reported a regression fit to Pearce's data in the temperature range 69 to 275°C

$$k_l = 1.07 \times 10^8 \exp\left[\frac{-71.2 \text{ kJ/mol}}{RT}\right] \text{ mg U/cm}^2/\text{h.} \quad (\text{eq. II-21})$$

Abrefah's expression was essentially equivalent to Trimble's regression fit and was almost certainly derived from the data extracted by Trimble. The small difference between the three regression fits, eqs. II-18, II-19, and, II-20, was attributed to differences in the data analyzed, differences in the temperature range, and data extraction variability.

The Arrhenius expressions derived by regression analysis of data compiled by Pearce (eqs. II-18, II-19, and II-20) were significantly different from the linear reaction rate constant Pearce recommended, eq. II-17. This highlights the fact that the expression Pearce recommended was derived solely from his own data rather than from all the data compiled in the review report. Moreover, eq. II-17 was based on parilinear kinetics rather than linear kinetics. The different kinetic models and different data sets explain the differences between eq. II-17 and the regression fits to data compiled by Pearce (eqs. II-18, II-19, and, II-20). The regression fits, eqs. II-18, II-19, and II-20, derived by regression analysis of data up to 1989 (i.e., compiled by Pearce¹⁵) were very similar to the regression fit of data up to 1985 compiled by Bennett et al., eq. 2-11, demonstrating a strong general consensus of uranium/oxygen reaction rates at temperatures up to 300°C, as summarized in Table 5.

The various analyses of the air oxidation kinetics data have produced a number of Arrhenius expressions, with the most recent in reasonably close agreement. In order to clarify the available information on air oxidation kinetics and to summarize this review, this author

reviewed and reanalyzed the available data in Pearce's report. That reanalysis produced an Arrhenius expression that was virtually identical to the other regression analyses results. The determined temperature dependence of the reaction rate of uranium oxidation in oxygen for the temperature range 38 to 300°C was

$$k_l = 1.09 \times 10^8 \exp\left[\frac{-71.3 \pm 2.1 \text{ kJ/mol}}{RT}\right] \text{ mg U/cm}^2/\text{h.} \quad (\text{eq. II-22})$$

In summary, uranium oxidation in dry air obeys linear kinetics at long times. The reaction rate has a strong temperature dependence with an energy of activation of ~70 kJ/mol (i.e., the rate increases five orders of magnitude over the temperature range 40 to 300°C). Shell, Trimble, Abrefah, and this author derived essentially equivalent Arrhenius rate expressions based on regression analysis of the literature data. Consequently, any one of these expressions, as summarized in Table 5, can represent uranium/oxygen reaction rates at temperatures less than 300°C. For traceability and completeness, this author's rate expression was recommended.

Table 5. Summary of uranium/oxygen reaction rate expressions.

Eq. No.	Rate Expression	Conditions	Reference
2-10	Linear: $k_l = 7.95 \times 10^8 \exp[-76.6/RT]$	40-300°C	Ritchie ¹⁸
2-11	Linear: $k_l = 1.21 \times 10^8 \exp[-73.1/RT]$	50-300°C	Bennett, et al. ²²
2-12	Paralinear: $k_p = 2.31 \times 10^4 \exp[-42.4/RT]$	117-177°C	Colmenares ⁹
2-13	$k_l = 2.31 \times 10^9 \exp[-91.5/RT]$		
2-15	Power law: $\Delta w/A = kt^{0.8} + 1.4$ $k_l = 3.25 \times 10^7 \exp[-70.9/RT]$	117-177°C	Colmenares ⁹
2-16	Paralinear: $k_p = 5.25 \times 10^3 \exp[-36.8/RT]$	38-300°C	Pearce ¹⁵
2-17	$k_l = 6.58 \times 10^9 \exp[-88.9/RT]$		
2-18	Linear: $k_l = 6.76 \times 10^7 \exp[-69.1/RT]$	38-300°C	Shell ⁴⁸
2-19	Linear: $k_l = 1.16 \times 10^8 \exp[-71.4/RT]$	38-450°C	Trimble & Welsh ⁴⁷
2-20	Linear: $k_l = 1.07 \times 10^8 \exp[-71.2/RT]$	69-275°C	Abrefah, et al. ⁴⁶
2-21	Linear: $k_l = 1.09 \times 10^8 \exp[-71.3 \pm 2.1/RT]$	38-300°C	This work

2. Uranium/Water Vapor Reaction

The oxidation reaction rate of uranium with water vapor is significantly higher than the reaction rate of uranium with dry air or oxygen gas. The oxidation reaction rate is a weak though complex function of the water vapor pressure and the amount of oxygen in the system; however, in anoxic conditions it varies simply according to the square root of the vapor pressure ($p^{0.5}$). In dry air and at low levels of moisture, the uranium/water vapor reaction rate increases rapidly with increasing water vapor pressure up to 5 kPa. In moist inert gas environments, the reaction rate is very sensitive to oxygen content and decreases rapidly and sigmoidally with increasing oxygen content, saturating at ~1000 vppm oxygen.⁹ This sensitivity to low oxygen levels indicates the importance of leak tight systems for accurately determining the kinetics of the uranium/anoxic water vapor reaction and may explain the high variability in reported rates. In environments intermediate in oxygen and water vapor content, the reaction rate is generally considered independent of both oxygen and water vapor pressure.

Anoxic and oxygenated water vapor reaction rates are treated separately in this review due to their different dependencies. The review of uranium/oxygenated water vapor kinetics was limited to intermediate atmospheres since the reaction rates for the transition regions (i.e., dry air to oxygenated water vapor and anoxic to oxygenated water vapor) were considered beyond the scope of this report.

Anoxic Water Vapor

There are a number of reviews of uranium oxidation in water vapor.^{9, 15, 18, 25, 30, 36, 45} The effect of small traces of oxygen (e.g., between 10 and 1000 vppm at 100°C) were significant, resulting in diminished rates similar to moist air. Hence oxygenated water vapor oxidation was treated in a separate section. The effects of inert gas on the reaction rate of water vapor oxidation were negligible.^{9, 14, 30, 55} In this report, data obtained in pure water vapor environments and water vapor in inert gas environments were not differentiated.

The oxidation of uranium in anoxic water vapor is much more aggressive than dry air oxidation. Due to its square root dependence on the water vapor pressure ($p^{0.5}$), the reaction rates were normalized by this parameter so that the units of uranium reaction rates with water vapor were mg U/cm²/h/kPa^{0.5}. The reaction rate is a strong function of temperature similar to that of dry air and has been expressed in an Arrhenius form by a number of workers. Several of the prominent Arrhenius expressions and the supporting data were reanalyzed and the conclusions are discussed in this section. A revised Arrhenius expression determined by linear regression analysis of literature data is presented and compared to the Arrhenius expressions reported in the literature. The temperature dependencies reported by Pearce¹⁵, Pearce and Kay,¹⁴ Ritchie²¹ and Trimble³⁵ are specifically discussed. Figure 13 displays the reaction rate expressions published in the literature and the revised Arrhenius dependence of all the data determined in this work by regression analysis.

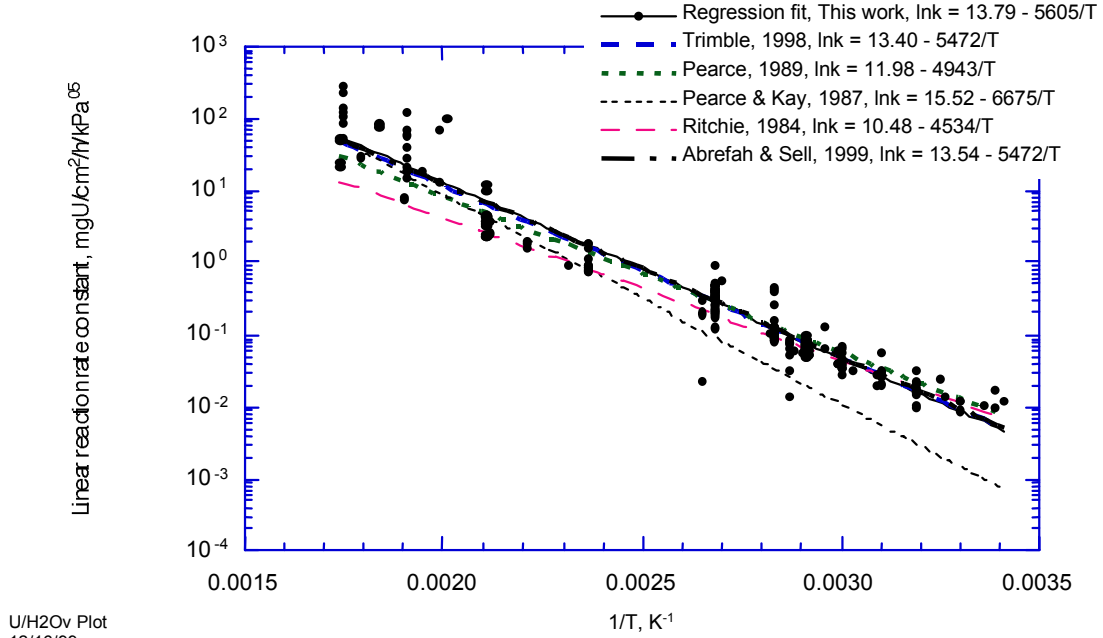


Figure 13. Summary of Arrhenius expressions derived for uranium oxidation in water vapor with vapor pressure less than 101 kPa and temperatures less than 302°C.

Ritchie published in 1984²⁵ some uranium oxidation rates derived from available literature data. Using revised refractive indices for uranium and uranium dioxide, Ritchie recalculated the uranium/water vapor oxidation rates reported by Grimes and Morris⁵⁶, which were obtained by interferometry. He plotted the reanalyzed data with other literature data and reported a “good fit” to the results as²¹

$$k_1/p^{0.5} = 3.56 \times 10^4 \exp\left[\frac{-37.7 \text{ kJ/mol}}{RT}\right] \text{ mg U/cm}^2/\text{h/kPa}^{0.5}. \quad (\text{eq. II-23})$$

This correlation, recommended by Ritchie for all the data he compiled, was essentially equivalent to the temperature dependent reaction rate of the reanalyzed Grimes and Morris’ data. All the data that Ritchie reviewed^{28, 30, 56, 57, 58, 59} were reanalyzed by this author using linear regression methods. Figure 14 shows the Arrhenius expressions recommended by Ritchie (eq. II-22), derived solely from the Grimes and Morris’ data that he reanalyzed,²⁵ and recently derived by a regression analysis of all the data by this author. Ritchie’s recommended expression was not equal to the Arrhenius expression determined by linear regression analysis of all the data and was apparently based only on the data he reanalyzed from Grimes and Morris and not on all the literature data that he reviewed.

Pearce and Kay derived the temperature dependence of uranium oxidation in water vapor from their experiments results as¹⁴

$$k_1/p^{0.5} = 5.50 \times 10^6 \exp\left[\frac{-55.5 \text{ kJ/mol}}{RT}\right] \text{ mg U/cm}^2/\text{h/kPa}^{0.5}. \quad (\text{eq. II-24})$$

Their results suggest a higher temperature dependence compared to that determined for all literature data.

Pearce reviewed data up to 1989 and recommended an Arrhenius expression based on linear regression analysis of all the data, excluding outlier data of Waber.³⁰ The reaction rate expression is

$$k_l/p^{0.5} = 1.60 \times 10^5 \exp\left[\frac{-41.1 \text{ kJ/mol}}{RT}\right] \text{ mg U/cm}^2/\text{h/kPa}^{0.5}. \quad (\text{eq. II-25})$$

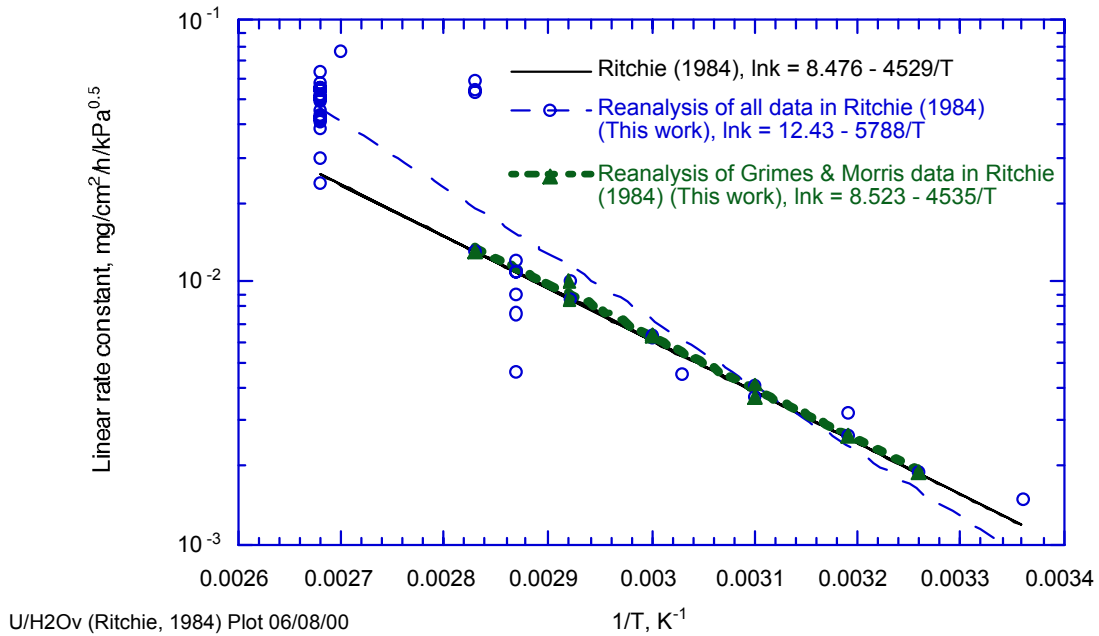


Figure 14. Reanalysis of Ritchie's²⁵ Arrhenius rate expression of the uranium/anoxic water vapor reaction.

Trimble performed a regression analysis of reaction rate data up to 1998.³⁵ The regression analysis included all the data reviewed by Pearce and some additional uranium-water vapor reaction rate data reported since 1989. The data were obtained directly from the original sources which eliminates the variability due to extraction from a graph of data (see above discussion in Section II.A.1). Trimble's analysis included results from oxidation tests at pressures both below and above 101 kPa. He recommended a square root pressure dependence at pressures below 101 kPa and a linear pressure dependence at pressures above 101 kPa for temperatures less than 295°C (568 K)

$$k_l/p^{0.5} = 6.60 \times 10^5 \exp\left[\frac{-45.5 \text{ kJ/mol}}{RT}\right] \text{ mg U/cm}^2/\text{h/kPa}^{0.5} \text{ at } p < 101 \text{ kPa} \quad (\text{eq. II-26})$$

$$k_l/p^{1.0} = 6.57 \times 10^4 \exp\left[\frac{-45.5 \text{ kJ/mol}}{RT}\right] \text{ mg U/cm}^2/\text{h/kPa}^{1.0} \text{ at } p > 101 \text{ kPa}. \quad (\text{eq. II-27})$$

Abrefah and Sell⁶⁰ reported a regression analysis of literature data normalized by $p^{0.5}$ in the temperature range 20-302°C. Their analysis is effectively equivalent to Trimble's expression at pressure less than 101kPa. The Arrhenius dependence of the reaction rate, derived by a regression fit of literature data up to 1998, was

$$k_l/p^{0.5} = 7.59 \times 10^5 \exp\left[\frac{-45.8 \text{ kJ/mol}}{RT}\right] \text{ mg U/cm}^2/\text{h/kPa}^{0.5}. \quad (\text{eq. II-28})$$

A regression analysis of the reaction rate data reported up to 1999 was performed as part of this work. That analysis evaluated the water vapor oxidation rates for the temperature range 20 to 302°C, and determined a temperature dependence of

$$k_l/p^{0.5} = 9.75 \times 10^5 \exp\left[\frac{-46.6 \pm 0.7 \text{ kJ/mol}}{RT}\right] \text{ mg U/cm}^2/\text{h/kPa}^{0.5}. \quad (\text{eq. II-29})$$

The regression fit to literature data up to 1999 calculated by this author was very similar to regression fits determined by Trimble (eq. II-25) and Abrefah et al. (eq. II-27). The regression fits of Trimble, Abrefah, et al., and this author resulted in slightly higher rates compared to Pearce (eq. II-24), whose fit did not include the Hayward, et al. 1992 data. The expressions reported by Pearce and Kay (eq. II-23) and Ritchie (eq. II-22), which were each derived from a single series of reaction rate measurements, were lower than the regression fit to all the literature data determined by this author. However, their expressions lie within the scatter of the literature data. The reaction rate expressions for the U/H₂O reaction are summarized in Table 6.

Table 6. Summary of uranium/anoxic water vapor reaction rate expressions.

Eq. No.	Rate Expression	Conditions ^a	Reference
2-22	Linear: $k_l/p^{0.5} = 3.56 \times 10^4 \exp[-37.7/RT]$	20-100°C	Ritchie ²⁵
2-23	Linear: $k_l/p^{0.5} = 5.50 \times 10^6 \exp[-55.5/RT]$	150-200°C	Pearce & Kay ¹⁴
2-24	Linear: $k_l/p^{0.5} = 1.60 \times 10^5 \exp[-41.1/RT]$	20-300°C	Pearce ¹⁵
2-25	Linear: $k_l/p^{0.5} = 6.60 \times 10^5 \exp[-45.5/RT]$	20-295°C	Trimble ³⁵
2-26	$k_l/p^{1.0} = 6.57 \times 10^4 \exp[-45.5/RT]$	p < 101 kPa p > 101 kPa	
2-27	Linear: $k_l/p^{0.5} = 7.59 \times 10^5 \exp[-45.8/RT]$	20-302°C	Abrefah & Sell ⁶⁰
2-28	Linear: $k_l/p^{0.5} = 9.75 \times 10^5 \exp[-46.6 \pm 0.7/RT]$	20-302°C	This work

^aAll data were obtained at pressure less than 101 kPa, except where noted.

Oxygenated Water Vapor

Many investigators, who reviewed the reaction rates of uranium in humid air and water vapor-oxygen environments, found that water vapor corrosion has a complex vapor pressure dependence.^{7, 8, 9, 10, 15, 18, 24, 28, 29, 30, 32, 33, 34, 36, 40, 45} Small amounts of moisture in oxygen (i.e., water vapor) significantly increase the reaction rate of uranium relative to dry oxygen. There are three regions of behavior: (a) at low relative humidity (<1-2%RH), the reaction rate strongly increases with increasing water vapor, (b) at intermediate relative humidity (2-90%RH), the reaction rate is essentially independent of vapor pressure and oxygen pressure for oxygen pressure above 1.33 kPa, and (c) at high relative humidity (>90%RH), the reaction rate increases as the one-fifth power of the vapor pressure increases ($p^{1/5}$), but this weak pressure dependence is lost in the data scatter.

At low relative humidity, Bennett, et al.²² and Pearce and Kay¹⁴ correlated the effects of moisture in oxygen (up to 2.5×10^4 vppm or 2.5% water vapor and temperatures up to 300°C) with one-third power of water vapor pressure ($p^{1/3}$). McGillivray, et al. modeled the effects of water vapor at low relative humidity (<4%RH) by Langmuir kinetics for temperatures between 0 and 350°C.¹⁰ At temperatures below 200°C, the vapor pressure dependence was fitted to a second order polynomial; however at higher temperature where the relative humidity was less than 0.5%RH a linear fit was used. At relative humidity greater than 90%RH, Colmenares⁹ correlated reaction rate data with a one-fifth power pressure dependence, $p^{1/5}$. Ritchie, et al.³² completed a systematic investigation of the uranium/water vapor-oxygen reaction over a temperature range of 40 to 102°C that demonstrated the reaction rate is independent of relative humidity between 11 and 75%RH. Figure 15 shows the Arrhenius expressions reported by Pearce¹⁵, Ritchie¹⁸ and Ritchie, et al.³², compared with that derived by linear regression of all the literature data by this author.

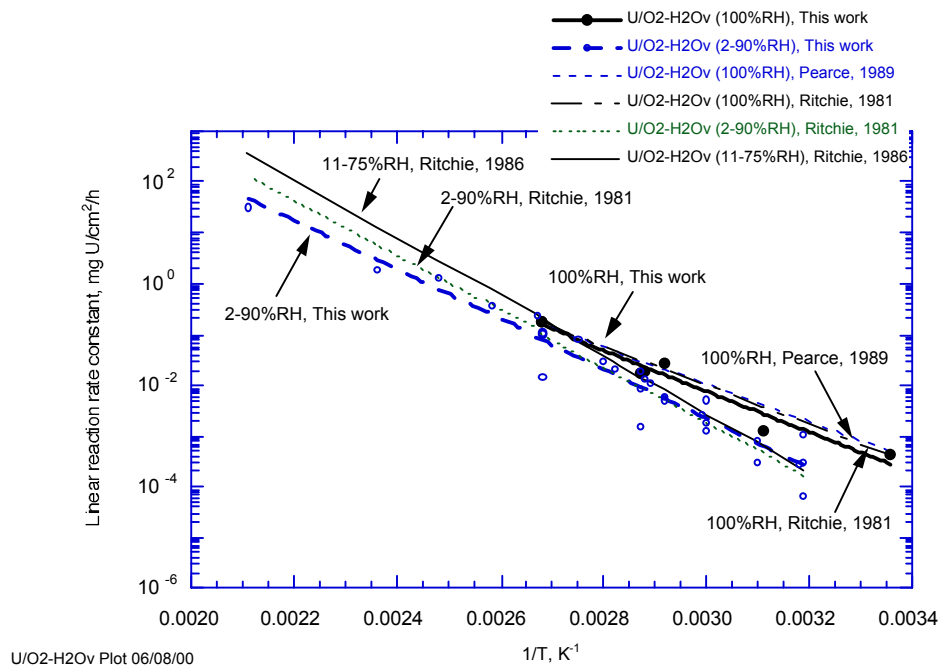


Figure 15. Summary of Arrhenius expressions derived for uranium oxidation in oxygenated water vapor at temperatures less than 302°C.

Ritchie reviewed reaction rates of uranium with water vapor-oxygen at relative humidity in the range 2-90%RH and at 100%RH.¹⁸ He reported an Arrhenius dependence of the uranium-water vapor-oxygen reaction rate of

$$k_l = 4.8 \times 10^{13} \exp\left[\frac{-104.7\text{kJ/mol}}{RT}\right] \text{ mg U/cm}^2/\text{h at 2-90\%RH and} \quad (\text{eq. II-30})$$

$$k_l = 4.6 \times 10^9 \exp\left[\frac{-74.5\text{kJ/mol}}{RT}\right] \text{ mg U/cm}^2/\text{h at 100\%RH.} \quad (\text{eq. II-31})$$

Ritchie, et al. reported experiment results of uranium oxidation tests in moist air at relative humidities between 11 and 75%RH and at temperatures between 40 and 100°C. A regression fit through all the experiment data resulted in³²

$$k_l = 5.65 \times 10^{14} \exp\left[\frac{-110.5\text{kJ/mol}}{RT}\right] \text{ mg U/cm}^2/\text{h} \quad (\text{eq. II-32})$$

comparable to the rate equation derived from literature data by Ritchie (eq. II-29) as seen in Figure 15.

Pearce reviewed the reaction rate of uranium/oxygen-water vapor at intermediate and 100%RH. At intermediate relative humidity and temperatures below 192°C, he proposed a $p^{1/3}$ pressure dependence to normalize the temperature dependence expression, although he stated that a pressure-independent expression fit the data equally well¹⁵

$$k_l / p^{0.3} = 2.75 \times 10^{11} \exp\left[\frac{-95.5\text{kJ/mol}}{RT}\right] \text{ mg U/cm}^2/\text{h/kPa}^{0.3} \text{ at 2-90\%RH.} \quad (\text{eq. II-33})$$

Pearce recommended a temperature dependence of the uranium/oxygenated-water vapor reaction rate at 100%RH, determined by regression analysis of literature data up to 1989, as

$$k_l = 1.61 \times 10^9 \exp\left[\frac{-71.4\text{kJ/mol}}{RT}\right] \text{ mg U/cm}^2/\text{h at 100\%RH.} \quad (\text{eq. II-34})$$

The temperature dependence was very similar to the uranium/dry air reaction (eq. II-21), but the pre-exponential was ten times greater.

This author re-evaluated the existing data up to 1999 for the reaction of uranium with water vapor-oxygen at intermediate and 100%RH relative humidity. Arrhenius expressions for the two relative humidity ranges were determined by linear regression analysis of the literature data. The temperature dependence of the reaction rate at 2-90%RH was determined to be

$$k_i = 8.21 \times 10^{11} \exp\left[\frac{-92.9 \pm 4.8 \text{kJ/mol}}{RT}\right] \text{mg U/cm}^2/\text{h} \quad (\text{eq. II-35})$$

and at 100%RH,

$$k_i = 8.65 \times 10^9 \exp\left[\frac{-76.9 \pm 7.0 \text{kJ/mol}}{RT}\right] \text{mg U/cm}^2/\text{h}. \quad (\text{eq. II-36})$$

The temperature dependence of the uranium/oxygenated-water vapor reaction rate derived by this author for 2-90%RH was somewhat less than reported by Ritchie¹⁸ for 2-90%RH and Ritchie et al.,³² for 11-75%RH. However, the temperature dependence at 100%RH was very similar to that reported by Pearce¹⁵ and Ritchie.¹⁸ The reaction rate expressions for U/O₂-H₂Ov are summarized in Table 5. The reaction rate of uranium in water saturated oxygen (100%RH) is around an order of magnitude higher than in dry oxygen, however it is one to two orders of magnitude less than the reaction rate in anoxic water vapor or water immersion.

Table 7. Summary of uranium/oxygenated water vapor reaction rate expressions at intermediate (2-90%RH) and 100%RH relative humidity.

Eq. No.	Rate Expression	Conditions	Reference
	Linear:		Ritchie ¹⁸
2-29	$k_i = 4.80 \times 10^{13} \exp[-104.7/RT]$	40-130°C, 2-90%RH	
2-30	$k_i = 4.60 \times 10^9 \exp[-74.5/RT]$	25-100°C, 100%RH	
	Linear:		Ritchie ³²
2-31	$k_i = 5.65 \times 10^{14} \exp[-110.5/RT]$	40-100°C, 11-75%RH	
	Linear:		Pearce ¹⁵
2-32	$k_i/p^{0.3} = 2.75 \times 10^{11} \exp[-95.5/RT]$	20-192°C, 2-90%RH	
2.33	$k_i = 1.61 \times 10^9 \exp[-71.4/RT]$	20-100°C, 100%RH	
	Linear:		This work
2-34	$k_i = 8.21 \times 10^{11} \exp[-92.9 \pm 4.8/RT]$	20-200°C, 2-90%RH	
2-35	$k_i = 8.65 \times 10^9 \exp[-76.9 \pm 7.0/RT]$	20-100°C, 100%RH	

3 Uranium/Water Reaction

A number of researchers have reviewed the reaction rate of uranium corrosion in water.^{30, 33, 35, 40, 42, 43, 45, 61, 62} Much of the original work was conducted over thirty years ago as part of fuel development and spent fuel storage studies. The rate and mechanism are considered to be the same as that of the uranium-water vapor reaction at saturation. Since the long term reaction rate in oxygenated water is the same as in anoxic water, only the uranium/anoxic water reaction kinetics are reviewed in this report.

The uranium/water reaction rate depends strongly on temperature, increasing by a factor of approximately one thousand from 100 to 300°C. Many investigations have studied the temperature dependence of the uranium/water reaction rate. However, most studies were completed before 1960 as part of early reactor fuel development efforts at the national laboratories, and the results were published only in technical reports. Moreover, the literature does not contain broad reviews of the uranium/water reaction as for dry air and anoxic and oxic water vapor, a probable consequence of the initial classification of the original reports. Since then these data have been declassified. Within the technical report literature, the temperature dependence of the U/H₂O reaction rate was sometimes summarized as Arrhenius plots, although the corresponding Arrhenius expressions were often not reported. This review reanalyzed and evaluated a few Arrhenius expressions derived from summary plots,^{33, 63} one from a regression fit,³⁵ and all available uranium/water reaction rate data up to 1999. The resulting Arrhenius expressions, summarized in Figure 2-10 show that the regression fit by this author and the other Arrhenius expressions are essentially the same and completely overlay each other.

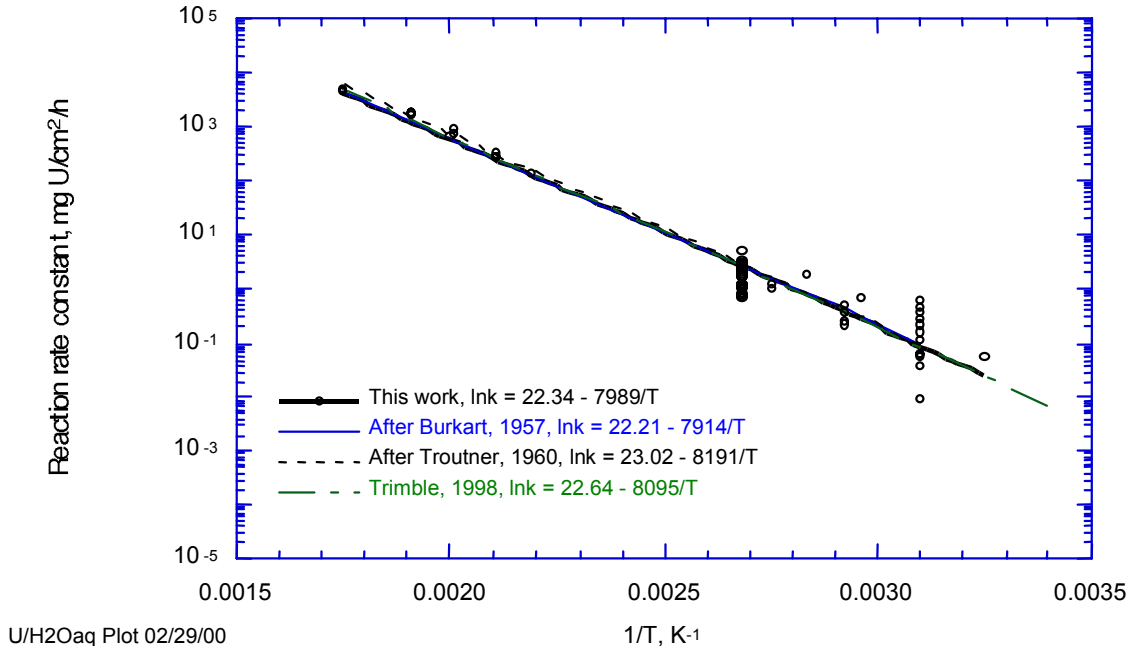


Figure 16. Summary of Arrhenius expressions derived for uranium oxidation in anoxic water and temperatures less than 302°C. Regression fits by this author and Trimble and the expressions derived from Burkart and Troutner completely overlay one another.

In a 1957 report,⁶³ Burkart published some corrosion results from a uranium fuel alloy development program at Bettis Atomic Power Laboratory. Burkart presented the Arrhenius dependence of the uranium/water reaction in a summary plot, which was based on previous work at Bettis⁶⁴ and by Howe and Jones,⁶⁵ but neglected to give the Arrhenius expression. This author derived the Arrhenius expression from the plot, which was valid in the temperature range 60-343°C,

$$k_i = 4.43 \times 10^9 \exp\left[\frac{-65.8 \text{ kJ/mol}}{RT}\right] \text{ mg U/cm}^2/\text{h.} \quad (\text{eq. II-37})$$

In 1960, Troutner investigated the mechanisms and kinetics of uranium corrosion in water and steam.³³ Troutner compared his reaction rate results to an Arrhenius plot of published and unpublished reference data in the range of 50 to 350°C,^{43, 66, 67, 68, 69} but did not publish the Arrhenius expression. This author derived the Arrhenius expression from Troutner's plotted data as

$$k_i = 9.90 \times 10^9 \exp\left[\frac{-68.1 \text{ kJ/mol}}{RT}\right] \text{ mg U/cm}^2/\text{h.} \quad (\text{eq. II-38})$$

Trimble collated literature data published before 1998 and determined a temperature dependent reaction rate by regression methods.³⁵ The Arrhenius expression for the uranium/water reaction at temperatures below 300°C was given as

$$k_i = 6.78 \times 10^9 \exp\left[\frac{-67.3 \text{ kJ/mol}}{RT}\right] \text{ mg U/cm}^2/\text{h.} \quad (\text{eq. II-39})$$

The regression analysis by Trimble (eq. II-38) was essentially identical to the summary expressions derived from figures in Burkart (eq. II-36) and Troutner (eq. II-37), while it included data from a number of additional sources.

This author reanalyzed the uranium/anoxic water reaction rate data reported before 1999 for temperatures below 300°C. The referenced data were essentially the same as analyzed by Trimble with a few revisions. Data from Waber,³⁰ originally reported in units of hydrogen gas generated, were found to be three orders of magnitude higher than reported by Trimble. The revised data fell within the scatter of the literature data, whereas Waber's data in Trimble's report were significantly lower. This error did not effect Trimble's regression fit, since he omitted Waber's data as outliers, consequently the regression fits by Trimble and this author were very similar. The Arrhenius dependence of the uranium/water reaction determined by this author was given as

$$k_l = 5.03 \times 10^9 \exp\left[\frac{-66.4 \pm 2.0 \text{ kJ/mol}}{RT}\right] \text{ mg U/cm}^2/\text{h.} \quad (\text{eq. II-40})$$

The four Arrhenius expressions reviewed in this section were essentially the same and completely overlay each other in Figure 16. This is not surprising since most of the data analyzed were the same for all the investigators. While the regression fits of Trimble (eq. II-38) and this author (eq. II-39) included data up to 1998, the majority of the data were compiled in a 1952 review by McWhirter and Draley, which was also referenced in the summary expressions by Burkart (eq. II-36) and Troutner (eq. II-37). Table 2-4 summarizes all four expressions. Therefore, equivalent Arrhenius expressions of the uranium/water reaction have been reported by investigators over a span of forty years. Consequently, there is high confidence in the validity of the temperature dependent reaction rates. The reaction rates of uranium with water are around 100 times higher than reaction rates in dry air in the temperature range 20-300°C, but have similar energies of activation (65-70 kJ/mol).

Table 8. Summary of uranium/water reaction rate expressions at temperatures less than 350°C.

Eq. No.	Rate Expression	Conditions	Reference
II-36	Linear: $k_l = 4.43 \times 10^9 \exp[-65.8/RT]$	60-343°C	after Burkart ⁶³
II-37	Linear: $k_l = 9.90 \times 10^9 \exp[-68.1/RT]$	50-350°C	after Troutner ³³
II-38	Linear: $k_l = 6.78 \times 10^9 \exp[-67.3/RT]$	20-300°C	Trimble ³⁵
II-39	Linear: $k_l = 5.03 \times 10^9 \exp[-66.4 \pm 2.0/RT]$	20-300°C	This work

4. Summary

The reactions of uranium with oxygen, water vapor, oxygenated water vapor and water all fit linear kinetics up to 300°C. The reaction rate of the uranium/oxygen reaction was around three orders of magnitude lower than the water driven reactions. The water vapor and water reactions exhibit similar rates and dependencies on oxygen addition. Above a threshold concentration, oxygen inhibits the water driven rates to values intermediate to the dry oxygen and anoxic water (vapor) rates. The transition from anoxic to oxygenated behavior occurs at an oxygen threshold concentration of 10-1000 vppm in water vapor and ~5 wppm in water. The water rate oxygen threshold is inferred from the observed anoxic/oxic transition at 70°C in air saturated water and the temperature dependence of the oxygen solubility in water. Arrhenius type reaction rate expressions were developed by standard regression analyses of the literature data published up to 1999. The regression fit rate expressions for the different environments are summarized in Table 9.

Table 9. Summary of rates of reaction for uranium with oxygen, water vapor, oxygenated water vapor and water at temperatures less than 300°C.

Reaction	Rate Expression mg/cm ² /h or mg/cm ² /h/kPa ^{0.5} (H ₂ Ov)	Conditions	Eq. No.
U/O ₂	Linear: $k_l = 1.09 \times 10^8 \exp[-71.3 \pm 2.1/RT]$	38-300°C	II-21
U/H ₂ Ov	Linear: $k_l/p^{0.5} = 9.76 \times 10^5 \exp[-46.6 \pm 0.7/RT]$	20-302°C	II-28
U/O-H ₂ Ov	Linear: $k_l = 8.21 \times 10^{11} \exp[-92.9 \pm 4.8/RT]$ $k_l = 8.65 \times 10^9 \exp[-76.9 \pm 7.0/RT]$	20-200°C, 2-90%RH 20-100°C, 100%RH	II-34 II-35
U/H ₂ Oaq	Linear: $k_l = 5.03 \times 10^9 \exp[-66.4 \pm 2.0/RT]$	20-300°C	II-39

C. Irradiation Effects on Uranium Metal Oxidation

The effects of irradiation on the reaction rate of uranium with oxygen and moist oxygen were reported in papers by Bennett and colleagues^{22, 24, 50, 51, 52, 70} and reviewed by Totemeier.⁴⁵ Bennett, et al. investigated the oxidation kinetics of unirradiated and irradiated uranium metal with 0-1200 ppm aluminum and 0-390 ppm iron. The uranium metal was irradiated in Magnox reactors at metal temperatures between 390 and 450°C to a maximum burnup of 9100 MWd/tU.⁷⁰ The surface area, density, swelling, and open porosity of the irradiated samples were determined by standard techniques. According to Bennett, et al. the swelling increased with irradiation, but the open porosity was independent of swelling, remaining at less than 5% for swelling up to 100%. Their conclusions are inconsistent with results for irradiated EBR-II metal fuel (~15% open porosity at 100% swelling)^{71, 72} and fundamental geometrical considerations.⁷³ Bennett, et al. discussed the possibility that machining of the samples may have closed the pores. They rejected this possibility that machining would have been unlikely to form air-tight seals. Yet one of their samples with 72% swelling exhibited 14.8% open porosity, consistent with the EBR-II data. As the open porosity measurements were probably low, the oxidation kinetic data did not seem affected by irradiation. For less than 22% swelling, the oxidation rate is less than a factor of two greater for irradiated uranium than for unirradiated uranium in the temperature range 100-250°C. Above 22% swelling, the oxidation rate increased with swelling exponentially. Bennett, et al. collated the increase in reaction rate due to irradiation at temperatures of 100-350°C as an exponential function of swelling and inverse temperature. The enhancement factor (EF) was given as^{22, 24}

$$EF = \exp\left[1.94 \times 10^4 \frac{S}{T^2}\right] \quad (\text{eq. II-41})$$

where S was the per cent swelling and T was the temperature in K. Bennett, et al. hypothesized that swelling resulted in break-up of the uranium surface during oxidation, creating more effective surface area. Generally, oxidation rates increase with temperature, so the positive slope of the 1/T fit was unexpected and could not be explained. In addition, this author found that the large data scatter obscured the influence of temperature, if any. Due to the mechanistic inconsistency of an inverse temperature dependence the reaction rate was assumed to be independent of temperature and related only to swelling. The author reanalyzed the Bennett data for temperatures between 100 and 300°C and plotted the enhancement factor (for the reaction rate of irradiated uranium in dry oxygen) as a function of swelling in Figure 17. The corresponding regression fit to the plotted data is

$$EF = 0.444 \exp[7.86 \times 10^{-2} S]. \quad (\text{eq. II-42})$$

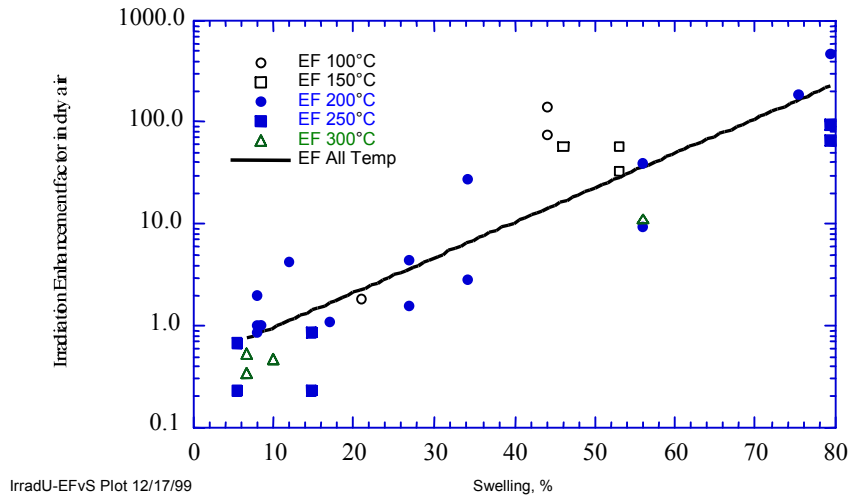


Figure 17. Reanalysis of irradiation enhancement factor dependence on swelling at temperatures between 100 and 300°C (after Bennett, et al.^{22, 24}).

Abrefah, et al., at Pacific Northwest National Laboratory (PNNL) also investigated the effect of irradiation on uranium metallic fuel corrosion.^{46, 60} They studied the oxidation kinetics of irradiated N-Reactor fuel (denoted as KW SNF in this discussion) in dry oxygen and water vapor environments. The fuel was stored in water at Hanford K-Basin for 12 to 28 years prior to testing. The chemical composition of N-reactor fuel, listed in Table 10, was similar to the material studied by Bennett, et al., while the average burnup, between 900 and 2700 MWd/tU,⁶⁰ was limited to the lower range of their data. At this low burnup, irradiation induced swelling is not significant. Linear reaction rates were derived from kinetic data obtained by thermogravimetric analysis. The reaction rate data of KW SNF with oxygen and water vapor are compared to the rate expressions of uranium metal determined by this author (see Figure 18). The water vapor data are normalized to saturation pressure for comparison purposes. The oxidation of N-Reactor spent fuel concluded that irradiation effects were negligible due to the low burnup, in apparent agreement with the literature data.

Table 10. Nominal composition of N-Reactor fuel samples used in the corrosion study.

Element	Amount, weight parts per million (wppm)
Aluminum	700-900
Beryllium	10
Boron	0.25
Cadmium	0.25
Carbon	365-735
Chromium	65
Copper	75
Hydrogen	2.0
Iron	300-400
Magnesium	25
Manganese	25
Nickel	100
Nitrogen	75
Silicon	124
Zirconium	65
Uranium	Balance

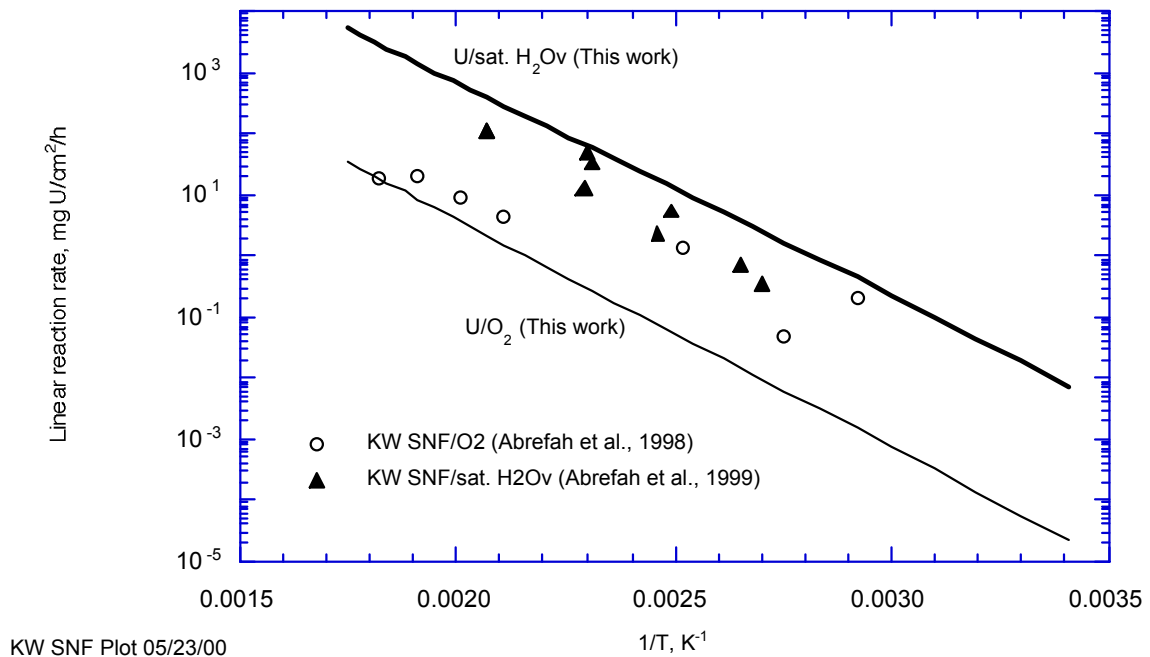


Figure 18. Reaction rates of N-reactor SNF with oxygen and with water vapor along with the temperature dependencies of uranium metal reactions determined in this work.

The KW SNF/O₂ reaction rates are similar to the literature data mean at temperatures above 200°C. At temperatures below 200°C, the KW SNF data are somewhat higher than the literature data, but this difference was not statistically significant. In water vapor, the KW SNF exhibited reaction rates lower than the mean reaction rates of the U/H₂Ov data at all temperatures up to 300°C. Abrefah, et al. evaluated the influence of oxygen in-leakage since oxygen is known to suppress water vapor reaction kinetics at very low concentrations. They adjusted the measured rates for this effect by multiplying by a factor of seven, derived from Colmenares' work⁹ on oxygen inhibition. The adjusted rates⁶⁰ are approximately equal to the regression fit of the unirradiated U/H₂Ov data suggesting that oxygen in-leakage may have occurred. In conclusion, the oxidation studies of N-Reactor spent fuel indicated that irradiation effects at low burnup were negligible, in agreement with the literature data. The similarity between oxidation rates of KW SNF and U metal is also consistent with dissolution rates of irradiated uranium metal fuel reported by Gray and Einziger at PNNL and Foncesbeck at Argonne National Laboratory-West (ANL-W).^{74, 75}

The effects of irradiation on uranium metal oxidation are summarized as follows. Irradiation does not increase the intrinsic oxidation rate of uranium metal. The apparent rate (normalized to geometric surface area) increases with irradiation-induced swelling. The enhancement factor due to irradiation is defined as an exponential function of swelling and is attributed to the associated increase in surface area. The oxidation rate of metal fuel irradiated to low burnup, which has negligible swelling, is expected to be similar to that of unirradiated U metal. Consistent with this, unirradiated uranium and irradiated KW SNF (which has a low burnup and negligible swelling) have essentially the same reaction rates in oxygen and water vapor environments, within the variability of the literature data.

D. Uranium-Hydride Effects on Uranium Metal Oxidation

Hydrogen is a product of the uranium/water reaction (cf. section II) that can be measured and used to derive the rate constant. Comparisons between metal loss rate determined by weight and by hydrogen gas measurements generally show that less than stoichiometric hydrogen is produced. Uranium hydride has been reported as a product of the uranium metal reaction with water^{6, 7, 16, 33, 67, 76} and with water vapor^{6, 7, 16, 28, 33, 76, 77, 78, 79} to account for this difference. The mechanism for uranium hydride formation is complex and not well understood.

The noted absence of any detectable hydride in some carefully performed experiments, yet its definite identification (by XRD and other methods) in the oxide of other experiments and in corroded fuel kept in storage, has contributed to the uncertainty in the mechanism. Where hydride was observed, the reported amount has varied widely from 2-60 wt%.^{16, 28, 78, 79} Uranium hydride was generally detected in uranium metal corrosion product in stagnant gas phase environments and at relatively short times in water oxidation. The water vapor atmosphere in contact with the uranium metal is confined or effectively closed to the outside. Such a condition can occur in a sealed system, in a crevice geometry, or a clad metal. In immersion oxidation tests performed on irradiated uranium, around 10% uranium hydride was observed in the reaction products of some of the samples that were not completely oxidized.⁷⁵ Since uranium hydride is an intermediate product that oxidizes to UO₂, a transient amount of residual UH₃ is expected to form while the U metal is still reacting and if the UH₃ oxidation rate is less than the U metal oxidation rate, as has been reported.^{80, 81}

In some studies, the presence of hydride has been speculated to increase the reaction rate of uranium metal oxidation. A hydrogen rich phase, postulated to be metastable monohydride, was observed in uranium-molybdenum alloys that failed by severe cracking. The authors proposed that the hydrides preferentially corroded, weakened the structure, and consequently caused severe cracking.^{63, 82} In work on N-reactor spent fuel oxidation kinetics, Abrefah, et al. speculated that the oxidation of hydride inclusions, which formed during wet storage, resulted in a higher apparent reaction rate due to the higher surface area of the hydride.⁴⁶ Obviously, the effect of hydride on uranium metal oxidation depends on the magnitude of its rate constant relative to the U metal oxidation rate constant. To evaluate the effect of uranium hydride on uranium metal oxidation, the oxidation kinetics of uranium hydride were reviewed.

The uranium hydride oxidation reactions with oxygen and water vapor are written as



Until recently, very little data were available on the oxidation kinetics of uranium hydride.⁸³ Recent work by Totemeier, et al. reports the oxidation kinetics and corrosion characteristics of hydride-bearing corrosion products formed on uranium fuel plates by water vapor reaction during dry storage.^{78, 79, 80, 84} The comprehensive study includes surface area measurements,

composition by x-ray diffraction, and oxidation kinetics in dry and moist atmospheres at temperature below and above ignition. The pertinent results are summarized here.

Uranium hydride was identified in the corrosion product by x-ray diffraction and the amount correlated with the extent of corrosion. Moderately to heavily corroded samples contained between 29 and 61% hydride and lightly corroded samples contained very little uranium hydride.⁸⁰ The samples were in powder form with specific surface areas from 0.51 to 1.00 m²/g. Reaction rates were independent of oxygen concentration between 4% and 20% O₂. In moist atmospheres the rates were slightly higher than in dry oxygen, but not enough to be statistically significant.⁸¹ Results from inert gas/water vapor tests were lower than expected and may have been depressed by oxygen leakage into the reaction system. The temperature dependence of the reaction rate in the temperature range 50-150°C is given as

$$k_l = 1.81 \times 10^6 \exp\left[\frac{-63 \pm 4 \text{kJ/mol}}{RT}\right] \text{ mg U/cm}^2\text{h in oxygen and} \quad (\text{eq. II-45})$$

$$k_l = 3.54 \times 10^4 \exp\left[\frac{-49.2 \text{kJ/mol}}{RT}\right] \text{ mg U/cm}^2\text{h in argon-4\%RH water vapor.} (\text{eq. II-46})$$

The Arrhenius dependence of the uranium hydride/oxygen reaction at temperatures less than 150°C is plotted in Figure 19 along with the regression fit of U metal/O₂ (eq. II-21). At these temperatures the surface area normalized reaction rate of uranium hydride with oxygen is slightly less than that of U metal. However, due to the uncertainty in the U metal oxidation rate, the uranium hydride reaction rate can be considered the same as the U metal.

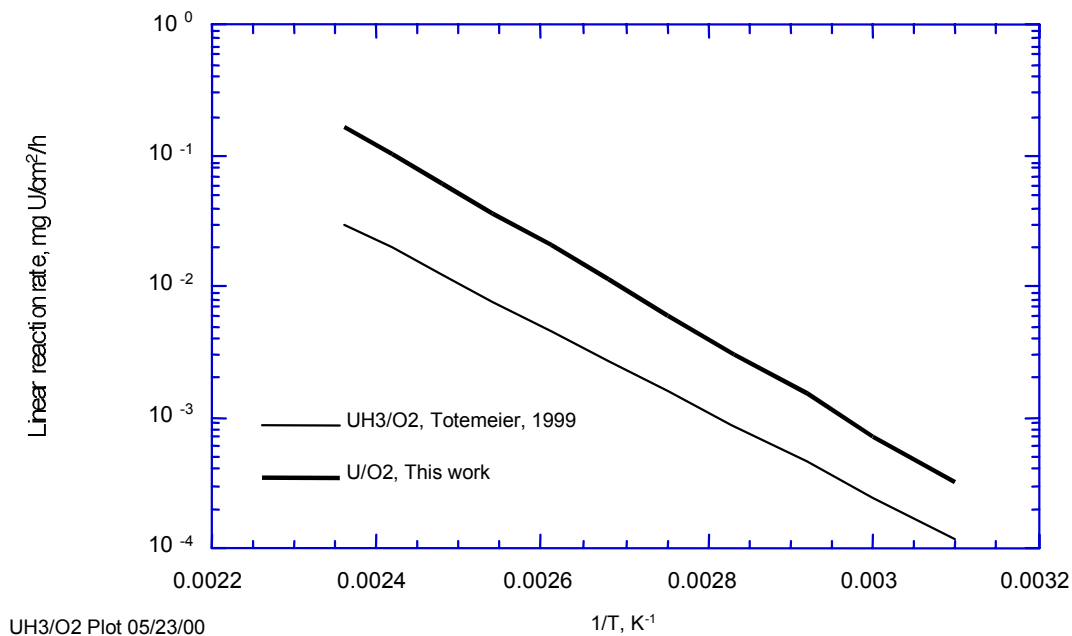


Figure 19. Arrhenius dependencies of the uranium-hydride/oxygen reaction rate (Totemeier, et al.⁸⁰) and uranium metal/oxygen reaction rate (this work).

III. OXIDATION RATES OF URANIUM METAL ALLOYS

Uranium alloys were investigated as part of reactor fuel development efforts to improve the corrosion resistance, density, and dimensional stability, and to limit fuel-cladding interactions at service temperatures and under irradiation. The addition of small amounts of alloying elements, particularly those that stabilize the gamma phase at lower temperatures, results in significant improvements in corrosion resistance compared to unalloyed uranium. The uranium alloys also typically exhibit higher strength, lower thermal expansion, and greater dimensional stability under irradiation. Due to the significant differences of the uranium alloys in corrosion, mechanical, physical and chemical behavior relative to unalloyed uranium metal, the alloys and the unalloyed metal were reviewed separately. However, the discussion is limited to uranium alloys of molybdenum, niobium, and zirconium, which were most relevant to DOE SNF. The majority of the reviewed work was published before 1960 in the United States in classified reports that have been subsequently declassified. More recently, irradiation performance of some U-alloys have been investigated in efforts to develop high fissile density fuel for low enriched high power research reactors, but these programs were limited to dimensional stability and fission gas induced-swelling rather than corrosion behavior. Few reviews of the mechanism and kinetics of uranium alloys oxidation in various media have been published.^{6, 19, 41, 43, 62, 63, 64, 85}

The uranium-molybdenum alloy corrosion reaction rate is dependent on microstructure and is lowest for the gamma phase. In general, the oxidation rates of high alloys in water were lower than that of unalloyed uranium at temperatures below 350°C. However, the differences between unalloyed and low alloy uranium (i.e., corresponding to alpha or beta phase) were not statistically significant. The temperature dependencies of uranium-molybdenum alloy oxidation rates were similar to that of unalloyed uranium, while the activation energies of the U-Nb and Zr-U alloys were lower, but not to a statistically significant extent.

This section discusses the general understanding of uranium alloy oxidation, kinetics and temperature dependencies of the oxidation rates, and reviews effects of irradiation on U-alloy corrosion.

A. Factors Affecting Uranium Alloy Oxidation

1. Microstructural Effects on Oxidation

The mechanism of uranium alloy oxidation is not well understood in microstructural terms. However, researchers observe that uranium alloys with a gamma phase microstructure exhibit the lowest oxidation rates.^{62, 85} In pure uranium, the gamma phase is stable only at temperatures above 776°C. The other two allotropic forms are the alpha phase at temperatures below 668°C and the beta phase at temperatures between 668°C and 776°C. The addition of elements highly miscible in the gamma phase (e.g., molybdenum, niobium and zirconium), lowers the equilibrium temperature (see Figures 20, 21 and 22) and stabilizes the gamma phase at temperatures below the equilibrium for pure uranium. The gamma phase in uranium alloys is actually metastable at temperatures below equilibrium and transforms to the equilibrium phase at sufficiently long times, dependent on the alloy content and temperature. Due to the time-temperature-transformation relationship, the minimum alloying amount necessary to maintain the gamma phase depends on the cooling rate. For example, the critical molybdenum additions in U-Mo alloys are 9.8 wt% Mo for normal cooling,⁶² 7 wt% Mo for water quenched cooling,⁶² and 6 wt% Mo for cooling of an atomized powder metallurgy process.⁸⁶

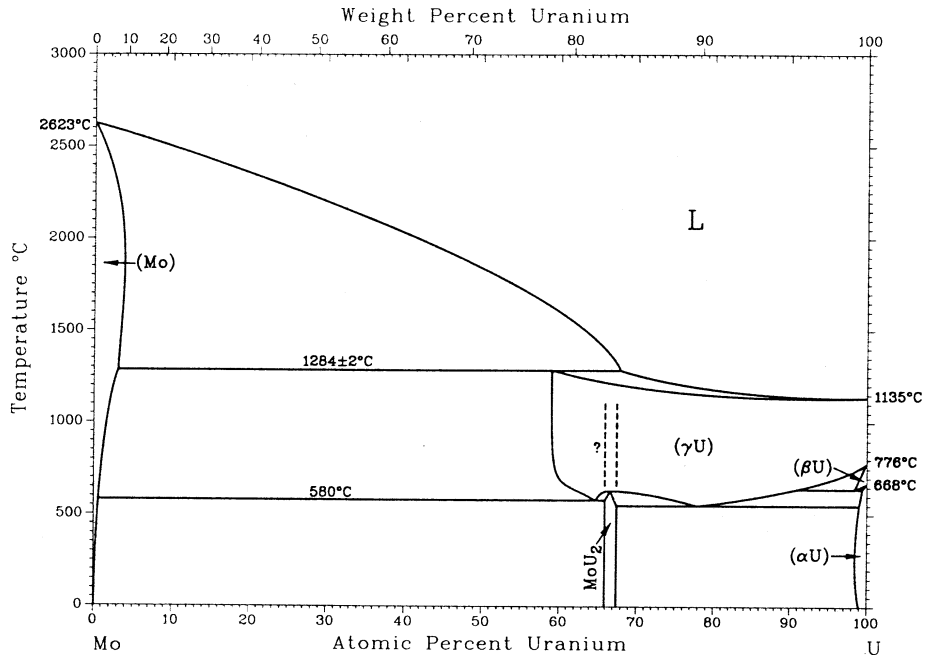


Figure 20. Uranium-molybdenum phase diagram indicating equilibrium gamma phase at a minimum temperature of 550°C and 12 at.% molybdenum.

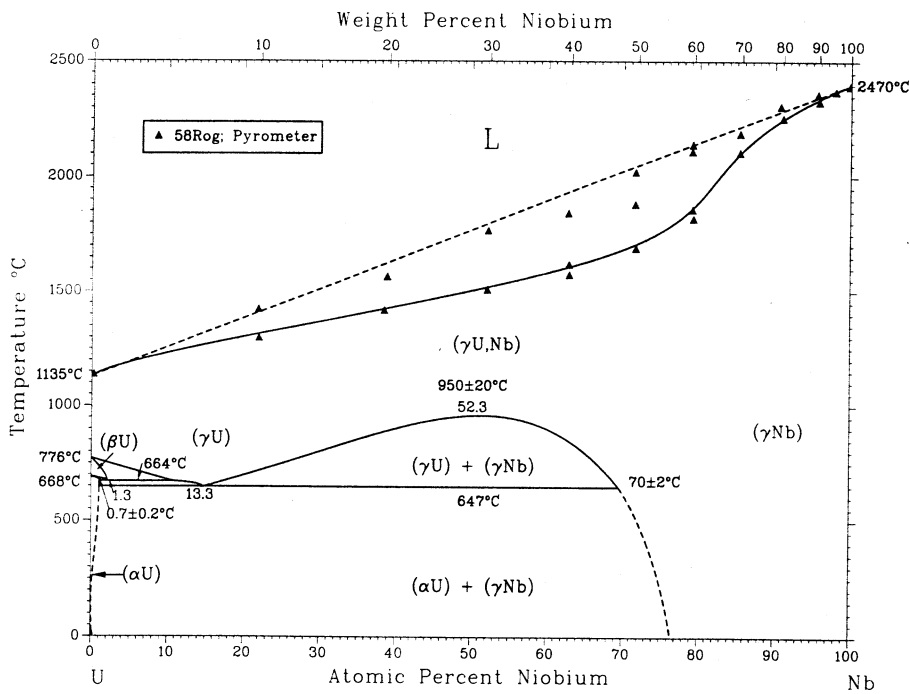


Figure 21. Uranium-niobium phase diagram indicating equilibrium gamma phase at a minimum temperature of 647°C and 13.3 at.% niobium.

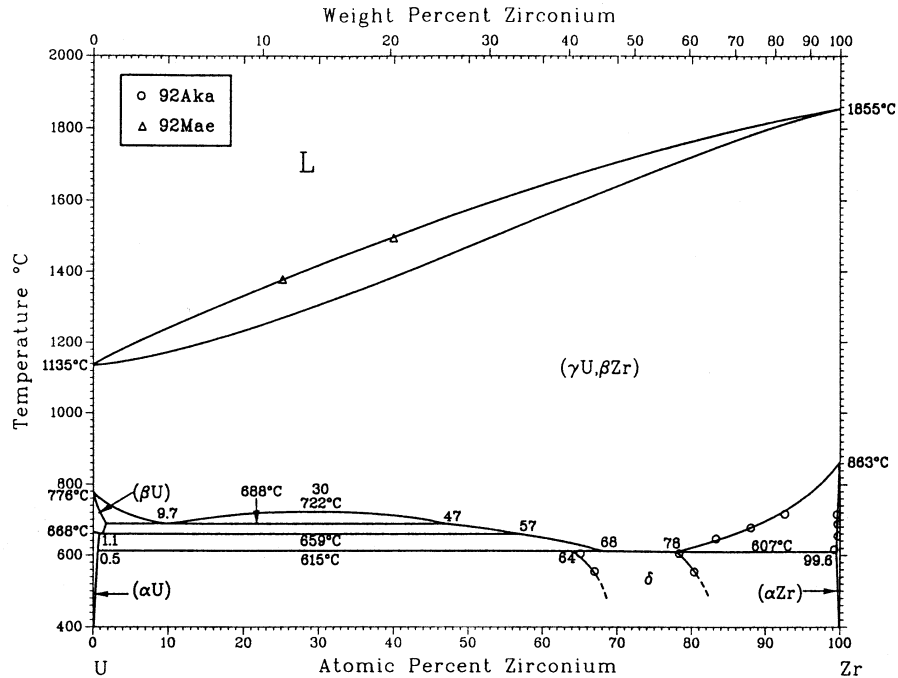


Figure 22. Zirconium-Uranium phase diagram indicating equilibrium gamma phase at a minimum temperature of 615°C and 68 to 75 at.% zirconium.

Under irradiation, the gamma phase is the stable phase for a range of fission rates and temperature conditions. Consequently, uranium alloys undergo phase reversion, wherein alloys in the equilibrium phase transform to the gamma phase, when subjected to a sufficiently high fission rate. The critical fission rate is not clearly established, but increases sharply with temperature, from 10^{12} fissions/cm³-sec at 371°C to 2×10^{13} fissions/cm³-sec at 427°C. The corrosion rates of U-Mo, U-Nb and Zr-U alloys remained unchanged after irradiation up to exposures of 2000 MWd/tU, although the times to discontinuous (matrix) failure for these alloys were significantly reduced.⁸⁷ More discussion on the premature discontinuous failure is presented in Section III.A.2.

2. Discontinuous Failure

The uniform oxidation rates of uranium alloys were much lower than those of unalloyed uranium. However, long-term resistance to corrosion of U alloys may not be greatly improved due to premature cracking and matrix breakup, which resulted in an apparent accelerating reaction rate at long times. Discontinuous failure, also called matrix breakup, is the severe cracking of the bulk or matrix material caused by preferential reaction of inhomogeneities in the matrix. For example, a hydrogen-rich secondary phase can form at the inhomogeneities and can initiate failure by embrittlement and localized stress, induced by volume mismatch of the hydride and matrix. Examples of matrix breakup caused by non-homogeneous reactions with water and humid air have been reported for uranium alloys.^{6, 63, 64} In these investigations, an apparent accelerating reaction rate after a period of stable linear kinetics was observed

concomitantly with severe cracking and matrix breakup of the samples. Since the non-homogeneous reaction and the consequential cracking results in increased specimen surface area, the apparent accelerating reaction rate was attributed to increased sample surface area rather than an intrinsic change in the reaction rate.

A non-homogeneous reaction resulting in an accelerating reaction rate has also been reported for unalloyed uranium metal. Troutner observed non-homogeneous attack and an accelerating reaction rate behavior for extruded uranium samples, containing impurity carbon, with water in the temperature range 170-500°C.³³ Based on the absence of non-homogeneous reactions in low carbon (<30ppm) samples, Troutner proposed that uranium-carbide stringers formed along the working direction and were preferentially attacked relative to the uranium metal, resulting in increased surface area and apparent accelerating rate. Waber's weight gain data of unalloyed uranium quenched from 800°C with 50% RH air at 75°C showed an accelerating rate after 3000 hours similar to that observed for the uranium alloys.⁶

The increase in surface area necessary to account for the apparent accelerating rates was derived from U-Mo and unalloyed uranium kinetic data. The surface area increase for U-Mo and pure uranium are comparable to each other for each environment and temperature condition evaluated. However, the apparent surface area increase is not well correlated with temperature or time. All of the U-Mo alloys exhibited induction periods of variable duration with 'normal' corrosion rates. Once discontinuous failure initiated, the corrosion rates were on the order of 100-10,000 times greater than the induction rates. These observations, coupled with metallographic evidence, indicate that the apparent increase in reaction rates was commensurate with an increase in reactive surface area. Unalloyed uranium metal may also exhibit accelerating rates at long exposure times and may be due to discontinuous failure.

B. Kinetics of Uranium-Molybdenum Oxidation

Retention of the gamma phase at low temperature is dependent on the cooling rate and molybdenum alloying content. The critical composition is 9.8 wt% Mo for normal cooling conditions and 7.0 wt% Mo for water quenched cooling. At temperatures below 575 to 600°C, the uranium gamma phase is metastable and transforms into the equilibrium alpha or beta phase. The time to transformation at temperature can be extended by increasing the alloying amount. Alloys with molybdenum content less than 8 wt% exhibit significantly higher reaction rates than uranium alloys with higher Mo content. For convenience in this report, the oxidation behavior of U-Mo alloys are discussed in terms of alloys with molybdenum content below and above 8 wt%. The reaction rates in humid air and water are discussed below.

1. U-Mo/Water Vapor Reaction

Waber² reported reaction rates of uranium-molybdenum alloys with moist air at 75°C. The experiments were performed in 50%RH air, but further details of the experiments were not given in the paper. Weight gains of U-Mo alloys with molybdenum between 2-10 wt% were plotted as a function of time on a log-log scale. At times exceeding 3000 hr, the reaction rate changed slope for alloys with less than 8 wt% Mo. The increased reaction rate correlated with severe cracking in the specimens. Therefore the increased reaction rate was attributed to the

concomitant increase in surface area generated by the cracking, rather than an intrinsic change in the material corrosion behavior.

The Waber data were reanalyzed and fit by regression analysis to exponential functions to derive the reaction kinetics. At times less than 3000 hr, the Power Law exponents (eq. I-4) for the oxidation of the 2-6 wt%Mo alloys were between 0.8 and 1.5 and the exponents for the 8-10 wt%Mo alloys were between 0.1 and 0.6, which suggested linear and parabolic (or cubic) kinetics, respectively. Unfortunately, the kinetics derived from Waber's data for the reaction of the 8-10 wt%Mo data with water vapor had a large uncertainty (i.e., Waber's data consisted of small weight gains of the 8-10%Mo alloys plotted on a log-log scale). Burkart observed linear kinetics for the reaction of 8-10% wt%Mo alloys with water vapor at higher temperature.⁶³ As there was large uncertainty in the low temperature kinetics, this author elected linear reaction kinetics to describe the reaction rate of high and low molybdenum alloys with humid air. The linear reaction rates of the U-Mo alloys derived from Waber are given in Table 11.

Table 11. Linear reaction rates of uranium-molybdenum alloys in humid air at 75°C and 50%RH (after Waber⁶).

Molybdenum Content in U-Mo Alloy %					
	2wt%	4wt%	6wt%	8wt%	10wt%
k ^a	5.95e-3	4.86e-3	2.15e-3	3.11e-5	1.08e-5

^aLinear reaction rate (mg wt gain/cm²/h). Average of two samples.

2. U-Mo/Water Reaction

The initial (i.e., induction period) reaction rate of uranium-molybdenum alloys with water was lower than the corresponding reaction of pure U metal by one to three orders of magnitude. However, the reaction rates in tests with small samples often accelerated after a certain time. The apparent accelerated rate corresponded to discontinuous failure^{63, 88} and the concomitant increase in surface area, analogous to the apparent rate transition observed in humid air and coincident with severe cracking.⁶ The rate of discontinuous failure and the rate of surface area increase have not been determined as a function of time or conditions, nor correlated with the apparent reaction acceleration. Therefore, the effects of discontinuous failure on the apparent reaction rate were not included in this review. This review does evaluate the corrosion rates of U/Mo during the induction period of the reaction.

The temperature dependence of the reaction rate of U-Mo alloys with water is depicted in Figure 23. The reaction rate data were grouped according to a molybdenum content threshold of 8 wt% that corresponded to the lowest critical composition of gamma phase stability for water-quenched alloys. For the data reviewed, all samples were heat treated at 800-850°C to

establish a gamma phase microstructure, unless otherwise noted. The reaction rate of as-cast U-Mo at 100°C was included to illustrate the effect of heat treatment. This author determined Arrhenius-type rate expressions by using standard linear regression methods. The low-Mo U alloys/water reaction was comprised of only a limited number of data, including only one datum at 343°C (as shown Figure 23). Since statistical analysis (i.e., Cook's Analysis) indicated that the one datum at 343°C had a very strong influence on the regression fit, the Arrhenius rate dependence was determined for two cases: (a) including all data (eq. III-1) and (b), excluding the single datum at 343°C, respectively

$$k_l = 1.28 \times 10^4 \exp\left[\frac{-37.8 \pm 8.2 \text{ kJ/mol}}{RT}\right] \text{ mg metal/cm}^2/\text{h at 100-343}^\circ\text{C and (eq. III-1)}$$

$$k_l = 1.15 \times 10^8 \exp\left[\frac{-66.5 \pm 12.2 \text{ kJ/mol}}{RT}\right] \text{ mg metal/cm}^2/\text{h at 100-178}^\circ\text{C. (eq. III-2)}$$

The temperature dependence of the U->8 wt%Mo/H₂O reaction rate is given as

$$k_l = 1.58 \times 10^6 \exp\left[\frac{-80.5 \pm 10.6 \text{ kJ/mol}}{RT}\right] \text{ mg metal/cm}^2/\text{h at 302-440}^\circ\text{C. (eq. III-3)}$$

The activation energy of the reanalyzed low Mo expression excluding the 343°C datum (eq. III-2) was twice that of the original expression (eq. III-1), which demonstrated the strong influence of the high temperature datum. The goodness of fit results for the two expressions were both acceptable with betas of 0.80 and 0.85 for eqs. III-1 and III-2, respectively. The high temperature datum (at 343°C) was within acceptable limits of variability (i.e., less than 3 times the standard deviation), so it could not be excluded as an outlier on purely statistical arguments. The temperature dependence (activation energy) of the U-low Mo water reaction excluding the 343°C datum (eq. III-2) was statistically the same, given the data scatter, as that of the high Mo alloy (eq. III-3). As the activation energy of eq. III-2 was more consistent with that of the high Mo rate expression (eq. III-3) and the temperature dependence of eq. III-1 was strongly influenced by the single datum at 343°C, (eq. III-2) (which omitted the single datum at 343°C) was considered the best fit for the U-low Mo/water reaction rate. The low Mo and high Mo trend lines, eq. III-2 and III-3 are depicted in Figure 23.

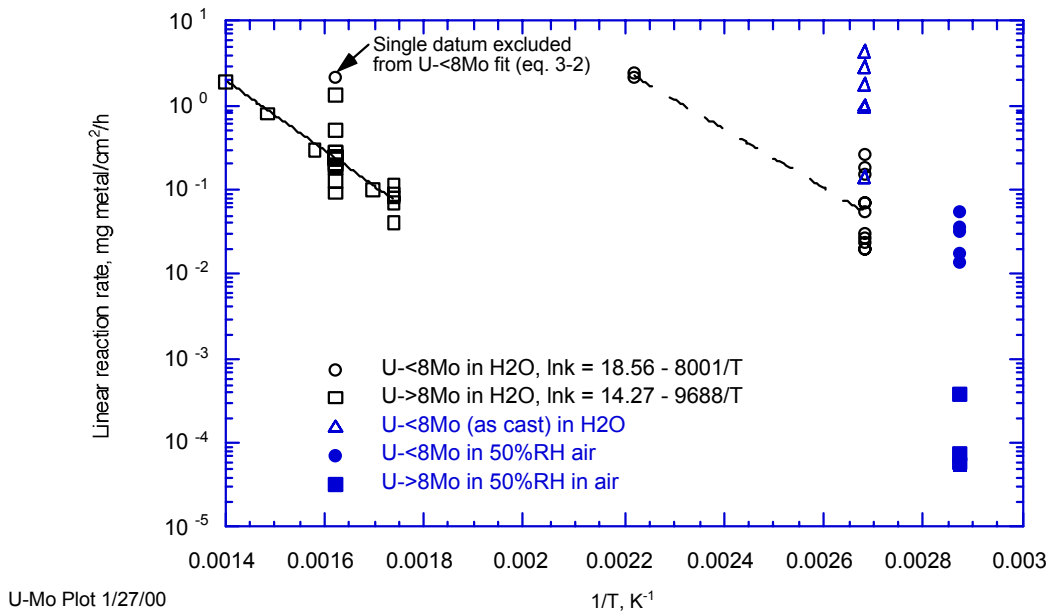


Figure 23. Summary of uranium-molybdenum alloy/water reaction rate at temperatures between 100 and 440°C.

The reaction rates of U-Mo with water were expected to be higher than the reaction rates with humid air, based on the uranium metal corrosion chemistry. There were no water reaction rate data at 75°C to compare with Waber's humid air data at 75°C. However extrapolations of equations III-2 and III-3 to 75°C were of the same order of magnitude as the humid air data for the corresponding alloys, considering the limited number of data, the uncertainty in the U-Mo/water rate expressions and the large extrapolation.

C. Kinetics of Uranium-Niobium Oxidation

Uranium-niobium is a highly gamma-miscible system like uranium-molybdenum. The corrosion rate of uranium-niobium alloys is microstructure-dependent and is lowest for the gamma phase. In phase diagram studies, the minimum niobium content for retaining the gamma phase was established between 2.0 and 4.0 wt%Nb⁸⁹ for water quench. At a cooling rate of 18°C/s, at least 4.9 wt% niobium content is necessary to retain the gamma phase.⁶² The gamma phase is metastable below temperatures of 400°C, transforming to the beta and alpha phase, but stability is increased with niobium content. A significant difference in reaction rate is observed for furnace-cooled and water-quenched alloys and for alloys with less than the minimum amount niobium for retaining the gamma phase upon cooling. For convenience, the reaction rate of uranium-niobium alloys with greater than 3 wt%Nb and cooled by quenching are discussed separately from alloys which have a lower Nb content or were slow cooled after heat treatment.

1. U-Nb/Water Reaction

A number of investigators^{41, 43, 62, 85, 90} have reviewed the reaction rate of uranium-niobium alloys with water. The reaction rate is significantly lower compared to the rate of unalloyed uranium. The mechanism of decreased corrosion rate is typical of high-miscibility gamma alloys. The U-Nb alloy forms an adherent oxide film, which is under compression and

epitaxial with gamma uranium. The oxide film induces a tensile stress on the metal substrate that eventually exceeds the elastic limit and leads to discontinuous cracks and failure.⁶² The reaction kinetics is linear.

This author determined the temperature dependence of the uranium-niobium/water reaction rate by regression analysis of literature data. A summary of the data and the resulting Arrhenius expressions are shown in Figure 24. The data were divided into two groups by the criteria of 3 wt% Nb alloy content and water quench cooling rate, threshold conditions for forming the gamma microstructure. The Arrhenius rate expressions for the U-<3wt%Nb/H₂O and U->3wt%Nb/H₂O reactions are respectively,

$$k_l = 7.19 \times 10^{11} \exp\left[\frac{-90.3 \pm 33.3 \text{ kJ/mol}}{RT}\right] \text{ mg metal/cm}^2/\text{h at } 100\text{-}178^\circ\text{C and (eq. III-4)}$$

$$k_l = 1.57 \times 10^4 \exp\left[\frac{-53.2 \pm 7.7 \text{ kJ/mol}}{RT}\right] \text{ mg metal/cm}^2/\text{h at } 100\text{-}343^\circ\text{C. (eq. III-5)}$$

The U-Mo data and the U-Nb data exhibit considerable scatter, largely because of the high experimental variability at the low temperature. While the corrosion rates of the U-high Nb/water reaction were significantly lower than those of the U-low Nb/water reaction, the Arrhenius temperature dependencies (the Arrhenius values) were statistically the same, within the variability of the data. Relative to the U-Mo/H₂O system, the U-Nb/H₂O reaction rates and temperature dependencies were statistically the same, within a 2-sigma statistical variation. The activation energies of the low alloy/water reactions alloys were 66.5 ± 12.2 for Mo and 90.3 ± 33.3 kJ/mol for Nb and those of the high alloy/water reactions were 80.5 ± 10.6 and 53.2 ± 7.7 kJ/mol, for Mo and Nb, respectively.

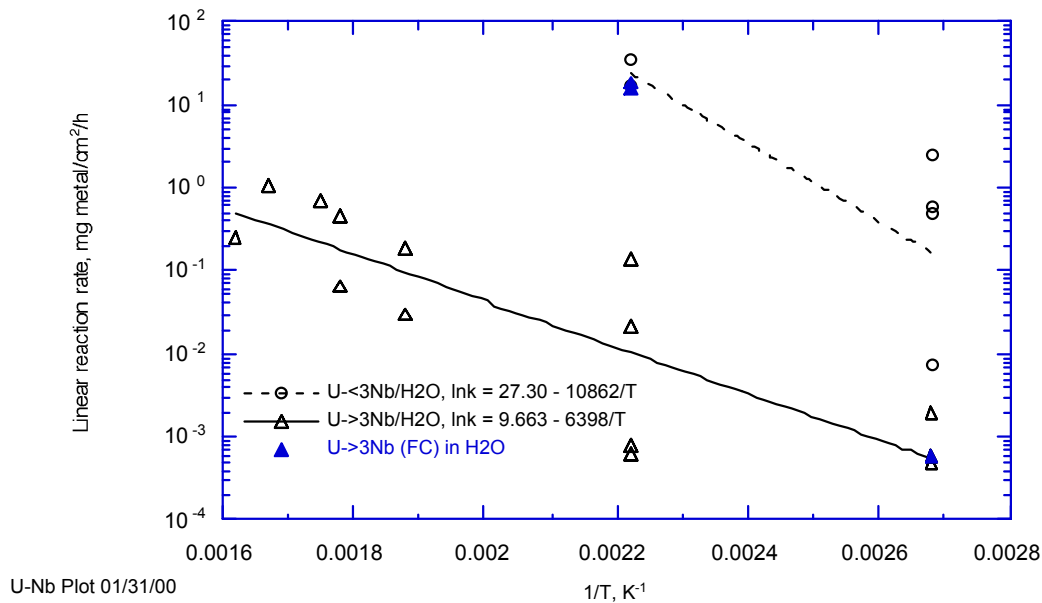


Figure 24. Summary of uranium-niobium alloy/water reaction rates at temperatures 100 to 343°C.

D. Kinetics of Zirconium-Uranium Oxidation

In the uranium-molybdenum and uranium-niobium alloys relevant to the DOE SNF inventory, uranium is the primary element and the other metal is the secondary element with composition limited to less than 30wt%. The uranium-zirconium alloys relevant to the DOE SNF inventory are zirconium-rich, with greater than 90% of the inventory consisting of fuel with a composition of ~95 wt% zirconium.⁹¹ Hence, the reaction rate data reviewed in this report were limited to zirconium-uranium alloys with at least 20 wt% Zr. The kinetics of the Zr-U/O₂ and Zr-U/H₂O reactions were linear and essentially independent of the uranium content at compositions between 20-97wt% zirconium. This author derived Arrhenius type expressions for the two systems employing linear regression analysis. Figure 25 displays the literature data and the regression fit Arrhenius expressions. In the high zirconium alloy, the corrosion behavior is largely governed by the zirconium. The magnitude and Arrhenius dependence of the Zr-U/H₂O reaction rate were similar to those of the U-Mo and U-Nb alloys, which were significantly less than the unalloyed U metal water oxidation rate. The following sections address the reaction rates of Zr-U in oxygen and in water.

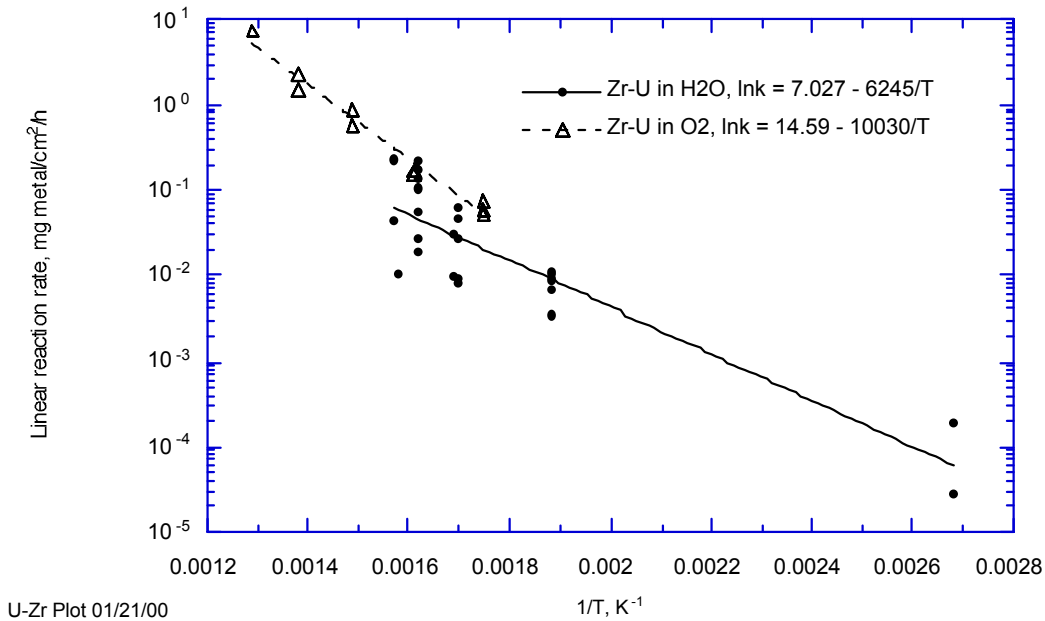


Figure 25. Summary of reaction rate of uranium-zirconium alloy with water and with oxygen at temperatures below 500°C.

1. Zr-U/Oxygen Reaction

Barnartt, et al.⁹² investigated the reaction rate of 50 wt% zirconium-uranium alloy in oxygen, and found linear kinetics for oxidation between 300 and 500°C and parabolic kinetics for the reaction at 200 and 250°C. Barnartt, et al. obtained separate fits for the annealed and as-cast samples with slightly different activation energies. For annealed samples at temperatures between 300 and 500°C, Barnartt determined an activation energy of 45.5 kJ/mol with linear kinetics. No activation energy was given for lower temperatures because of large scatter in the data. However, the parabolic rate constants were reported as 3.0×10^{-5} (mg/cm²)²/h and 18.0×10^{-5} (mg/cm²)²/h at 200 and 250°C, respectively. This author reanalyzed the annealed and as-cast data at temperatures between 300 and 500°C as one data set by standard linear regression methods, which provided a reasonably good fit given as

$$k_l = 2.17 \times 10^6 \exp\left[\frac{-83.4 \pm 4.5 \text{ kJ/mol}}{RT}\right] \text{ mg metal/cm}^2/\text{h.} \quad (\text{eq. III-6})$$

Matsui, et al.⁹³ investigated the oxidation behavior of 20 wt% zirconium-uranium alloy in oxygen. Matsui and associates fit their data to parabolic (i.e., mixed parabolic and linear) kinetics in the temperature range 150 to 230°C and to linear kinetics at temperatures between 370 and 450°C. The activation energies of the rate constants at temperatures below 230°C were reported as 100.3 ± 4.8 kJ/mol for k_l and 70.7 ± 13.3 kJ/mol for k_p .

2. Zr-U/Water Reaction

Reaction rate data for zirconium-uranium alloys with water were reported in a small number of references.^{41, 64, 85, 94, 95} The reviewed rate data were in the temperature range 100-360°C with an alloy composition range of from 40 to 97 wt% zirconium, except one datum for >20 wt% Zr. Bauer reported the maximum, minimum, and mean corrosion rates of U-90.7 wt%Zr alloy. However the minimum rate data were excluded from this analysis as outliers. The temperature dependence of the U-Zr (20-97 wt%)/H₂O reaction rate for temperatures between 100 and 363°C is

$$k_l = 1.13 \times 10^3 \exp\left[\frac{-51.9 \pm 5.5 \text{ kJ/mol}}{RT}\right] \text{ mg metal/cm}^2/\text{h.} \quad (\text{eq. III-7})$$

The reaction rate of zirconium-uranium alloys with water was around five orders of magnitude lower than the reaction rate of unalloyed uranium with water and had similar temperature dependence. The water reaction rate of Zr-U was slightly lower than that of U-Mo and U-Nb, but not significantly.

At temperatures above 300°C, the oxidation reaction rates of zirconium-uranium alloys in oxygen were higher than those in water (see Figure 25); however at lower temperature, the oxygen reaction rate was lower than the water rate, based on an extrapolation of the high temperature oxygen rate data. This crossover in the oxygen and water rates for the Zr-U system contrasts with pure uranium which has a reaction rate in water approximately 200 times higher than in oxygen at temperatures between 20 and 350°C (cf. Section II). The crossover in the Zr-U rates can be explained by the greater temperature dependence of the reaction rate in air compared to water. In addition, the higher reaction rates for zirconium-uranium alloys in air compared to water might be due to the difference in the microstructure of the samples or the resultant oxide. The alloy samples tested in air by Barnartt were cold-rolled or slow cooled after heating to gamma phase which would result in mixed phases or epsilon phase, respectively, whereas the samples studied in water were gamma heated and quenched to retain the gamma phase.

E. Irradiation Effects on Uranium Alloy Oxidation

The irradiated uranium alloys corrosion rates were investigated in the 1940s and 1950s as part of the reactor fuel development programs managed by Bettis Atomic Power Laboratory. The results of the reaction rate tests, mechanistic studies, and microstructural analyses were summarized in a series of reports.^{63, 64, 87, 88} In reactor, the corrosion rates of U-Mo, U-Nb and U-Zr samples exposed to high temperature water were unchanged relative to out-of-reactor measurements. In fact, observations indicated that radiation promoted the stability of the gamma phase and even caused phase reversion to the gamma phase at sufficiently high fission rates.⁸⁷ The average corrosion rates of irradiated samples tested out of reactor were the same as unirradiated samples, however the times to discontinuous failure of some of the alloys were significantly reduced and were proportional to the exposure. The reaction rates and times to failure for U-Mo and U-Nb alloys irradiated up to 2000 MWd/tU are shown in Table 12. The U-Mo alloys exhibited a reduction in time to failure at 302°C, but there was no change at 343°C. The one datum for irradiated U-10wt% Nb also showed a significant decrease in time to failure. Figure 26 compares the corrosion rates of irradiated uranium alloys with those of the unirradiated uranium-alloys reaction rates calculated from eq. III-3 for U-Mo and eq. III-5 for U-Nb. The irradiated U-alloys data were relatively few and had a scatter of around one order of magnitude. Essentially, the corrosion rates were the same as unirradiated U-alloys, considering the scatter of the data.

Table 12. Corrosion rates of non-irradiated and irradiated (gamma quenched) uranium alloys.⁸⁷

Temperature, °C	Sample No.	Composition	Exposure, MWd/t	Avg. Corrosion rate, mg/cm ² /h	Days to Failure	
302	30C	U-12 wt%Mo	0	0.09	52-66	
	80C		0	0.11	45-52	
	81		230	0.05	14-21	
	40		650	0.05	7-14	
	61		835	0.01	14-21	
	8		1250	0.05	1-7	
	0		1575	0.05	7-14	
	51		1690	0.04	1-7	
	90		2000	0.04	1-7	
	343		6	U-10.5 wt%Mo	0	0.24
5		0	0.25		21-35	
13		445	0.26		22-28	
12		900	0.20		35-42	
11		1050	0.30		22-28	
30		U-12 wt%Mo	0	0.25	21-35	
29			0	0.20	21-35	
27			445	0.30	20-22	
26			900	0.11	22-28	
24			940	0.13	35-42	
F-25			U-10 wt%Nb	0	0.25 – 1.33	35
F-5				500	0.23	NR
F-4				720	1.87	NR
F-3				820	4.01	2-3

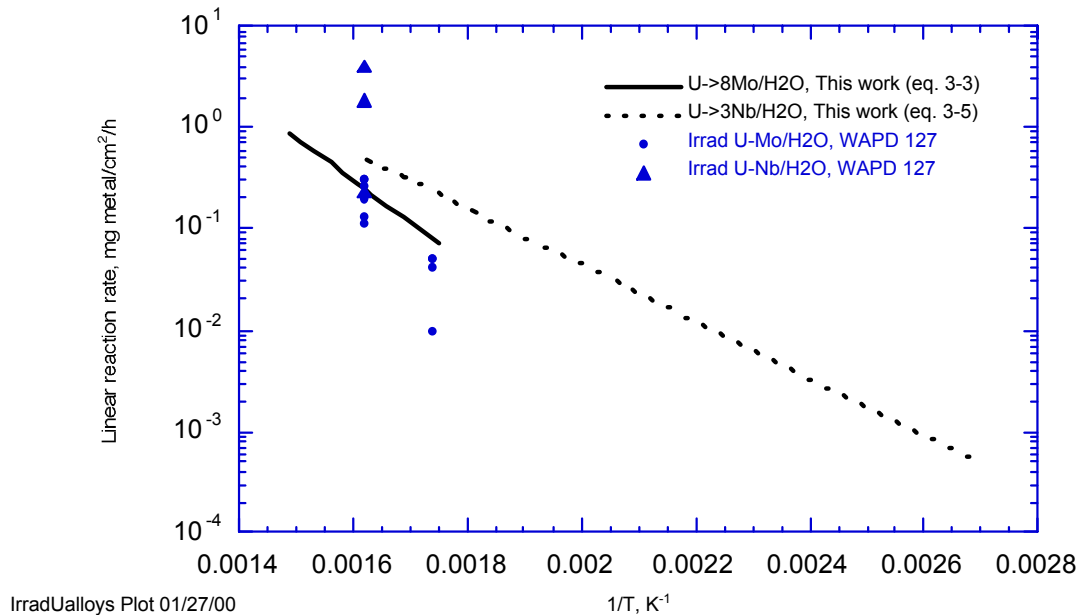


Figure 26. Reaction rates of irradiated uranium-molybdenum and uranium-niobium alloys in water at temperatures between 100 and 400°C.

F. Summary of Uranium Alloy Oxidation

The oxidation rates of uranium-molybdenum, uranium-niobium and zirconium-uranium alloys were dependent on the microstructure with the lowest rates corresponding to gamma phase. Retention of the gamma phase was a function of alloy composition and cooling rate with minimum compositions of 7 and 3-4 wt% for water quenching of molybdenum and niobium alloys, respectively. The corrosion rate data of U-Mo and U-Nb were reasonably grouped using these compositions and water quench cooling as critical values. The uniform reaction rates of the gamma phase alloys were significantly lower than those of unalloyed uranium. At long times, the samples exhibited an accelerated rate and discontinuous premature failure by matrix breakup. The phenomenon of matrix breakup is not peculiar to uranium alloys, but was also observed in unalloyed uranium exposed to high temperature water. Matrix breakup collated with observations of a hydride phase in the U-alloys and with high carbon impurity levels in pure uranium. Discontinuous failure probably occurs by preferential attack along non-homogeneous secondary phases, such as hydrides for the alloys or carbide stringers in pure uranium, that resulted in cracks and an increased surface area. Arrhenius-type rate expressions for U-Mo, U-Nb and Zr-U water reactions were determined by linear regression analyses of the literature data and are summarized in Table III-3. The high Mo and Nb and Zr-U alloys had similar corrosion rates that were approximately four to five orders of magnitude lower than for unalloyed uranium. In contrast, the corrosion rates of the low Mo and Nb alloys were slightly less than those of unalloyed uranium, but not significantly. The temperature-dependent expressions were somewhat limited in range of temperature because of the paucity of data. With this caveat and the significant scatter in the data, the activation energies of the water reaction with U-Mo, U-Nb

and Zr-U alloys were essentially the same and constant over temperatures between 100 and 350°C. The temperature dependencies were comparable to those of unalloyed uranium/water reaction, which suggests a similar rate-determining mechanism. According to the data reviewed, irradiation did not effect uniform oxidation rate of uranium alloys; however the time to failure for some alloys was decreased significantly.

Table 13. Summary of rates of reaction for uranium-molybdenum, uranium-niobium and zirconium-uranium alloys with oxygen and water at temperatures less than 500°C.

Reaction	Rate Expression mg/cm ² /h or mg/cm ² /h/kPa ^{0.5} (H ₂ O _v)	Conditions	Eq. No.
U-<8wt%Mo/H ₂ O	Linear: $k_l = 1.15 \times 10^8 \exp[-66.5 \pm 12.2/RT]$	100-178°C	III-2
U->8wt%Mo/H ₂ O	$k_l = 1.58 \times 10^6 \exp[-80.5 \pm 10.6/RT]$	302-440°C	III-3
U-<3wt%Nb/H ₂ O	Linear: $k_l = 7.19 \times 10^{11} \exp[-90.3 \pm 33.3/RT]$	100-178°C	III-4
U->3wt%Nb/H ₂ O	$k_l = 1.57 \times 10^4 \exp[-53.2 \pm 7.7/RT]$	100-343°C	III-5
U-Zr(50wt%)/O ₂	Linear: $k_l = 2.17 \times 10^6 \exp[-83.4 \pm 4.5/RT]$	300-500°C	III-6
U-Zr(20-97wt%)/H ₂ O	Linear: $k_l = 1.13 \times 10^3 \exp[-51.9 \pm 5.5/RT]$	100-363°C	III-7

IV. OXIDATION RATES OF ALUMINUM-BASED DISPERSION FUELS

The aluminum-based dispersion fuels in the DOE spent nuclear fuel inventory were used primarily in domestic and foreign research and test reactors. The aluminum dispersion fuels consist of uranium-bearing fuel particles discontinuously dispersed within an aluminum alloy matrix. The fuel particles of the Al dispersion fuels are composed of UAl_x, U₃O₈, or U_xSi_y fuel particles.⁹⁶ The uranium intermetallic alloys, such as U-Al and U-Si, are differentiated from the solid solution alloys, like U-Mo, U-Nb and U-Zr, because the intermetallic alloys form compounds or structures with discrete stoichiometry within the host phase (e.g., UAl_x and U_xSi_y) rather than solid solutions with a range of compositions. The matrix corrosion rate determines in large part the bulk reaction rates of aluminum dispersion fuels. The reaction rates of the fuel compounds are also of interest, due to the possibility of localized corrosion leading to accelerated radionuclide release.

The oxidation processes and kinetics discussed in this report are limited to pure water, therefore they are not directly applicable to corrosion in water chemistry that is very different. The corrosion rate of aluminum alloys is known to be sensitive to water chemistry variations in conductivity, pH, and impurity levels.^{97, 98, 99} Specifically, aluminum is susceptible to localized

attack as pitting in water chemistries of high conductivity and impurities such as chlorine and copper.^{97, 98, 99} The dependence of aluminum corrosion behavior on water chemistry has been observed in fuel storage basins across the DOE Complex at Hanford, Idaho National Engineering and Environmental Laboratory, Brookhaven National Laboratory, Oak Ridge National Laboratory and Savannah River Site.¹⁰⁰ In fuel storage basins with water chemistry of conductivity $>50 \mu\text{S}/\text{cm}$ and chlorine levels $>6 \text{ ppm Cl}$, aluminum based spent nuclear fuel and aluminum alloy materials have exhibited pitting rates many times greater than the general corrosion rate.^{100, 101, 102, 103, 104, 105, 106} In fuel storage basins which have maintained pure water through demineralization ($\sim 1\text{-}3 \mu\text{S}/\text{cm}$ conductivity and $<1 \text{ ppm Cl}$), the aluminum alloys have exhibited low corrosion rates and no pitting over time periods of ten years or longer.^{100, 102, 103, 105, 106}

The aluminum dispersion fuel work spans four decades of research reactor fuel development and is still ongoing as part of the Reduced Enrichment of Research and Test Reactor (RERTR) Program. However, there are relatively few papers reporting oxidation rates of aluminum-based dispersion fuels or the reaction rates of uranium intermetallic alloys. Data for the aluminum-based uranium aluminides were for aluminum-rich uranium alloys with compositions of Al-(1.9-53 wt%)U, which have a multi-phase microstructure of uranium aluminide intermetallics (UAl_2 , UAl_3 and UAl_4) and aluminum matrix. There were almost no studies reporting the reaction rate of uranium oxide and uranium silicide dispersions, except a few corrosion tests of fuel plates with defected cladding. Rate data for U_xSi_y were correlated as a supplement to the Al based dispersion data. Tri-uranium octaoxide (U_3O_8) oxidation has been studied as part of uranium dioxide studies and its behavior is covered in the second volume of this report. The reaction rate of aluminum alloys has been studied independently from aluminum matrix dispersion fuels and is well characterized in the temperature range of interest of most research reactors (i.e., less than 100°C). The corrosion rates of aluminum dispersion fuels have also been mostly limited to temperatures below 100°C . However, a few investigators reported corrosion rates at higher temperatures as part of research programs studying oxidation behavior at storage or stabilization/ treatment process conditions. Most of the work on uranium silicides was performed before 1975 as part of U.S. and Canadian fuel development programs for naval ship propulsion and electric power generation.

This review includes the oxidation kinetics of aluminum-based dispersion fuels with oxygen, anoxic water vapor and water, and the reaction rate of aluminum alloys in pure water. This author developed Arrhenius-type expressions via regression analyses, where sufficient data were available. The reaction rate of Al- UAl_x was essentially the same as that of Al alloys, with little variability in the data. The reaction rate of Al dispersions of U_3O_8 and U_xSi_y (derived from defected fuel plates) showed a large scatter, over 6 orders of magnitude, with insufficient data to make any conclusions. The reaction rates of U-Si intermetallics were slightly higher than Al alloy, but still around 10,000 times lower than the rate of unalloyed uranium. A summary of the recommended rate expressions is presented in the last section.

A. Oxidation Mechanisms of Aluminum-Based Dispersion Fuels

There are few studies of the oxidation mechanism of Al dispersion nuclear fuels, but the oxidation behavior is generally considered to be determined by the aluminum matrix, which constitutes the majority of the fuel volume. There has been no observation reported of localized attack of the fuel particles with respect to the Al matrix. For example, surface characterization of

Al-UAl_x specimens reacted with saturated water vapor revealed a uniform corrosion layer of hydrated aluminum oxide, similar to that observed on aluminum, with no indication of preferential attack.¹⁰⁷

1. Microstructural Effects on Oxidation

The aluminum-based dispersion fuels typically have fuel volume percentages of 20 vol% for UAl_x and U₃O₈ and 30 vol% for U_xSi_y intermetallics. Typical microstructures of irradiated dispersion fuels for the three fuel dispersoids are shown in Figure 27.

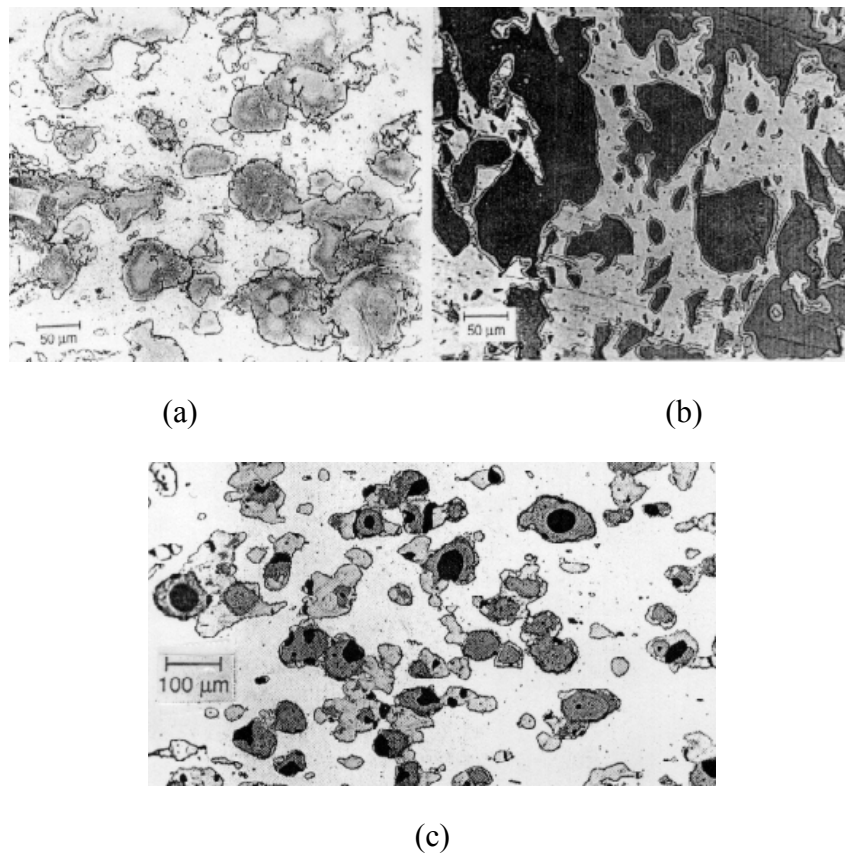


Figure 27. Typical microstructures of aluminum-based dispersion fuels irradiated to 80-90% burnup with Al matrix (light phase) and fuel dispersions (dark phase) of (a) UAl_x, (b) U₃Si₂, and (c) U₃O₈.⁹⁶

The fuel particles (darker phase) are distributed uniformly throughout the aluminum alloy matrix (light phase) and have a volume fraction low enough to prevent interconnectivity of fuel particles. Due to this design and other inherent fuel properties, the three fuel types exhibit good irradiation performance with little fission gas release, low swelling and an acceptably low amount of fuel-matrix interaction. The UAl_x and U_xSi_y fuel dispersions may consist of multiple compounds depending on composition and heat treatment. The constituent phases of the U-Al and U-Si intermetallic systems are discussed in this section since the microstructure effects the corrosion behavior.

The aluminide dispersions, Al- UAl_x , are by composition aluminum-rich uranium alloys. However, the Al-U alloys are referred to as Al- UAl_x throughout this report for consistency and to emphasize the dispersoid/matrix microstructure. The uranium-aluminum system includes three uranium aluminide compounds, UAl_2 , UAl_3 , and UAl_4 , with uranium fractions of 81.5 wt%, 74.6 wt%, and 65.3 wt%, respectively (see Figure 28). The phase composition with respect to aluminum-uranium solid solution and uranium aluminide intermetallic compounds depends on the uranium content of the alloy and the processing conditions. The microstructure of an equilibrated alloy of high aluminum (≥ 35 wt% Al) consists of UAl_4 intermetallic in an aluminum matrix with a small amount (≤ 0.06 wt%) of dissolved U^{96} and that of a high uranium content (>64.2 wt% U) consists of $UAl_4 + UAl_3$, $UAl_3 + UAl_2$ or $UAl_2 + Al-U$ solid solution. Fabricated dispersion fuels in practice however, are not at equilibrium, so that all three compounds form, denoted as UAl_x , along with aluminum. The typical phase distribution for an Al- UAl_x (68.8 wt%U) alloy, reported for ATR fuels, is about 7 wt% UAl_2 , 76 wt% UAl_3 , 13 wt% UAl_4 , and 4 wt% Al.¹⁰⁸

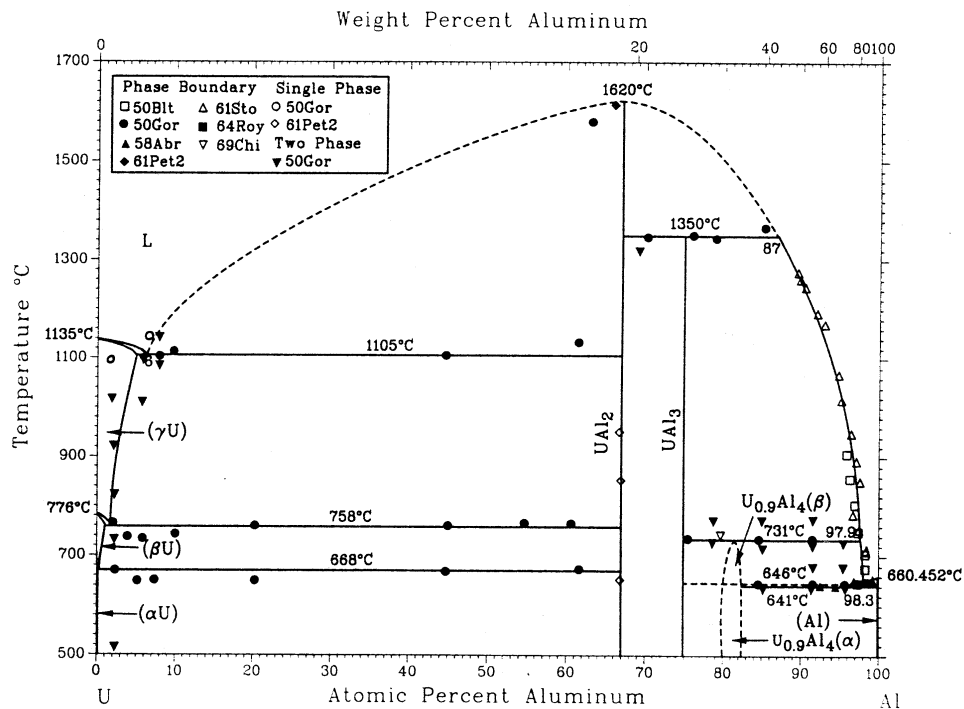


Figure 28. Phase diagram of the aluminum-uranium system.

The dispersed particles are brittle relative to the aluminum matrix, but in the case of uranium aluminides, ductility can be retained by rapid cooling resulting in non-equilibrium phases of UAl_2 and UAl_3 dispersed throughout a ductile aluminum matrix.⁶² The uranium aluminides are stable under irradiation to high fission density and burnup. At burnups to 80 at% ^{235}U , the swelling rate averages approximately 4 vol% per 10^{27} fissions/ m^3 , and fuel-matrix interaction is not significant. Since uranium aluminides exhibit limited swelling up to high burnup and fission density, the uranium loading is limited by fabricability, which limits the U content to around 35-40 wt% U in practice.⁹⁶

There are a number of phases in the uranium-silicon system (see Figure 29), of which USi , U_3Si_2 and U_3Si are the most significant to fuel alloys. The uranium fractions of the compounds are 89.5 wt%, 92.7 wt%, and 96.0 wt%, respectively. The delta phase U_3Si is of particular importance because it has the highest uranium density of these compositions and it exhibits the greatest corrosion resistance as a monolith in high temperature water. However, since U_3Si exhibits relatively high fission gas swelling rates at low or moderate fission densities, its use is limited to reactors with a rod-type fuel geometry, such as many Canadian reactors.⁹⁶ In the U.S. where the major fuel geometry of aluminum-based dispersion fuels is the plate-type, U_3Si_2 is the preferred compound because of its stable swelling behavior and medium-density uranium loading. U_3Si_2 (7.3 wt%Si) forms directly from the melt while U_3Si forms by lengthy heating near the peritectoid temperature $930^\circ C$,¹⁰⁹

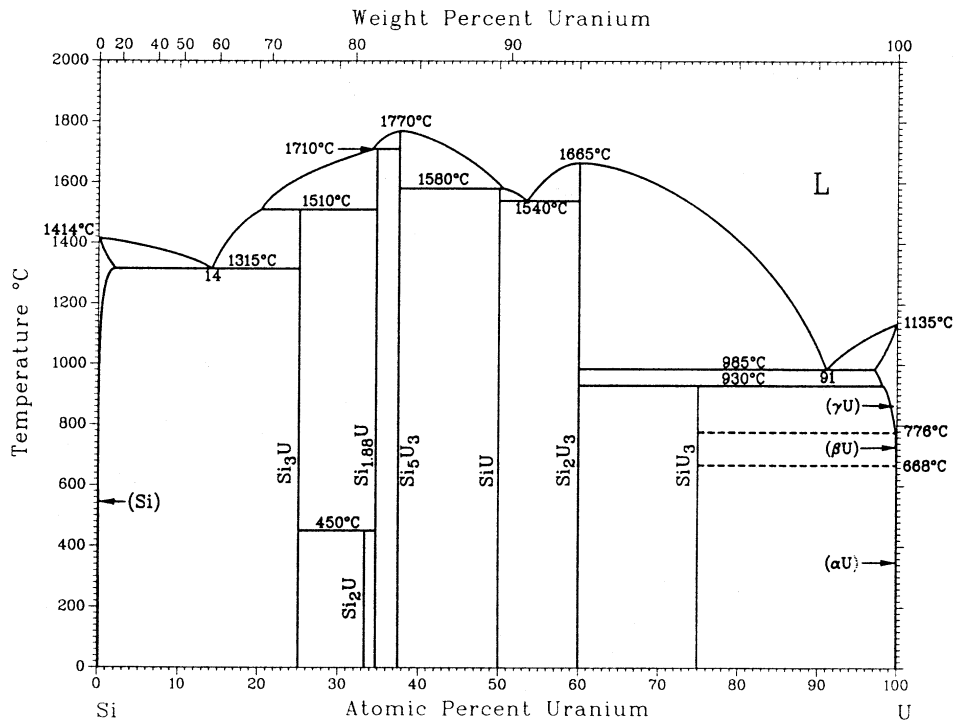


Figure 29. Phase diagram of uranium-silicon system.

As-cast alloys of delta phase composition (3.8 wt%Si) consist of uranium and U₃Si₂ particles. Consequently, alloys of delta phase composition (3.8 wt%) must be heat treated to form the delta phase U₃Si microstructure. The U₃Si phase grows around the U₃Si₂ particles by a sluggish reaction sensitive to local variation in silicon content. Most uranium silicide fuels consist of a mixture of several of the uranium silicide phases and possibly uranium-silicon solid solution. The corrosion resistance is sensitive to microstructure and composition, with delta phase exhibiting the best performance. All reaction rates are reported for the heat-treated condition, unless otherwise noted.

2. Oxidation Mechanism of Aluminum-Based Dispersion in Water

In aluminum-based dispersions, the aluminum matrix typically comprises 70-80 vol% of the fuel material; consequently, it dominates the corrosion behavior of the high-aluminum fuels. Therefore, the oxidation mechanism of aluminum-based dispersion fuels is considered the same as that of the aluminum matrix with similar reaction kinetics and corrosion products. At temperatures above 80°C, aluminum forms hydrated aluminum oxide (boehmite) in water according to the reaction



Similarly, hydrated aluminum oxide (boehmite) was observed as the reaction product of Al-UAl_x (i.e., Al-10-18 wt%U) alloys/ water vapor reaction.^{107, 110} Aluminum oxidation rates are initially very rapid and decrease with time as a protective oxide layer forms. The initial kinetics are usually described by parabolic or parilinear models. However, after the initial rapid development of the oxide film, the long-term corrosion rates of aluminum-based dispersions are adequately described by linear kinetics. In this report, linear kinetics serve to model the reaction rates of Al-based dispersion fuels and aluminum alloys, consequently, the reaction rates are only applicable to corrosion at long times in pure water chemistry.

B. Kinetics of Aluminum Alloy Oxidation

1. Al-Alloy/ Water Reaction

Aluminum alloys have been researched for over fifty years as a potential cladding material for nuclear reactor fuel elements. Its relative high abundance, high strength, low neutron absorption and general good corrosion behavior qualified it for consideration. The corrosion rates of aluminum alloys reported by a number of investigators were reviewed in this report.^{111, 112, 113, 114, 115, 116, 117, 118} The aluminum alloy data were reviewed to evaluate whether the aluminum based dispersion fuels behave like aluminum or behave like uranium. The review was limited to the oxidation rates of aluminum alloys types 6061 and 8001, which are typical of alloys used in reactor applications. The long term linear corrosion rate of Al alloys is dependent on the specific alloy, differing by factors of 2 to 4. However, a single rate expression for the Al alloys/water reaction was derived from all the alloy data to illustrate the general corrosion rate of aluminum alloys. The scatter of the pooled data is within a factor of ten of the mean (see Figure 30) and is

attributable to both alloy to alloy variation as well as measurement variability. The Arrhenius expression for the Al alloys/water reaction was determined as

$$k_l = 4.29 \exp\left[\frac{-32.8 \pm 1.8 \text{ kJ/mol}}{RT}\right] \text{ mg metal/cm}^2/\text{h at 25-360}^\circ\text{C.} \quad (\text{eq. IV-3})$$

Although the reaction product of aluminum oxidation changes from bayerite ($\text{Al}(\text{OH})_3$) at low temperatures to boehmite (AlOOH) at temperatures above $70\text{-}80^\circ\text{C}$, the long term reaction rate was correlated by a single Arrhenius expression from 30°C to 360°C (see Fig. 30). There is high confidence in this conclusion based on an R value of 0.95 for the regression fit and the long time period over which the low temperature data were obtained. The low temperature data were collected over a period of ten to thirteen years as part of corrosion surveillance monitoring programs at fuel storage basins with good water chemistry at the INEEL¹¹⁸ and at Hanford.¹⁰⁶ The sample coupons were weighed every six to twelve months over a period of ten to thirteen years, so they are a very good indication of long term corrosion of aluminum alloys in pure water.

Lam, et al. also investigated the reaction rate of aluminum alloys 1100, 5052, and 6061 in 200°C saturated water vapor. They reported Arrhenius expressions for aluminum alloys 1100 and 6061 based on a power law regression fit to reaction rate data at 150 and 200°C . The resulting exponents were between 0.40 and 0.55,¹¹⁹ consistent with parabolic kinetics. However, the power law regression fits did not correlate well with the data at longer times, suggesting a paralinear kinetic model that changes from an initial parabolic rate to linear kinetics at long times. This author derived linear reaction rates based on Lam, et al.'s data at long times. The linear rates of Al alloy oxidation in water vapor were consistent with the regression fit of literature data for the water oxidation.

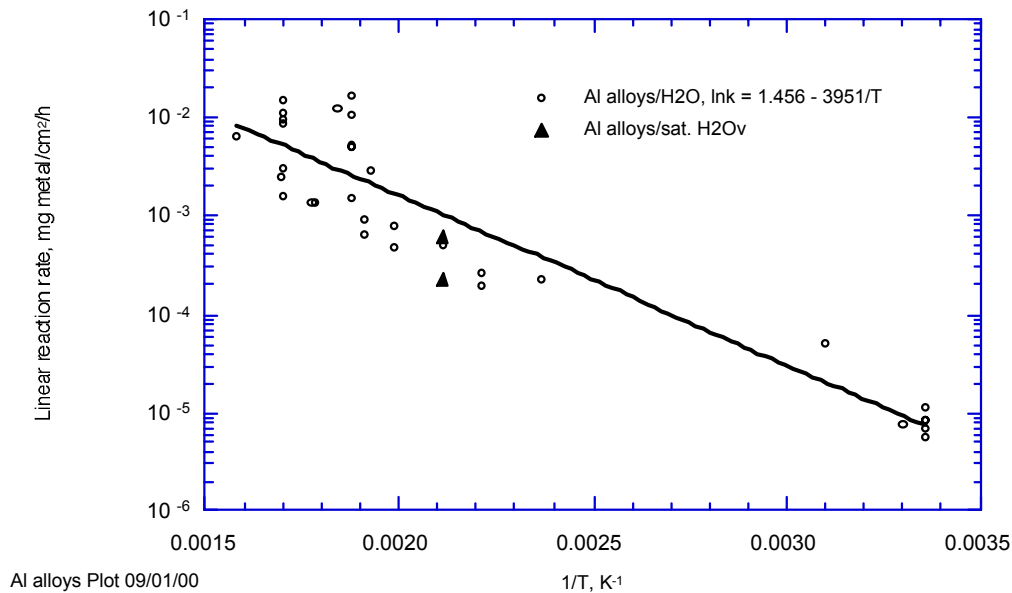


Figure 30. Summary of reaction rates of aluminum alloys (types 6061 and 8001) with water and saturated water vapor at temperatures between 30 and 360°C .

C. Kinetics of Aluminum Matrix-Uranium Aluminide Oxidation

The oxidation reaction rates of aluminum matrix-uranium aluminide (Al-UAl_x) dispersion fuels are similar to rates of aluminum alloys that form the matrix. The Al dispersion fuel oxidation exhibits a significant temperature dependence, but not as strong as uranium metal and its alloys. Oxidation is generally modeled by parabolic or paralinear kinetics, but at long times corrosion rates proceed by linear or quasi-linear growth. All the reaction rate data in this report were converted to linear reaction rates for use in describing reaction rates at long times and comparison purposes. This author determined Arrhenius expressions for the Al-UAl_x/H₂O reaction by regression analysis. The reaction rate data of Al-UAl_x in H₂O and saturated water vapor and the Arrhenius expression are shown in Figure 31, along with the Arrhenius expression for aluminum alloys derived in this work (eq. IV-3). The saturated water vapor reaction rate was similar to the reaction rate for immersion in water. The reaction rate and temperature dependence of Al-UAl_x dispersion fuels oxidation were essentially the same as those of aluminum alloys, which is a million times less than the rate of unalloyed uranium.

1. Al-UAl_x/Water Vapor Reaction

In support of spent fuel storage and disposition, Lam, et al. at the Savannah River Site recently investigated the reaction rate of aluminum-uranium alloys in saturated water vapor.^{107, 110, 119, 120} Lam, et al. investigated the corrosion rate of aluminum alloys and aluminum-uranium alloys with 10 and 18 wt% uranium in 200°C saturated water vapor. This author derived linear reaction rates from the portion of their data at long corrosion times. The reaction rate of Al-UAl_x alloys in saturated water vapor at 200°C was 2 to 8 x 10⁻⁴ mg/cm²/h. This was essentially the same as the reaction rate of 7.4x10⁻⁴ mg/cm²/h for Al-UAl_x in water (see Figure 31). These data indicate that the mean oxidation rates of Al-UAl_x are equivalent for water and water vapor, as was the case for oxidation rates of uranium metal.

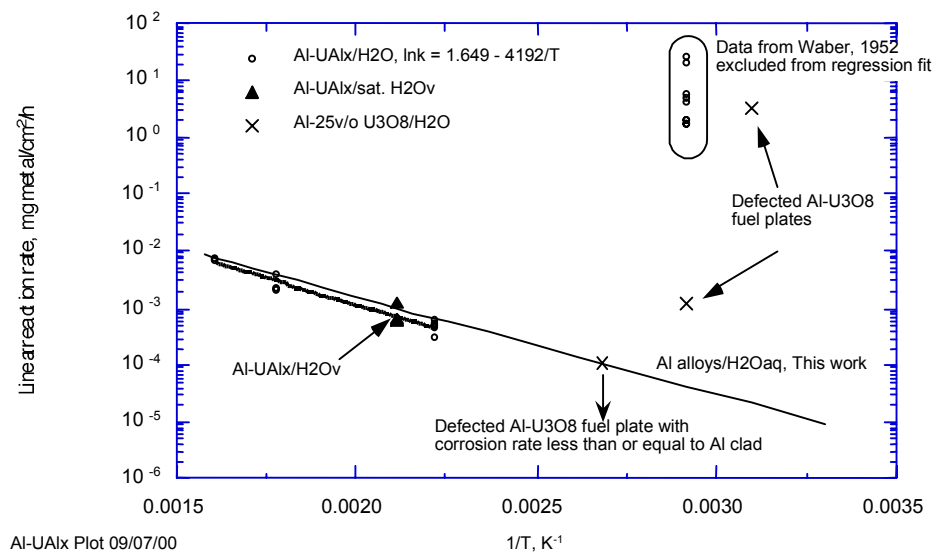


Figure 31. Summary of reaction rates of aluminum-based dispersions with uranium aluminide (equivalent to Al-1.9-53 wt%U alloys) and uranium-oxide with water and saturated water vapor at temperatures less than 360°C.

2. Al-UAl_x/Water Reaction

Few investigators have reviewed the reaction rates of aluminum-uranium aluminide dispersions with water.^{30, 62, 121, 122} The reaction rate of Al-UAl_x with water is governed (or “controlled”) by the corrosion behavior of the aluminum matrix. The reaction rates of Al-UAl_x with water are essentially the same as for the aluminum alloys with water, slightly smaller than the rate of U alloys/water, and much smaller than unalloyed U/ H₂O. The Al-UAl_x/H₂O and Al alloys/H₂O rates of reaction depend moderately on temperature, increasing by a factor of ten between 200 and 350°C. This author determined Arrhenius type expressions by regression analysis of the literature data.

The Al-UAl_x data showed little scatter except for one group of data at 70°C reported by Waber (see Figure 31), which were not included in the regression analysis. In Waber’s review of the corrosion of uranium and uranium alloys,³⁰ he reported weight change data for Al-UAl_x (1.9-30 wt% uranium) in water at 70°C and at 178°C. The reaction rates derived from the 178°C data were consistent with oxidation rates reported by other investigators in this temperature range, however the reaction rates at 70°C were 10,000 times higher than corrosion rates derived from release rate data at 25°C.^{123, 124, 125} Based on an evaluation of the inconsistency between Waber’s 70°C rate data and the other low temperature data, the 70°C rate data reported by Waber were excluded as outliers because they did not satisfy quality assurance requirements. Waber did not provide a primary reference of the 70°C data, nor did he present any experiment details of the 70°C tests, therefore the test controls under which the data were obtained could not be determined. On the other hand, the release rate data by Wiersma and Mickalonis¹²³ and Gray^{124, 125} were obtained under research programs that satisfy quality assurance requirements. The 178°C data were included in the regression analysis because the original source of the data was properly referenced,¹²⁶ details of the corrosion experiment were provided in the primary reference by Arendt and Binger¹²⁶ and corroborating data from other investigators were consistent with the oxidation rates. The Arrhenius dependence of Al-UAl_x (1.9-53 wt%U) dispersion fuel with water was determined by regression analysis of the literature data, excluding Waber’s 70°C data. The linear reaction rate temperature dependence determined by this author is given as

$$k_l = 5.20 \exp \left[\frac{-34.9 \pm 2.3 \text{ kJ/mol}}{RT} \right] \text{ mg metal/cm}^2/\text{h at 178-350}^\circ\text{C.} \quad (\text{eq. IV-4})$$

The reaction rates of Al-UAl_x dispersion fuel in water were essentially the same as those of the aluminum alloys. The oxidation rates of Al-UAl_x correlated by eq. IV-4 are also consistent with dissolution rates of Al-UAl_x reported by Wiersma and Mickalonis at Savannah River Technology Center¹²³ and Gray at Pacific Northwest National Laboratory.^{124, 125} In comparison to unalloyed uranium metal, the Al-based aluminide dispersion fuels exhibited much lower corrosion rates in water. The reaction rates were a million times lower than unalloyed U and around ten times lower in magnitude than the gamma phase U alloys (i.e., U-Mo, U-Nb and Zr-U). The temperature dependence of the Al-based dispersion reaction rates was not as strong as unalloyed U or the U alloys, with an activation energy of around 35-40 kJ/mol compared to 60-80 kJ/mol, respectively.

D. Kinetics of Aluminum Matrix-Uranium Oxide Oxidation

Uranium oxide aluminum-based dispersion fuels were used on a limited basis (and comprise a limited inventory) because of their higher uranium loading relative to other aluminum-based nuclear fuel compositions. There were a few studies that investigated the corrosion behavior of Al-U₃O₈ dispersion fuels with defected cladding.^{127, 128, 129} Peacock recently reviewed the properties of Al-U₃O₈ fuel.¹³⁰ Peacock considered the corrosion behavior generally the same as that of the aluminum matrix, since the reaction rate of U₃O₈ with water is very small in comparison. The experience with failed fuel in basin storage was consistent with this expectation. Peacock observed no corrosion of 53 wt%U₃O₈ core material in failed elements after one year storage.¹³⁰ However, reaction rates derived from defected cladding studies were not conclusive. Peacock's studies were designed to quantify macroscopic weight changes of fuel elements and were not designed to measure the rates of reaction of dispersion fuel. However, in the absence of other kinetic data, these macroscopic performance data were used by this author to derive reaction rates. Reaction rates derived from defected clad samples have a large uncertainty due to variations in the defect geometry, which affect the exposed fuel surface area or the formation of crevices that corrode preferentially. The uncertainty is exacerbated at low temperatures because of very small reaction rates and the resultant small weight changes. There was a large scatter in the rate data, ranging from less than 10⁻⁵ to ~4 mg metal/cm²/h at temperatures below 100°C (see Figure 31). The reaction rates of Al-U₃O₈/H₂O were expected to be similar to that of Al alloys, as in the case of Al-UAl_x dispersion fuels. The low range of the data was similar to long term linear reaction rates of Al alloys as expected, but the high range of the data was a factor of 10⁶ higher. Although some rate data were greatly different from the long-term linear reaction rate of Al alloys, the magnitude of the high rates was similar to the initial reaction rates of Al alloy oxidation, which exhibits parabolic kinetics. The high range of the data might be attributed to several factors: (a) the initial fast reaction of fresh, exposed metal, (b) accelerated corrosion in crevice geometries, or (c) uncertainties in the derivation in the rates from the raw data.

E. Kinetics of Aluminum Matrix-Uranium Silicide Oxidation

The reaction rate of aluminum matrix-uranium silicide fuel has been studied as part of the RERTR Program. Corrosion tests were limited to weight gain measurements of defected cladding plates in boiling water. As there was a scarcity of aluminum matrix U-Si dispersion data, the reaction rate of uranium silicide intermetallic alloys were also included. Specifically, the reaction rates of U₃Si (3.8 wt% Si stoichiometric) and U₃Si₂ (7.3 wt% Si stoichiometric) with oxygen and with water were reviewed. These reaction rates do not represent the corrosion rates of the aluminum-based U_xSi_y dispersion fuel (which is ~30 vol% U-Si and 70 vol% aluminum alloy matrix), but do provide rate data pertinent to radionuclide release since they are the reaction rates of the dispersed fuel particles. The corrosion resistance of U_xSi_y intermetallics is sensitive to microstructure and composition.^{109, 131} The data reviewed are for samples in the heat-treated condition, except where noted. The reaction rates of uranium-silicide intermetallic alloys with oxygen and water were a strong function of temperature. The temperature dependencies in oxygen and water were essentially the same and were similar to those of unalloyed uranium and uranium alloys. The magnitude of the U_xSi_y reaction rates were approximately 10,000 times lower than those of unalloyed uranium, which was around a factor of ten higher than for the gamma stabilized uranium alloys.

1. Al-U_xSi_y/Water Reaction

The corrosion behavior of Al-U_xSi_y in water was studied as part of the RERTR Program.¹³² The published weight gain measurements on defected fuel plates exposed to boiling water were used by this author to derive reaction rates. The mini-plates were fabricated with fuel particles of different uranium-silicide compositions dispersed in aluminum alloy matrix and clad in aluminum alloy Type 8001. Holes were machined through the plates to simulate through-wall defects and tested in boiling, distilled water at 100°C for 168 hours. The reported weight change was converted to metal loss rate using the volume fractions of aluminum matrix and fuel and the reaction product stoichiometry for the separate reactions. The uncertainties inherent in reaction rates derived from defected cladding corrosion tests were discussed under Al-U₃O₈ oxidation (cf. Section IV.C).

There was a large variation in the derived reaction rate data for Al-U_xSi_y/H₂O (see Figure 32) as with the Al-U₃O₈ reaction rates derived from defected cladding corrosion tests. One plate with U₃Si fuel composition had no measurable weight gain, similar to Al alloys tested. The predicted weight gain on the Al cladding, based on eq. IV-3, should have been measurable but was not, therefore casting doubt on the results. The fuel plate in question is shown on Figure 32 as having a rate equivalent to or lower than aluminum alloys, whereas most of the defected fuel plates exhibited a reaction rate $\sim 10^5$ times greater than the rate of aluminum alloys and 100-1000 times greater than uranium-silicide intermetallics. The high range of data was unexpected since the reaction rate of aluminum matrix dispersion fuel is considered equivalent to the reaction rate of the aluminum alloy. Possible explanations for the high reaction rates are similar to those of the Al-U₃O₈ dispersions. The high rates might reflect the initial parabolic oxidation of freshly exposed metal (defects were machined holes), an accelerated corrosion in crevices, or uncertainties in the surface area and weight change data. An experimental program designed to measure the kinetics of oxidation reaction of Al matrix U-Si dispersions is recommended to clarify variation among the rates of reaction.

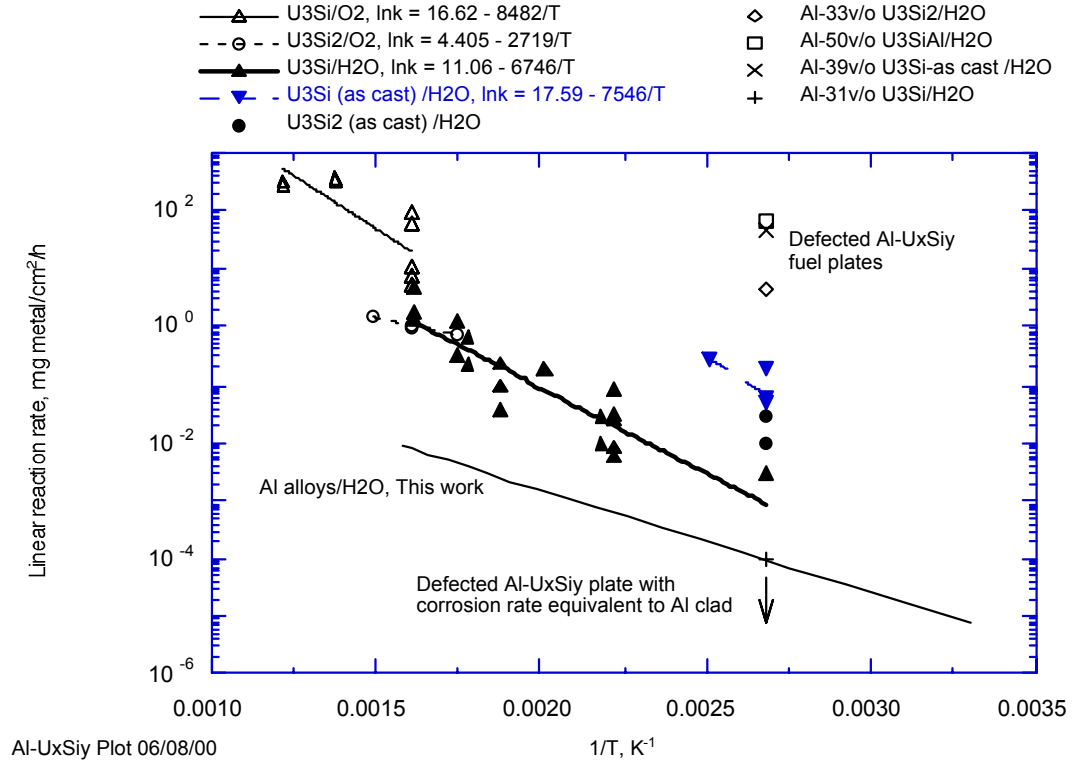


Figure 32. Summary of reaction rates of uranium-silicide intermetallic alloys and defected aluminum-based uranium silicide dispersion fuels with oxygen and water at temperatures below 550°C.

2. U_xSi_y /Oxygen Reaction

Feraday¹³³ and Snyder,¹³¹ respectively, reported the reaction rate of delta phase U_3Si and U_3Si_2 in air. The U_3Si data were reported at temperatures between 350 and 550°C and the U_3Si_2 data at temperatures between 300 and 400°C. A multi-layered reaction product formed on the oxidized U_3Si samples. The outermost layer spalled off and was identified as U_3O_8 . Underlying layers were identified as UO_2 with two adherent, innermost layers that were probably USi_2 . Average reaction rates for U_3Si/O_2 were derived from Feraday's data, based on linear kinetics. There was some scatter in the data, as seen in Figure 32. A regression fit of the data by this author resulted in the Arrhenius expression,

$$k_l = 1.65 \times 10^7 \exp \left[\frac{-70.5 \pm 17.9 \text{ kJ/mol}}{RT} \right] \text{ mg metal/cm}^2/\text{h at 350 to 550}^\circ\text{C. (eq. IV-5)}$$

Snyder reported parabolic kinetics for the U_3Si_2/O_2 data. Pseudo linear rates at long times were derived by this author and used to calculate an Arrhenius expression for U_3Si_2 oxidation in air,

$$k_l = 8.19 \times 10^1 \exp \left[\frac{-22.6 \pm 2.7 \text{ kJ/mol}}{RT} \right] \text{ mg metal/cm}_2/\text{h at 300 to 400}^\circ\text{C. (eq. IV-6)}$$

Based on this analysis, the activation energy of U_3Si_2/O_2 reaction is 50% less than that of U_3Si/O_2 and the reaction rate is less by approximately a factor of ten. The activation energy of U_3Si , 70.5 ± 17.9 kJ/mol, was similar to that of pure uranium and uranium alloys (Zr-U/ O_2), 71.3 and 83.4 ± 4.5 kJ/mol, respectively. Above $300^\circ C$, the oxidation rate of uranium-silicide intermetallic alloys in air were 10-100 times lower than unalloyed uranium.

3. U_xSi_y /Water Reaction

A few investigators^{43, 62, 85, 134} have reviewed the kinetics of U_3Si and U_3Si_2 oxidation in water. The reaction rate is sensitive to the microstructure as seen by differences in the reaction rates of U_3Si in the as-cast and deltized condition. Figure 32 shows the reaction rates of U_3Si (deltized and as-cast) with water and the Arrhenius dependence determined by regression analysis. The temperature dependent reaction rate of deltized U_3Si with water is

$$k_l = 6.36 \times 10^4 \exp \left[\frac{-56.1 \pm 6.1 \text{ kJ/mol}}{RT} \right] \text{ mg metal/cm}^2/\text{h at 100 to } 343^\circ C. \quad (\text{eq. IV-7})$$

The Arrhenius expression for the as-cast U_3Si /water reaction was determined as,

$$k_l = 4.37 \times 10^7 \exp \left[\frac{-62.7 \pm 33.7 \text{ kJ/mol}}{RT} \right] \text{ mg metal/cm}^2/\text{h at 100 and } 125^\circ C. \quad (\text{eq. IV-8})$$

The uncertainty of (eq. IV-8) is high due to the few number of data; however, the Arrhenius expression was included because it is consistent with oxidation rate data of Bourns at $300^\circ C$ in water.¹⁰⁹ The temperature dependencies of deltized and as-cast alloys were considered equivalent considering the variability. At $100^\circ C$, the as-cast expression predicts a reaction rate approximately two orders of magnitude greater than that of heat treated U_3Si . A few reaction rate data for U_3Si_2 at $100^\circ C$ are shown in Figure 32 for comparison and are intermediate to the as-cast and heat-treated U_3Si reaction rates.

The reaction rates of uranium-silicide intermetallic alloys are many times less than that of unalloyed uranium, but slightly higher than the gamma stabilized uranium alloys. The temperature dependencies of the U-Si intermetallic reactions in oxygen and water environments, with the exception of U_3Si_2/O_2 , are the same as those of unalloyed uranium and uranium alloys. The large variability and paucity of reaction rate data for oxidation of aluminum-based uranium-silicide dispersion fuels made it impossible to recommend a best estimate. Reasons for the large scatter in the defected clad Al- U_xSi_y dispersion fuel rate data are the same as for the Al- U_3O_8 fuel with defected clad, namely, uncertainty in sample surface pre-oxidation, in sample geometry and in the derivation of rates from the raw data. Further kinetic studies of the Al- U_xSi_y/H_2O water reaction are necessary to better determine the reaction rate. An experimental program specifically designed to quantify Al- U_xSi_y fuel meat reaction rates would benefit this effort.

F. Summary of Aluminum-Based Dispersion Fuel Oxidation

The oxidation rates of aluminum-based dispersion fuels are controlled by the oxidation of the aluminum alloy matrix. The reaction rates reported here are for advanced corrosion with a developed oxide growth, which obeys linear kinetics. The initial rates of reaction, during formation of the protective rate-limiting oxide layer, for Al-based dispersion fuels and Al alloys were significantly higher than reaction rates on metal with mature, existing oxide coating. The linear reaction rates of Al-UAl_x with compositions of Al-(1.9-53 wt%) uranium were similar to the reaction rates of aluminum alloys. There were few data for the Al-U₃O₈ and Al-U_xSi_y/H₂O reactions and they exhibited a large variability. However, the relative reaction rates of uranium silicide intermetallic fuel were only slightly higher than the aluminum matrix, indicating that a localized corrosion mechanism is unlikely. The reaction rates of uranium-silicon intermetallic fuels were many times less than that of unalloyed uranium, but slightly higher than the gamma stabilized uranium alloys.

This author derived Arrhenius expressions for Al alloys, Al-UAl_x dispersion fuels and U-Si intermetallics by regression analysis, summarized in Table 14. The temperature dependencies of the U-Si intermetallics reactions in oxygen and water environments, with the exception of U₃Si₂/O₂, are the same as those of unalloyed uranium and uranium alloys. The aluminum alloys and aluminum matrix dispersions exhibited smaller temperature dependence than the U-Si intermetallic and U metal, with an activation energy of 35-40 kJ/mol compared to 70-80 kJ/mol.

In the temperature range 178-350°C, the aluminum-based uranium aluminides exhibited reaction rates with water similar to those of the aluminum alloys. There were some low temperature reaction rate data not consistent with higher temperature data reported in the literature, which were excluded from the regression fit Arrhenius expression (cf. discussion in Section IV.C). At 200°C, the reaction rates of aluminum alloys and Al-UAl_x dispersion fuels with saturated water vapor were similar to the immersion rate data. These data indicate that the mean oxidation rates of Al-UAl_x are equivalent for water and water vapor, as was the case for oxidation rates of uranium metal. While the reaction rate of Al-UAl_x with water was consistent with the reaction rate of aluminum alloys with water, there is too much variability of the reaction rate data of Al-U₃O₈ and Al-U_xSi_y/H₂O (derived from defected cladding corrosion tests) to draw a conclusion. An experimental program to study the reaction kinetics of Al-U₃O₈ and Al-U_xSi_y/H₂O reaction is recommended to better determine the reaction rates.

Table 14. Summary of rates of reaction of aluminum alloys, aluminum matrix uranium aluminide dispersions and uranium silicides with oxygen and water at temperatures less than 550°C.

Reaction	Rate Expression, mg/cm ² /h, Linear:	Conditions	Eq. No.
Al alloys/H ₂ Oaq	$k_l = 4.29\exp[-32.8 \pm 1.8/RT]$	25-360°C	IV-3
Al-UAl _x /H ₂ Oaq	$k_l = 5.20\exp[-34.9 \pm 2.3/RT]$	178-350°C	IV-4
U ₃ Si/O ₂	$k_l = 1.65 \times 10^7 \exp[-70.5 \pm 17.9/RT]$	350-550°C	IV-5
U ₃ Si ₂ /O ₂	$k_l = 8.19 \times 10^1 \exp[-22.6 \pm 2.7/RT]$	300-400°C	IV-6
U ₃ Si/H ₂ Oaq (Delta)	$k_l = 6.38 \times 10^4 \exp[-56.1 \pm 6.1/RT]$	100-343°C	IV-7
U ₃ Si/H ₂ Oaq (As-cast)	$k_l = 4.37 \times 10^7 \exp[-62.7 \pm 33.7/RT]$	100-125°C	IV-8

V. CONCLUSIONS

This review has critically evaluated the kinetics of uranium metal, uranium alloys and aluminum-based dispersion fuels with oxygen, water vapor, and water, based on available literature data. The water-corrosion aspects of this review were limited to pure water corrosion; corrosion data for water chemistry expected in the repository environment were not available at the outset of this project. The oxidation processes and kinetics discussed in this report are limited to pure water, therefore they are not directly applicable to corrosion rates of SNF in water chemistry that is significantly different. Linear or parabolic kinetics was observed for all fuel types in the three groups. Linear reaction rates were developed for all fuel types. In the case of systems with parabolic kinetics, linear reaction rates were determined for times after initial parabolic oxide growth. Temperature dependent reaction rates for the different systems were developed by standard regression methods. The regression fits to the literature data were compared to Arrhenius rate expressions where available. In some instances, the revised expressions differed little from existing correlations and were noted in the text. The recommended Arrhenius dependent reaction rates of uranium metal, alloys, and aluminum-based dispersion fuels are summarized in Table 15. In this section, the reaction rates of the three fuel types with oxygen and with water are summarized and the major conclusions are presented.

Table 15. Summary of rates of reaction for uranium metal, uranium alloys and aluminum-based dispersion fuels with oxygen, water vapor, oxygenated water vapor, and water at temperatures less than 300°C.

Reaction	Rate Expression ^a mg/cm ² /h or mg/cm ² /h/kPa ^{0.5} (H ₂ Ov)	Conditions	Eq. No.
Uranium metal			
U/O ₂	Linear: $k_t = 1.09 \times 10^8 \exp[-71.3 \pm 2.1/RT]$	38-300°C	II-21
U/H ₂ Ov	Linear: $k_t/p^{0.5} = 9.76 \times 10^5 \exp[-46.6 \pm 0.7/RT]$	20-302°C	II-28
U/O ₂ -H ₂ Ov	Linear: $k_t = 8.21 \times 10^{11} \exp[-92.9 \pm 4.8/RT]$ $k_t = 8.65 \times 10^9 \exp[-76.9 \pm 7.0/RT]$	20-200°C, 2-90%RH 20-100°C, 100%RH	II-34 II-35
U/H ₂ Oaq	Linear: $k_t = 5.03 \times 10^9 \exp[-66.4 \pm 2.0/RT]$	20-300°C	II-39
Uranium alloys			
U-<8wt%Mo/H ₂ O	Linear: $k_t = 1.15 \times 10^8 \exp[-66.5 \pm 12.2/RT]$	100-178°C	III-2
U->8wt%Mo/H ₂ O	$k_t = 1.58 \times 10^6 \exp[-80.5 \pm 10.6/RT]$	302-440°C	III-3
U-Zr(50wt%)/O ₂	Linear: $k_t = 2.17 \times 10^6 \exp[-83.4 \pm 4.5/RT]$	300-500°C	III-6
U-Zr(20-97wt%)/H ₂ O	Linear: $k_t = 1.13 \times 10^3 \exp[-51.9 \pm 5.5/RT]$	100-363°C	III-7
Al-UAl _x /H ₂ Oaq	Linear: $k_t = 5.20 \exp[-34.9 \pm 2.3/RT]$	178-350°C	IV-4
U ₃ Si/O ₂	Linear: $k_t = 1.65 \times 10^7 \exp[-70.5 \pm 17.9/RT]$	350-550°C	IV-5
U ₃ Si ₂ /O ₂	Linear: $k_t = 8.19 \times 10^1 \exp[-22.6 \pm 2.7/RT]$	300-400°C	IV-6
U ₃ Si/H ₂ Oaq (Delta)	Linear: $k_t = 6.38 \times 10^4 \exp[-56.1 \pm 6.1/RT]$	100-343°C	IV-7
U ₃ Si/H ₂ Oaq (As-cast)	$k_t = 4.37 \times 10^7 \exp[-62.7 \pm 33.7/RT]$	100-125°C	IV-8
^a Activation energy in kJ/mol, R is 8.314 x 10 ⁻³ kJ/mol/K and T in Kelvin			

The reaction rates of uranium metal, uranium alloys and uranium silicide with oxygen were similar (see Figure 33). Of the uranium alloys, only zirconium-uranium alloys had a substantial amount of published data from various sources. There were no oxidation studies of aluminum-based dispersion fuels; therefore the reaction rate of uranium silicide was included in this review to illustrate the fuel particle (of an Al-based dispersion) corrosion rate relative to other fuel types. The temperature dependencies were the same for the three fuel types with activation energies of around 75 kJ/mol. The magnitude of the reaction rates of uranium metal and uranium silicide were essentially the same, and that of the zirconium-uranium alloy was slightly less.

The reaction rates in oxygen were at least 1000 times lower than the rate of the U metal/water reaction shown in Figure 34. At temperatures below 350°C, the unalloyed uranium/water reaction rate is between 10,000 and 100,000 times greater than the reaction rates of the gamma phase uranium alloys, aluminum-based dispersion fuels and uranium silicide with water. The non-gamma phase U alloys (U-<8wt%Mo) reaction rate in water was slightly lower than the pure uranium, but not to a statistically significant extent. Rate data for U-Nb alloys exhibited the same difference in reaction rates for gamma phase and non-gamma phase alloy contents (cf. Section III.C). The Al-based aluminide dispersions and Zr-U alloys have the lowest reaction rates in water, which can be attributed to the small fraction of fuel and the good corrosion resistance of the aluminum and zirconium major alloying elements. The temperature dependencies of the reaction rates of the unalloyed uranium, uranium alloys and uranium intermetallics were the same, within a 2-sigma statistic, with an activation energy of around 75 kJ/mol. The reaction rate of Al-based aluminide dispersions in water had an activation energy about 50% lower at 35 kJ/mol, which was the same as for solid Al alloys.

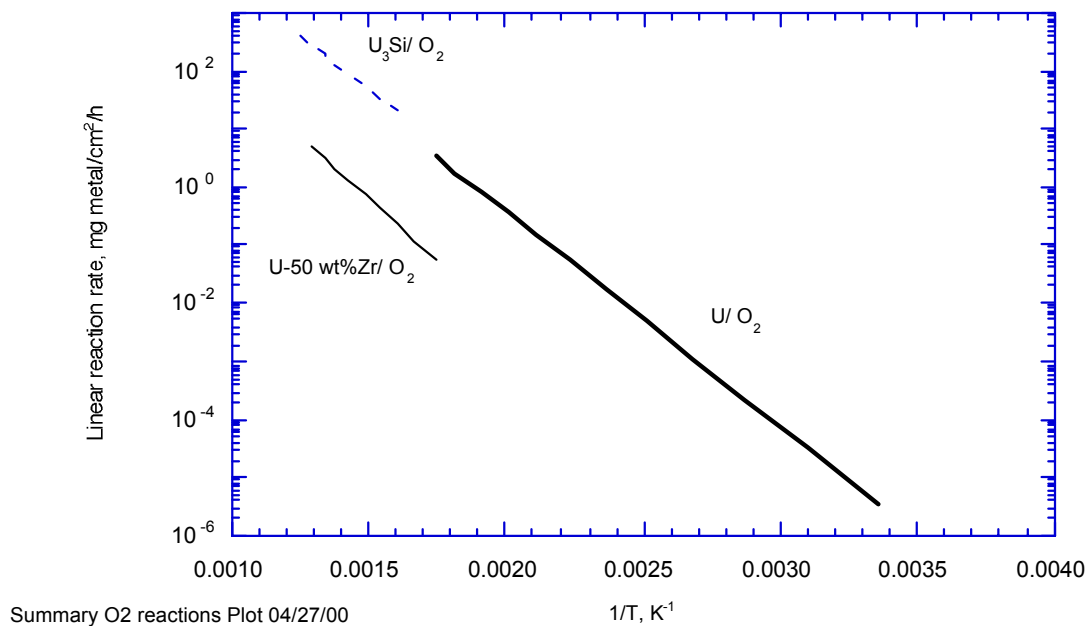


Figure 33. Summary of reaction rates of uranium metal, zirconium-uranium alloy and uranium silicide intermetallic with oxygen at temperatures less than 550°C.

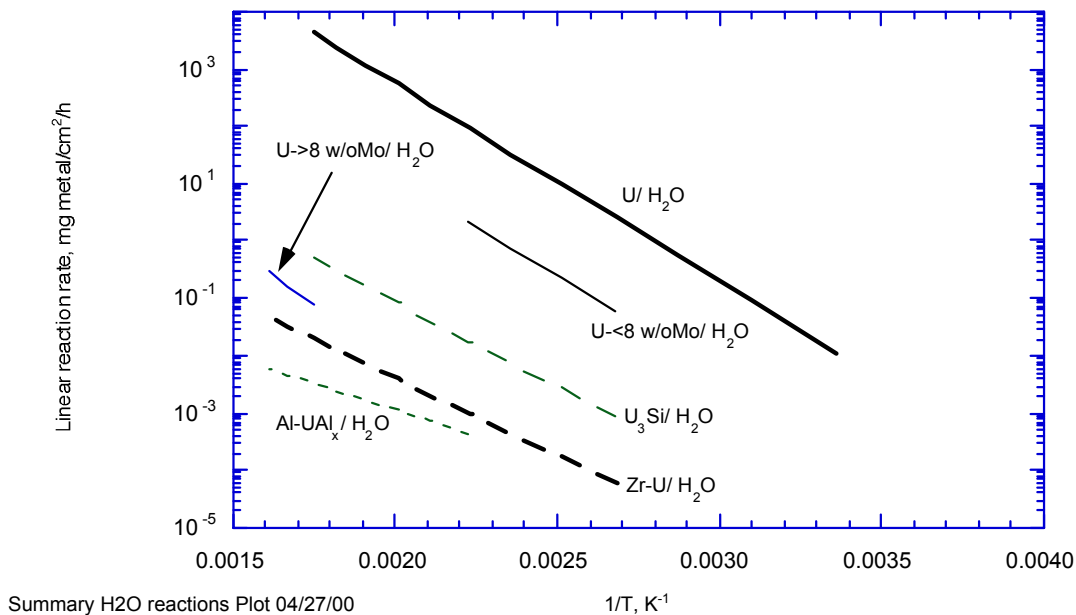


Figure 34. Summary of reaction rates of uranium metal, uranium alloys and aluminum-based dispersion fuels with water at temperatures less than 350°C.

In conclusion, the uranium metal/water reaction exhibited the highest reaction rate of the fuel types and environments that were reviewed. Consequently, the N-Reactor fuel is considered the bounding fuel type for corrosion of metal fuels and alloys. The reaction rate in anoxic, saturated water vapor was essentially the same as the water reaction rate. In oxygenated water vapor, the reaction rate was intermediate to the water and oxygen reaction rate. The reaction rates of gamma phase uranium alloys in water were significantly lower than that of unalloyed uranium metal, however non-gamma phase uranium alloys exhibited reaction rates similar to uranium metal. At very long times, uranium alloys and unalloyed uranium with high carbon exhibited an apparent increase in reaction rate due to discontinuous failure. The apparent increased reaction rate was attributed to the increase in surface area not accounted for in the normalized rate, rather than to an increase in the inherent reaction rate. The reaction rates of aluminum-based dispersions were generally considered to be determined by the aluminum matrix behavior, which has a reaction rate much lower than pure uranium. The Arrhenius rate expression of aluminum-based aluminide dispersions was consistent with this, however the reaction rates of Al-based uranium oxide and uranium silicide dispersion fuels with water were inconclusive due to the large scatter and paucity of data. The long term intrinsic reaction rates of irradiated and unirradiated fuel were determined to be similar. The apparent reaction rate increases at high burnup as a function of swelling due to the increased surface area. Research to clarify the oxidation rates of U-Mo alloys at low temperatures and the influence of shortened failure times of irradiated alloys on radionuclide release rates and an experimental program to study the reaction kinetics of Al-U₃O₈ and Al-U_xSi_y/H₂O reaction are recommended.

ACKNOWLEDGMENTS

Research and analysis for this document was conducted for the Department of Energy National Spent Nuclear Fuel Program under contract to the Idaho National Engineering and Environmental Laboratory.

The author acknowledges H. H. Loo of Bechtel BWXT Idaho, LLC for his support for this work. The author acknowledges M.A. Ebner of Bechtel BWXT Idaho, LLC for numerous discussions and extensive review of this report. R. Pahl of Argonne National Laboratory-West provided many helpful suggestions and review of this report. The author benefited from discussions with T. C. Totemeier and M. Meyer of Argonne National Laboratory-West, P. S. Lam of Savannah River Site, and D. J. Trimble of Fluor Daniel Hanford, Inc. K.W. Scott of Bechtel BWXT Idaho, LLC edited and prepared the report for publication.

REFERENCES

- ¹ Lockheed-Martin Idaho Technologies Company, Inc., 1999, *DOE Spent Nuclear Fuel Information in Support of TSPA-SR*, DOE/SNF/REP-0047, Rev. 0, Idaho National Engineering and Environmental Laboratory: Idaho Falls, ID.
- ² Scully, J. C., 1990, *The Fundamental of Corrosion*, 3rd Edition, Oxford: Pergamon Press, p. 226.
- ³ Uhlig, H. H. and R. W. Revie, 1985, *Corrosion and Corrosion Control: An Introduction to Corrosion Science and Engineering*, 3rd Edition, New York: John Wiley & Sons, p. 441.
- ⁴ Kofstad, P., 1966, *High-Temperature Oxidation of Metals*, New York: John Wiley & Sons, p. 340.
- ⁵ Evans, U. R., 1964, *An Introduction to Metallic Corrosion*, 2nd Edition, New York: St. Martin's Press, p. 253.
- ⁶ Waber, J. T., 1958, "The Corrosion Behavior of Plutonium and Uranium," *Proceedings of Conference for Peaceful Uses of Atomic Energy, International Atomic Energy Association (IAEA) in Geneva*, pp. 204-214.
- ⁷ Orman, S., 1976, "Oxidation of Uranium and Uranium Alloys," in *Physical Metallurgy of Uranium Alloys*, J. J. Burke, et al. (eds.), Chestnut Hill, MA: Brook Hill Publishing Company, pp. 815-833.
- ⁸ Colmenares, C. A., 1975, "The Oxidation of Thorium, Uranium, and Plutonium," *Progress in Solid State Chemistry*, Vol. 9, pp. 139-329.
- ⁹ Colmenares, C. A., 1984, "Oxidation Mechanisms and Catalytic Properties of the Actinides," *Progress in Solid State Chemistry*, Vol. 15, pp. 257-364.
- ¹⁰ McGillivray, G. W., D. A. Geeson, and R. C. Greenwood, 1994, "Studies of the Kinetics and Mechanism of the Oxidation of Uranium by Dry and Moist Air – a Model for Determining the Oxidation Rate Over a Wide Range of Temperatures and Water Vapour Pressures," *Journal of Nuclear Materials*, Vol. 208, pp. 81-97.
- ¹¹ Balooch, M. and A. V. Hamza, 1996, "Hydrogen and Water Vapor Adsorption on and Reaction with Uranium," *Journal of Nuclear Materials*. Vol. 230, pp. 159-170.
- ¹² Manner, W. L., J. A. Lloyd, and M. T. Paffett, 1999, "Reexamination of the Fundamental Interactions of Water with Uranium," *Journal of Nuclear Materials*, Vol. 275, pp. 37-46.
- ¹³ Allen, G. C., I. R. Trickle, and P. M. Tucker, 1981, *Philosophical Magazine B*, Vol. 43, p. 689.

- ¹⁴ Pearce, R. J. and P. Kay, 1987, *The Reaction of Uranium in the U-O₂-H₂O and U-H₂O Systems*, TPRD/B/0954/R87, Central Electricity Generating Board, Berkeley Nuclear Laboratories: Berkeley, UK.
- ¹⁵ Pearce, R., J., 1989, *A Review of the Rates of Reaction of Unirradiated Uranium in Gaseous Atmospheres*, RD/B/6231/R89, Central Electricity Generating Board, Berkeley Nuclear Laboratories: Berkeley, UK.
- ¹⁶ Baker, M. M., L. N. Less, and S. Orman, 1966, "Uranium + Water Reaction Part 1. Kinetics, Products and Mechanism," *Transactions of the Faraday Society*, Vol. 108, No. 62, pp. 2513-2524.
- ¹⁷ Leibowitz, L., et al., 1961, "The Kinetics of Oxidation of Uranium Between 125° and 250°C," *Journal of the Electrochemical Society*, Vol. 108, No. 12, pp. 1155-1160.
- ¹⁸ Ritchie, A. G., 1981, "A Review of the Rates of Reaction of Uranium with Oxygen and Water Vapour at Temperatures Up to 300°C," *Journal of Nuclear Materials*, Vol. 102, pp. 179-182.
- ¹⁹ Schnizlein, J. G., et al., 1959, *Ignition Behavior and Kinetics of Oxidation of the Reactor Metals, Uranium, Zirconium, Plutonium and Thorium, and Binary Alloys of Each*, ANL-5974, Argonne National Laboratory: Lemont, IL.
- ²⁰ Catlow, C. R. A. and A. B. Lidiard, 1974, *Thermodynamic Nuclear Procedure*, Vienna: International Atomic Energy Agency, pp. 27-41.
- ²¹ Ritchie, A. G., 1984, "The Kinetics of the Initial Stages of the Reaction of Uranium with Oxygen," *Journal of the Less-Common Metals*, Vol. 98, pp. 193-214.
- ²² Bennett, M. J. and R. J. Pearce, 1985, "The Oxidation of Irradiated Uranium in Air at 50-300°C," *Nuclear Fuel Performance*, British Nuclear Energy Society: London, pp. 111-113.
- ²³ Hayward, P. J., et al., 1992, "Oxidation of Uranium in Argon-25% Oxygen at 190-610°C," *Journal of Nuclear Materials*, Vol. 187, pp. 215-222.
- ²⁴ Pearce, R. J., M. J. Bennett, and J. B. Price, 1988, "Oxidation of Irradiated Uranium in Moist Air," *Nuclear Energy*, Vol. 27, pp. 305-309.
- ²⁵ Ritchie, A. G., 1984, "The Kinetics and Mechanism of the Uranium-Water Vapour Reaction – an Evaluation of Some Published Work," *Journal of Nuclear Materials*, Vol. 120, pp. 143-153.
- ²⁶ Colmenares, C., R. Howell, and T. McCreary, 1981, *Oxidation of Uranium Studied by Gravimetric and Positron-Annihilation Techniques*, UCRL-85549, Lawrence Livermore National Laboratory: Livermore, CA.

- ²⁷ Hayward, P. J., et al., 1994, "Oxidation of Uranium in Steam," *Journal of Nuclear Materials*, Vol. 217, pp. 82-92.
- ²⁸ Kondo, T., F. H. Beck, and M. G. Fontana, 1974, "A Gas Chromatographic Study on the Kinetics of Uranium Oxidation in Moist Environments," *Corrosion*, Vol. 30, pp. 330-339.
- ²⁹ Orman, S., 1963, "The Effect of Certain Gases on the Rate of Oxidation of Uranium by Water Vapour," *Chemistry and Industry*, pp. 1692-1693.
- ³⁰ Waber, J. T., 1958, *A Review of the Corrosion Behaviour of Uranium*, LA-2035, Los Alamos National Laboratory: Los Alamos, NM.
- ³¹ Orman, S., G. Picton, and J. C. Ruckman, 1969, "Uranium Oxides Formed in Air and Water in the Temperature Range 200-375°C" *Oxidation of Metals*, Vol. 1, No. 2, p. 199.
- ³² Ritchie, A. G., R. C. Greenwood, and S. J. Randles, 1986, "The Kinetics of the Uranium-Oxygen Water Vapour Reaction Between 40 and 100°C," *Journal of Nuclear Materials*, Vol. 139, pp. 121-136.
- ³³ Troutner, V. H., 1960, *Mechanisms and Kinetics of Uranium Corrosion and Uranium Core Fuel Element Ruptures in Water and Steam*, HW-67370, Hanford Atomic Products Operation: Richland, WA.
- ³⁴ Weirick, L. J., 1960, *The Oxidation of Uranium in Low Partial pressures of Oxygen and Water Vapor at 100°C*, SAND83-0618, Sandia National Laboratories: Albuquerque, NM.
- ³⁵ Trimble, D. J., 1998, *Reaction Rate Constant for Uranium in Water and Water Vapor*, HNF-2853, Duke Engineering & Services Hanford, Inc.: Richland, WA.
- ³⁶ Haschke, J. M., 1998, "Corrosion of Uranium in Air and Water Vapor: Consequences for Environmental Dispersal," *Journal of Alloys and Compounds*, Vol. 278, pp. 149-160.
- ³⁷ Baker, L., and J. D. Bingle, 1966, "The Kinetics of Oxidation of Uranium Between 300 and 625°C," *Journal of Nuclear Materials*, Vol. 20, pp. 11-21.
- ³⁸ Allen, G. C., P. M. Tucker, and R. A. Lewis 1984, "X-Ray Photoelectron Spectroscopy Study of the Initial Oxidation of Uranium Metal in Oxygen + Water-Vapour Mixtures," *Journal of Chemical Society, Faraday Transactions 2*, Vol. 80, pp. 991-1000.
- ³⁹ Winer, K., et al., 1987, "Interaction of Water Vapor with Clean and Oxygen-Covered Uranium Surfaces," *Surface Science*, Vol. 183, pp. 67-99.
- ⁴⁰ Baker, M. M., L. N. Less, and S. Orman, 1966, "Uranium + Water Reaction Part 2. Effect of Oxygen and Other Gases," *Transactions of Faraday Society*, Vol. 62, pp. 2525-2530.
- ⁴¹ Waber, J. T., 1952, *A Review of the Corrosion of Uranium and Its Alloys*, LA-1524, Los Alamos National Laboratory: Los Alamos, NM.

- ⁴² Mollison, W. A., G. C. English, and F. Nelson, 1945, *Corrosion of Tuballoy in Distilled Water*, CT-3055, University of Chicago, Metallurgical Laboratory Report: Chicago, IL.
- ⁴³ McWhirter, J. W. and J. E. Draley, 1952, *Aqueous Corrosion of Uranium and Alloys: Survey of Project Literature*, ANL-4862, Argonne National Laboratory: Chicago, IL.
- ⁴⁴ Waber, J. T., 1948, *An Analysis of Project Data on the Corrosion of Uranium in Various Media*, LA-1381, Los Alamos National Laboratory: Los Alamos, NM.
- ⁴⁵ Totemeier, T. C., 1995, *A Review of The Corrosion and Pyrophoricity Behavior of Uranium and Plutonium*, ANL/ED/95-2, Argonne National Laboratory: Idaho Falls, ID.
- ⁴⁶ Abrefah, J., et al., 1998, *Dry Air Oxidation Kinetics of K-Basin Spent Nuclear Fuel*, PNNL-11786, Pacific Northwest National Laboratory: Richland, WA.
- ⁴⁷ Trimble, D. J., 1998, *Reaction Rate Constant for Dry Air Oxidation of K Basin Fuel*, HNF-SD-SNF-CN-019, Duke Engineering & Services Hanford, Inc.: Richland, WA.
- ⁴⁸ Shell, L. S., 1997, "A Model for the Evolution of Gas Pressure and Composition During Sealed Storage of Metallic Uranium Fuel," *Department of Nuclear Engineering*, Massachusetts Institute of Technology: Cambridge, MA, p. 115.
- ⁴⁹ Baker, M. M. and L. N. Less, eds. 1981, "Review of the Rates of Reaction of Uranium with Oxygen and Water Vapour at Temperatures Up to 300°C [Unpublished Report]," A. G. Ritchie (ed.), *Journal of Nuclear Material*, Vol. 102, pp. 170-182.
- ⁵⁰ Bennett, M. J., B. L. Myatt, and J. E. Antill, 1974, "The Oxidation Behaviour of Highly Irradiated Uranium in Dry Carbon Dioxide at 375-500°C and in Dry Air at 200-300°C," *Journal of Nuclear Materials*, Vol. 50, pp. 2-10.
- ⁵¹ Bennett, M. J., et al., 1975, "The Oxidation Behaviour of Uranium in Air at 50-300°C," *Journal of Nuclear Materials*, Vol. 57, pp. 221-236.
- ⁵² Bennett, M. J. and B. L. Myatt, 1977, "The Effect of the Aluminum Content of Uranium Upon Its Oxidation Behaviour in Carbon Dioxide and Air," *Journal of Nuclear Materials*, Vol. 66, pp. 37-43.
- ⁵³ Owen, L. W. and J. R. Alderton, eds., 1981, [Unpublished Report], *Journal of Nuclear Materials*, ed. A. G. Ritchie, Vol. 102, pp. 170-182.
- ⁵⁴ Trimble, D. J., 1999, *Personal Communication*.
- ⁵⁵ Magnani, N. J., 1974, *The Reaction of Uranium and Its Alloys with Water Vapor at Low Temperatures*, SAND-74-0145, Sandia National Laboratory: Albuquerque, NM.

- ⁵⁶ Grimes, J. H. and J. R. Morris, 1965, *Uranium Corrosion Studies, Part 2. The Rate of Reaction of Polished Uranium and Water Vapor at Various Temperatures*, AWRE Report No. 0-68/65, Atomic Weapons Research Establishment: Berkeley, CA.
- ⁵⁷ Corcoran, V. J., C. Johnston, W. J. Metcalfe, and J. Thorpe, 1965, *The Water Vapor Corrosion of uranium and Its Prevention*, AWRE Report No. 0-42/65, Atomic Weapons Research Establishment: Berkeley, CA.
- ⁵⁸ Kondo, T., et al., 1964, "Gas Chromatographic and Gravimetric Studies of Uranium Oxidation Mechanism," *Corrosion*, Vol. 20, pp. 314-320.
- ⁵⁹ Orman, S., 1964, *Uranium Compatibility Studies, Part 2. The Effect of Water Vapor Pressure in an Oxygen Free Atmosphere in the Corrosion Rate of Uranium at 100°C*, AWRE Report No. 0-25/64, Atomic Weapons Research Establishment: Berkeley, CA.
- ⁶⁰ Abrefah, J. and R. L. Sell, 1999, *Oxidation of K-West Basin Spent Nuclear Fuel in Moist Helium Atmosphere*, PNNL-12167, Pacific Northwest National Laboratory: Richland, WA.
- ⁶¹ Tyfield, S. P., 1988, "Corrosion of Reactor Grade Uranium in Aqueous Solutions Relevant to Storage and Transport," *Nuclear Energy*, Vol. 27, pp. 91-98.
- ⁶² Wilkinson, W. D., 1962, *Uranium Metallurgy*, Vol. 2, New York: Interscience Publishers, pp. 757-1490.
- ⁶³ Burkart, M. W. and ed., 1957, *Development and Properties of Uranium-Base Alloys Corrosion Resistant in High-Temperature Water, Part III. Corrosion Mechanism of Uranium-Base Alloys in High Temperature Water*, WAPD-127-Part III, Westinghouse Electric Corporation: Pittsburgh, PA.
- ⁶⁴ McGeary, R. K. and ed., 1957, *Development and Properties of Uranium-Base Alloys Corrosion Resistant in High-Temperature Water, Part I, Alloys without Protective Cladding*, WAPD-127-Part IV, Westinghouse Electric Corporation: Pittsburgh, PA.
- ⁶⁵ Howe, J. P. and T. O. Jones, 1955, "Coatings and Corrosion," *National Nuclear Energy Series Div. VIII*.
- ⁶⁶ Draley, J. E. and J. W. McWhirter, 1953, *Effects of Metal Purity and Heat Treatment on the Corrosion of Uranium in Boiling Water*, ANL-5029, Argonne National Laboratory: Chicago, IL.
- ⁶⁷ Schroeder, J. B., D. A. Vaughan, and C. M. Schwartz, 1959, "Aqueous Uranium Corrosion at 100°C." *Journal of the Electrochemical Society*, Vol. 106, No. 6, pp. 486-489.
- ⁶⁸ Dillon, R. L., ed. 1960, Report HW-67370, [Unpublished], V. H. Troutner (ed.), Hanford Atomic Products Operation.

- ⁶⁹ Bown, H. C., J. E. Minor, and R. G. Post, eds., 1960, HW-67370, [Unpublished Report], V. H. Troutner (ed.), Hanford Atomic Products Operation.
- ⁷⁰ Bennett, M. J. and J. B. Price, 1981, "The Oxidation Behaviour of Uranium in Air at 348-765 K," *Journal of Nuclear Materials*, Vol. 101, pp. 44-55.
- ⁷¹ Pahl, R. G., E. M. Franklin, and M. A. Ebner, 1994, "Technical Assessment of Continued Wet Storage of EBR-II Fuel," *Proceedings of DOE National Spent Fuel and Fissile Material Management Conference*. American Nuclear Society: Salt Lake City, pp. 223-230.
- ⁷² Einzinger, R. E. and B. R. Seidel, 1979, "Irradiation Performance of Metallic Driver Fuel in Experimental Breeder Reactor II to High Burnup," *Nuclear Technology*, Vol. 50, pp. 25-39.
- ⁷³ Barnes, R. S., 1964, "A Theory of Swelling and Gas Release for Reactor Materials," *Journal of Nuclear Materials*, Vol. 2, pp. 135-148.
- ⁷⁴ Gray, W. J. and R. E. Einzinger, 1998, *Initial Results from Discolution Rate Testing of N-Reactor Spent Fuel Over a Range of Potential Geologic Repository Aqueous Condition*, DOE/SNF/REP-022, PNNL-11894, Pacific Northwest National Laboratory: Richland, WA.
- ⁷⁵ Fannesbeck, J. E., J. R. Krsul, and S. G. Johnson, 1998, "ERB-II Blanket Fuel Leaching Test Using Simulated J-13 Well Water," *Proceedings of Third Topical Meeting on DOE Spent Nuclear Fuel and Fissile Materials, Vol. 2, September 1998*, American Nuclear Society: Charleston, SC.
- ⁷⁶ Waber, S. F. and J. T. Waber, 1951, *The Reaction of Uranium with Purified Water*, LAMS-1841, Los Alamos Scientific Laboratory: Los Alamos, NM.
- ⁷⁷ Hopkinson, B. E., 1959, "Kinetics of the Uranium-Steam Reaction," *Journal of the Electrochemical Society*, Vol. 106, No. 2, pp. 102-106.
- ⁷⁸ Totemeier, T. C., et al., 1998, *Metallic Uranium ZPPR Fuel: Corrosion Characteristics and Corrosion Product Oxidation Kinetics*, ANL-98/11, Argonne National Laboratory: Idaho Falls, ID.
- ⁷⁹ Totemeier, T. C., et al., 1998, "Characterization of Corroded Metallic Uranium Fuel Plates," *Journal of Nuclear Materials*, Vol. 256, pp. 87-95.
- ⁸⁰ Totemeier, T. C., R. G. Pahl, and S. M. Frank, 1999, "Oxidation Kinetics of Hydride-Bearing Uranium Metal Corrosion Products," *Journal of Nuclear Materials*, Vol. 265, pp. 308-320.
- ⁸¹ Totemeier, T. C., 1999, *Oxidation of ZPPR Fuel Corrosion Products: National Spent Nuclear Fuel Program FY 1999 Final Report*, ANL-99/21, Argonne National Laboratory: Idaho Falls, ID.
- ⁸² Burkart, M. W. and B. Lustman, 1958, "Corrosion Mechanism of Uranium-Base Alloys in High Temperature Water," *Journal of Metals*, Vol. 10, No. 26.

- ⁸³ Robinson, S. L. and G. L. Thomas, 1996, *Uranium Hydride Formation and Properties: A Review with Commentary on Handling and Disposition*, SAND96-8206, Sandia National Laboratory: Albuquerque, NM.
- ⁸⁴ Totemeier, T. C. and R. G. Pahl, 1998, "Oxidation Kinetics of Reaction Products Formed in Uranium Metal Corrosion," *DOE Spent Nuclear Fuel and Fissile Materials Management*, American Nuclear Society: Charleston, SC, p. 271.
- ⁸⁵ Tipton, C. R., Jr., ed. 1960, "Materials," 2nd Ed. *Reactor Handbook, Vol. I.*, Interscience Publishers Inc.: New York.
- ⁸⁶ Meyer, M., 1999, *Personal Communication*.
- ⁸⁷ Jones, L. J. and ed., 1957, *Development and Properties of Uranium-Base Alloys Corrosion Resistant in High-Temperature Water. Part IV, Radiation Stability of Uranium-Base Alloys*, WAPD-127-Part I, Westinghouse Electric Corporation: Pittsburgh, PA.
- ⁸⁸ Cohen, I., E. F. Losco, and eds., 1957, *Development and Properties of Uranium-Base Alloys Corrosion Resistant in High-Temperature Water. Part II. Alloys with Protective Cladding*, WAPD-127-Part II, Westinghouse Electric Corporation: Pittsburgh, PA.
- ⁸⁹ Dwight, A. E. and M. H. Mueller, 1956, *Constitution of the Uranium-Rich U-Nb and U-Nb-Zr Systems*, ANL-5581, Argonne National Laboratory: Argonne, IL.
- ⁹⁰ Draley, J. E., S. Greenberg, and W. E. Ruther, 1957, *The High Temperature Aqueous Corrosion of Uranium Alloys Containing Minor Amounts of Niobium and Zirconium*, ANL-5530, Argonne National Laboratory: Argonne, IL.
- ⁹¹ Idaho National Engineering and Environmental Laboratory, 1998, *DOE Spent Nuclear Fuel Information in Support of TSPA-VA*.
- ⁹² Barnartt, S., R. G. Charles, and E. A. Gulbransen, 1957, "Oxidation of 50 Weight Per Cent Uranium-Zirconium Alloy," *Journal of the Electrochemical Society*, Vol. 104, No. 4, pp. 218-221.
- ⁹³ Matsui, T., et al., 1993, "Oxidation of U-20 at% Zr Alloy in Air at 423-1063 K," *Journal of Nuclear Materials*, Vol. 199, pp. 143-148.
- ⁹⁴ Bauer, A. A., 1959, *An Evaluation of the Properties and Behavior of Zirconium-Uranium Alloys*, BMI-1350, Battelle Memorial Institute: Columbus, OH.
- ⁹⁵ Thomas, D. E., 1954, *Corrosion of Zirconium-Uranium Alloys*, WAPD-MDM-24, Westinghouse Electric Corporation.
- ⁹⁶ Hofman, G. L. and J. L. Snelgrove, 1994, "Dispersion Fuels," in *Nuclear Materials*, B. R. T. Frost (ed.), Weinheim, New York, Basel, Cambridge, Tokyo: VCH Publishers Inc., pp. 45-108.

- ⁹⁷ Godard, H. P., 1960, "The Corrosion Behavior of Aluminum in Natural Waters," *The Canadian Journal of Chemical Engineering*, Vol.38, p. 167.
- ⁹⁸ Pathak, B. R. and H.P Godard, 1968, "Equation for Predicting the Corrosivity of Natural Fresh Waters to Aluminum," *Nature*, Vol. 218, p. 893.
- ⁹⁹ Ailor, W.H., 1969, "A Review of Aluminum Corrosion in Tap Waters," *Journal of Hydronautics*, Vol. 3, p. 105.
- ¹⁰⁰ Howell, J. P., 1996, "Durability of Aluminum-Clad Spent Nuclear Fuels in Wet Basin Storage," *Paper No. 128 of Corrosion 96, National Association of Corrosion Engineers*.
- ¹⁰¹ Howell, J. P., P. E. Zapp, and D.Z. Nelson, 1993, "Corrosion of Aluminum Alloys in a Reactor Disassembly Basin," *Paper No. 709 of Corrosion 93, National Association of Corrosion Engineers*.
- ¹⁰² Howell, J.P. and P.E. Zapp, 1994, "Effect of Water Conductivity on Corrosion of Aluminum Alloys in Spent Fuel Storage," *Paper No. 118 of Corrosion 94, National Association of Corrosion Engineers*.
- ¹⁰³ Howell, J.P., 1997, "Corrosion Surveillance in Spent Fuel Storage Pools," *Paper No. 107 of Corrosion 97, National Association of Corrosion Engineers*.
- ¹⁰⁴ Chandler, G.T., R.L. Sindelar, and P.S. Lam, 1997, "Evaluation of Water Chemistry on the Pitting Susceptibility of Aluminum," *Paper No. 104 of Corrosion 97, National Association of Corrosion Engineers*.
- ¹⁰⁵ Howell, J.P. and S.D. Burke, 1996, "The Corrosion of Aluminum-Clad Spent Nuclear Fuel in Wet Basin Storage," *Proceedings of DOE Spent Nuclear fuel and fissile material management, American Nuclear Society, Reno, NV*, p. 49.
- ¹⁰⁶ Johnson, A.B. and S.P. Burke, 1996, "Corrosion of uranium fuel and basin materials in Hanford K East and K West fuel storage facilities," *Proceedings of DOE Spent Nuclear Fuel and Fissile Material Management, American Nuclear Society, Reno, NV*, p. 41.
- ¹⁰⁷ Lam, P. S., R. L. Sindelar, and K. Y. Barrett, 1998, "Corrosion of Aluminum-Uranium Alloys in Water Vapor at 200°C," *Proceedings of Material Research Society Winter Annual Meeting, Boston, MA*.
- ¹⁰⁸ Whitcare, R. F., 1990, *The UAl_x Fuel Dispersion System*, EGG-PRP-8783, Rev. 2, EG&G Idaho, Inc.: Idaho Falls, ID.
- ¹⁰⁹ Bourns, W. T., 1968, *Corrosion Testing of Uranium Silicide Fuel Specimens*, AECL-2718, Atomic Energy of Canada Limited: Chalk River, Ontario.
- ¹¹⁰ Lam, P. S., R. L. Sindelar, and H. B. Peacock, Jr., 1998, *Vapor Corrosion of Aluminum Cladding Alloys*, WSRC-MS-98-00333, Westinghouse Savannah River Co.: Aiken, SC.

- ¹¹¹ LaQue, F. L. and H. R. Copson, (eds.), 1963, *Corrosion Resistance of Metals and Alloys*, 2nd ed., Reinhold Publishing Corporation: New York.
- ¹¹² Draley, J. E., et al, 1958, "High Temperature Aqueous Corrosion of Aluminum Alloys," *Proceedings of Second International Conference on the Peaceful Uses of Atomic Energy*. United Nations: Geneva.
- ¹¹³ Draley, J. E. and W. E. Ruther, 1967, *Corrosion of Aluminum Alloys by Flowing High Temperature Water*, ANL-7227, Argonne National Laboratory: Argonne, IL.
- ¹¹⁴ Breden, C. R. and N. R. Grant, 1969, *Summary of Corrosion Investigations on High Temperature Aluminum Alloys*, ANL-5546, Argonne National Laboratory, Argonne, IL.
- ¹¹⁵ Grant, N. R., 1961, *Summary of Corrosion Investigations of High-Temperature Aluminum Alloys*, ANL-6204, Argonne National Laboratory: Argonne, IL.
- ¹¹⁶ Aas, S. and K. Videm, 1965, "Improved Aluminum Alloys as Fuel Cladding Material in Water-Cooled Power Reactors," *Proceedings of the Third International Conference on the Peaceful Uses of Atomic Energy*, United Nations: Geneva.
- ¹¹⁷ Ayers, J. A., R. L. Dillon, and R. J. Lobsinger, 1958, "The Use of Aluminum as Fuel Cladding in Pressurized Water Power Reactors," *Proceedings of the Second International Conference on the Peaceful Uses of Atomic Energy*, United Nations: Geneva.
- ¹¹⁸ Johnson, A. B., 1994, "Bases for Extrapolating Materials Durability in Fuel Storage Pools," *Proceedings of the Topical DOE Spent Nuclear Fuel-Challenges and Initiatives*, American Nuclear Society: Salt Lake City, UT, pp. 83-88.
- ¹¹⁹ Lam, P., R. L. Sindelar, and H. B. Peacock, Jr., 1997, *Vapor Corrosion of Aluminum Cladding Alloys and Aluminum-Uranium Fuel Materials in Storage Environments*, WSRC-TR-97-0120, Westinghouse Savannah River Co.: Aiken, SC.
- ¹²⁰ Lam, P. S., R. L. Sindelar, and K. Y. Barrett, 1998, *Corrosion of Aluminum-Uranium Alloys in Water Vapor at 200°C*, WSRC-MS-98-00858, Westinghouse Savannah River Company: Aiken, SC.
- ¹²¹ Peacock, H. B. and R. L. Frontroth, 1989, *Properties of Aluminum-Uranium Alloys*, WSRC-RP-89-489, Westinghouse Savannah River Co.: Aiken, SC.
- ¹²² Ruther, W. E. and J. E. Draley, 1959, *Corrosion of Aluminum-Uranium Alloys in High-Temperature Water*, ANL-6053, Argonne National Laboratory: Lemont, IL.
- ¹²³ Wiersma, B.J. and J.I. Mickalonis, 1998, *Preliminary Report on the Dissolution Rate and Degradation of Aluminum Spent Nuclear Fuels in Repository Environments*, WSRC-TR-98-00290 (U), Savannah River Technology Center: Aiken, SC.

- ¹²⁴ Gray, W.J., 2000, *Dissolution Rates of Aluminum-Based Spent Fuels Relevant to Geologic Disposal*, PNNL-11979/WSRC-TR-2000-00042, Pacific Northwest National Laboratory: Richland, WA.
- ¹²⁵ Gray, W.J., 1998, "Corrosion of Aluminum-Based Spent Fuel Under Geologic Disposal Conditions," *Proceedings of Third Topical Meeting on DOE Spent Nuclear Fuel and Fissile Materials, Vol. 2, September 1998*, American Nuclear Society: Charleston, SC.
- ¹²⁶ Arendt, J. W. and W. W. Binger, 1945, *Corrosion of Aluminum-Uranium Alloys*, CT-3029, University of Chicago Metallurgical Laboratory: Chicago.
- ¹²⁷ De Souza Santos, T. D., H. M. Haydt, and C. T. de Freitas, 1965, "Experimental Studies on the Fabrication of Thin Fuel Plates with U₃O₈-Al Cermets," *Proceedings of the Third International Conference on Peaceful Uses of Atomic Energy, Geneva: United Nations*.
- ¹²⁸ Stahl, D., 1982, *Fuels for Research and Test Reactors*, Status Review: July 1982, ANL-83-5, Argonne National Laboratory: Argonne, IL.
- ¹²⁹ Durazzo, M. and L. V. Ramanathan, 1988, "Aqueous Corrosion of U₃O₈-Al Cermet Cores," *Proceedings of the 10th International Congress on Metallic Corrosion*, Key Engineering Materials: Madras, India, pp. 1577-1586.
- ¹³⁰ Peacock, H. B., 1990, *Properties of U₃O₈-Aluminum Cermet Fuel*, WSRC-RP-89-981, Westinghouse Savannah River Co.: Aiken, SC.
- ¹³¹ Snyder, M. J. and W. H. Duckworth, 1959, *Properties of Some Refractory Uranium Compounds*, BMI-1223, Battelle Memorial Institute: Columbus, OH.
- ¹³² Wiencek, T. C., 1995, *Summary Report on Fuel Development and Miniplate Fabrication for the RERTR Program, 1978 to 1990*, ANL/RERTR/TM-15, Argonne National Laboratory: Argonne, IL.
- ¹³³ Feraday, M. A., 1971, *The Oxidation, Hydriding and Aqueous Corrosion of U₃Si Alloys*, AECL-3862, Atomic Energy of Canada Limited: Chalk River, Ontario.
- ¹³⁴ Bourns, W. T., 1965, *A Literature Survey of U₃Si Corrosion*, AECL-2609, Atomic Energy of Canada Limited: Chalk River, Ontario.